Establishment of Appropriate Guidelines for Use of the Direct and Indirect Design Methods for Reinforced Concrete Pipe

Prepared for:

AASHTO Standing Committee on Highways

Prepared by:

Ian D. Moore, Neil A. Hoult and Katrina MacDougall

Queen`s University

Department of Civil Engineering, 58 University Avenue, Kingston, ON, K7L 3N6 Canada

March 2014

The information contained in this report was prepared as part of NCHRP Project 20-07, Task 316, National Cooperative Highway Research Program.

Acknowledgements

This study was requested by the American Association of State Highway and Transportation Officials (AASHTO), and conducted as part of National Cooperative Highway Research Program (NCHRP) Project 20-07. The NCHRP is supported by annual voluntary contributions from the state Departments of Transportation. Project 20-07 is intended to fund quick response studies on behalf of the AASHTO Standing Committee on Highways. The report was prepared by Ian Moore, Neil Hoult, and Katrina MacDougall of Queen's University. The work was guided by a task group included Henry Cross (South Carolina DOT), Cecil L. Jones (Diversified Engineering Services, Inc.), Michael G. Katona (Washington State University), Thomas P. Macioce (Pennsylvania DOT), John J. Schuler(Virginia DOT), Scott A. Anderson (Federal Highway Administration), and Josiah W. Beakley (American Concrete Pipe Association). The project was managed by Waseem Dekelbab, NCHRP Senior Program Officer.

TABLE OF CONTENTS

SUMMARY

The performance of Indirect Design and Direct Design procedures for structural design of reinforced concrete culverts was investigated. Tests performed on three 24 in. diameter and two 48 in. diameter pipes revealed that the Indirect Design procedure leads to safe load capacity estimates, ranging from 54% to 81% of those observed in the buried pipe tests. Direct Design calculations for those tests were also safe, with calculated load capacity falling between 19% and 77% of the observed values. Furthermore, Direct Design estimates of expected moment arising from the effects of surface loads on shallow buried pipes were between 3 and 4 times higher than those calculated from strains measured during the experiments.

Semi-empirical design procedures like Indirect Design would normally be expected to produce larger areas of required steel than design procedures based on rational assessments of expected moment and moment capacity (like the calculations performed as part of the Direct Design Method). As observed by others previously, the steel requirements calculated using Direct Design for small diameter reinforced concrete pipes can actually be greater than those that arise from Indirect Design. Various simplifications associated with Direct Design estimates of moment capacity were examined, and it was found that these discrepancies between Direct Design and Indirect Design outcomes can largely be addressed by using a 'thick ring' moment adjustment factor to eliminate conservatism associated with thin ring theory, and by using Modified Compression Field Theory to employ more sophisticated approximations for the concrete response and to enforce compatibility between the steel reinforcing and the concrete. Since these two techniques can be used to eliminate the larger estimates of steel area that may otherwise arise from the Direct Design of small diameter pipes, and since both design methods were found to produce safe designs, there appears to be no need for guidelines that restrict use of either of the design procedures for pipes of specific diameter or burial depth.

Three changes to the AASHTO LRFD Bridge Design Specifications are recommended: the introduction of a simple adjustment factor to eliminate conservatism associated with thin ring theory, the introduction of commentary indicating that the evidence collected during this research project supports a free choice by the designer regarding which design method to employ, and the introduction of commentary which suggests that Modified Compression Field Theory can be used to obtain more sophisticated estimates of flexural and shear capacity during Direct Design. A change is also suggested regarding the calculation of load spreading below surface loads. Calculations of surface load effects at the crown should continue to employ the

depth of burial to the top of the pipe, but calculations for surface load effects on springline and invert moments could consider load spreading from the surface to the depth of burial of the springline and invert, respectively.

CHAPTER 1 BACKGROUND

Currently, in the AASHTO LRFD Bridge Design Specifications, reinforced concrete pipe can be designed according to one of two methods; the indirect design method or the direct design method. The Indirect Design Method uses tables to select the appropriate pipe class (thickness, reinforcement, and concrete strength) for a given fill height and installation type. The method is based on three-edge-bearing tests and observed crack widths. The Direct Design Method is a more theoretical design method where four separate structural design limit states are considered: flexure, thrust, shear (diagonal tension), radial tension, and crack control. These two methods may give different answers for design of equivalent pipe, depending upon size, loading and installation requirements. The Indirect Design Method is based on a comparison of field moments versus test moments. The Direct Design Method has simplifying assumptions for reinforcement conditions, as well as limitations on the steel and concrete properties that may not allow for a pipe to be designed to its true strength. There has been uncertainty regarding the relative performance of both methods, whether they both produce safe designs for all situations, and which method is most appropriate for specific pipe sizes and burial depths, to eliminate unneeded expense. Recent suggestions for determining appropriate guidelines for which design method to use have ranged from taking the lower steel area requirement of the two designs, to using the Direct Design Method for pipes with an inner diameter larger than 36” and the Indirect Design Method for pipes 36” and smaller.

Objectives

The objectives of this research are to:

(1) review the strengths and weaknesses of the Indirect and Direct Design methods and compare their design outcomes (e.g. the areas of steel required for specific loading conditions);

(2) conduct tests that permit evaluation of the performance of the two design methods relative to measurements of demand (the loads that develop) and resistance (the ability of the reinforced concrete test pipes to resist those demands);

(3) produce guidance regarding when each method is most appropriate, and possible revisions to make their design outcomes more consistent (including revisions to the AASHTO LRFD Bridge Design Specifications, Section 12).

CHAPTER 2 RESEARCH APPROACH

The project was divided into various tasks:

- a literature search to review the development of both design methods and to summarize the strengths and weaknesses of the two procedures
- testing of small and medium diameter pipes to compare observed performance with calculations according to Section 12 of the AASHTO LRFD Bridge Design Specifications
- work clarifying how both the service limit states and strength limit states apply to the Indirect and Direct Design Methods in Section 12.10, to determine the reasons for differences on outcomes from the two design procedures, and to prepare draft guidelines for when a particular method may or may not be appropriate
- evaluation of potential changes to ultimate strength calculations during Direct Design so the two methods might produce more similar design outcomes
- draft revisions to Section 12 of the AASHTO LRFD Bridge Design Specifications so that both design methods more closely correlate
- identification of future research or immediate implementation if sufficient data already exists
- preparation of this final report describing the entire research effort.

The research agency is Queen's University (QU).

CHAPTER 3 FINDINGS AND APPLICATIONS

3.1 Introduction

The research findings are presented in the six following areas:

- An overview of the literature review and the two design methods, discussing their pros and cons, their treatment of limit states, and previous studies examining their relative performance;
- A description of the experimental work performed on small and medium sized reinforced concrete pipes;
- A comparison of the experimental results and design calculations to gage the current level of safety associated through comparisons of design calculations with observed performance;
- The investigation of potential changes to the Direct Design procedures for estimating ultimate moment capacity;
- A comparison of the steel requirements calculated using Direct Design and Indirect Design, considering the current specifications and the effect of potential changes to those specifications;
- A discussion of when to use Direct and Indirect Design, and proposed changes to the AASHTO LRFD Bridge Design Specifications.

3.2 Literature review and overview of the two design methods

3.2.1 Introduction

Before the 19th century, little work was performed developing the theory of pipe design. Brown (2002) presents a history of pipe-flow equations showing work in the development of flow equations as early as 1770 by Antoine Chezy. In the 1900's, as cities grew and the demand for concrete pipes increased, so did the need for a standardized method of design to ensure the adequate strength of pipes. With the addition of steel reinforcement to concrete pipe walls around 1900, pipes were able to reach higher capacities and work began to determine the strength required by these pipes (Ontario Concrete Pipe Association, 2011). The following literature review outlines the development of pipe design theory beyond 1900, and discusses the two current methods of pipe design: the Indirect Design Method and the Direct Design Method. It also summarizes the current implementations of the two design methods as well as

previous research performed to evaluate and compare them. The review discusses studies of both demand (the loads that develop on a buried rigid pipe) and the resistance (the ability of the pipe to support the demand). The equations presented below are taken from the American Association of State Highway and Transportation Officials LRFD Bridge Design Specifications (2007) subsequently referred to as AASHTO LRFD Bridge Design Code. The acronym LRFD stands for Load and Resistance Factor Design.

3.2.2 Early Theories

In the early 1900's Marston developed a load theory to assess rigid pipes in the ground by first analyzing their behavior in trench conditions. Marston used the theory of Janssen (1895) for pressures in silos to develop his own theory in relation to pipes. He defined the gravity loading on the pipe as the column of soil above the crown of the pipe across the width of the trench excavation. This force was modified to account for the friction forces transferred across the vertical planes on the sides of the trench (shear on the interfaces between the column of soil and the undisturbed soil, Zhao and Daigle, 2001). Factors in Marston's load equation include the soil's specific weight and type, the external diameter of the pipe and the trench width, and soil parameters unit weight, coefficient of lateral earth pressure, and frictional strength along the sides of the trench.

Marston also developed equations for the embankment condition, where he proposed that the prism of soil overlying the pipe can be considered to have sides rising vertically upwards from the pipe springlines, and these also transfer load to or from the surrounding soil by means of friction (depending on whether the pipe is more compressible or less compressible that the soil beside it, respectively).In 1932, Schlick, a colleague of Marston, developed an equation to define the critical width at which point the trench burial load equation no longer applied and an embankment load equation had to be employed (Moser, 2001). This width is known as the transition width; the point where the weight of the soil column overlying a pipe in a wide trench is equal to the embankment load.

Spangler (1933) later developed three installation conditions using Marston's earth load theory and worked to determine the strength of buried rigid pipe that was required to support the predicted load. Spangler developed ratios, known as bedding factors, which related the cracking load in buried rigid pipe installations to the cracking load in three-edge bearing tests. The cracking load is reached when cracks of width measuring 0.01-in.at the inner or outer surface of

the pipe begin to form (ASTM C76-11). Bedding factors were developed for trench and embankment conditions. However the trench bedding factor excluded the effects of lateral pressure from the soil onto the pipe, and the embankment bedding factor only partially included lateral pressure. The bedding conditions defined were developed to suit analysis and not ease of construction (Concrete Pipe Design Manual, 2011).

3.2.3 Pipe Design Developments of Heger and his coworkers

In the 1970's the American Concrete Pipe Association (ACPA) sponsored a research project undertaken by Frank Heger and his colleagues from Simpson Gumpertz & Heger Inc. that resulted in the Soil Pipe Interaction Design and Analysis (SPIDA) program. The development of SPIDA was based on a number of research initiatives. Heger and McGrath (1980) presented a design method that includes considerations for flexural strength involving reinforcement tension, concrete compression, concrete radial tension, stirrup radial tension, and diagonal tension. Limiting crack width of 0.01-inch was defined as a serviceability limit. Heger (1982) then presented a new structural design method for reinforced concrete pipe based on extensive tests performed on pipes, box sections, slabs and curved slabs. Additionally, Heger and McGrath (1982) discussed use of new semi-empirical equations for the shear strength of pipe and suggested how the shear design equations used at that time did not accurately assess shear strength in pipe. Further work examining radial tension strength of pipes by Heger and McGrath (1983) presented equations to predict radial tension strength from tests subjecting the inside face of the curved member to flexural tension. These results were empirically determined from a limited number of three edge bearing tests.

Heger and McGrath (1984) then studied crack widths during a number of tests on pipes, box sections, straight and curved slabs, and suggested that other crack widths might be appropriate (the use of crack width of 0.01-in as a serviceability limit was seemingly an arbitrary choice with limited data connecting it to pipe durability). They presented design equations and a control factor that permits consideration of various different crack widths, and these were incorporated into the 1983 AASHTO Bridge Specification. Heger and Liepens (1985) examined the stiffness of flexurally cracked reinforced pipe. They used correlations between computed and measured deflections of pipe under three edge bearing and developed coefficients for calculation of wall stiffness that were incorporated into the SPIDA program. In 1988, using SPIDA to run various simulations, Heger developed a new idealized pressure distribution defining soil loads around the circumference of concrete pipes, and recommended five new standard installation types.

Heger's new pressure diagram differed from earlier established theories, and included the effect of voids or zones of low stiffness backfill that often occur under the pipe haunches. Although the results were based on limited field tests to support the theoretical calculations, other researchers have reported test results that support Heger's earth pressure distributions (e.g. Wong et al. 2006).

3.2.4 Common Elements of Pipe Design

Introduction

Indirect Design is based on using the results of three-edge bearing tests and empirical 'bedding factors' to consider the impact of burial on the load capacity. Direct Design was developed from the finite element method (FEM) as discussed later in this section, and employs analysis of soil and other loads to determine moment, thrust and shear in the pipe. Despite the differences in loading analysis, certain aspects of pipe design are common to both approaches.

Installation Types

The original installation types were based on the early work of Marston (1913) and Spangler (1933), however more recent research has led to modified installation types. The research performed by Heger (1988) used a number of different simulations to develop the four Standard Installation Direct Design (SIDD) installation types currently considered: Type I (highest quality), Type II (lower quality), Type III (least quality), and Type IV (no quality control). These installation conditions are used in both Indirect and Direct Design and as outlined in Table 1.

Concrete pipe analyses

Three computer analyses were developed in support of Direct Design by Heger and his collaborators:

1. Soil Pipe Interaction Design and Analysis Program (SPIDA) – a finite element analysis which explicitly models the soil, the pipe, and their interaction;
2. Standard Installation Direct Design (SIDD) – a structural analysis of the pipe ring using the Heger soil pressure distributions to determine the moments, thrusts, and shears;
3. PIPECAR –employing moment, thrust and shear factors associated with the four standard installation types, pipe self-weight, fluid, earth and vehicle loads.

Table 1. Standard embankment installation soils and minimum compaction requirements from AASHTO LRFD Bridge Design Code Table 12.10.2.1-1.

Installation Type	Bedding Thickness	Haunch and Outer Bedding	Lower Side
Type 1	For soil foundation, use B_c/2.0 ft minimum, not less than 3.0 in. For rock foundation, use B_c ft minimum, not less than 6.0 in.	95% SW	90% SW, 95% ML, or 100% CL
Type 2—Installations are available for horizontal elliptical, vertical elliptical, and arch pipe	For soil foundation, use B_c/2.0 ft minimum, not less than 3.0 in. For rock foundation, use B_c ft minimum, not less than 6.0 in.	90% SW or 95% ML	85% SW, 90% ML, or 95% CL
Type 3—Installations are available for horizontal elliptical, vertical elliptical, and arch pipe	For soil foundation, use B_c/2.0 ft minimum, not less than 3.0 in. For rock foundation, use B_c ft minimum, not less than 6.0 in.	85% SW, 90% ML, or 95% CL	85% SW, 90% ML, or 95% CL
Type 4	For soil foundation, no bedding required. For rock foundation, use B_c/2.0 ft minimum, not less than 6.0 in.	No compaction required, except if CL, use 85% CL	No compaction required, except if CL, use 85% CL

Vertical Arching Factor

The vertical arching factor (VAF) is used to account for the manner in which load redistributes within the soil as a result of the stiffness of the pipe relative to the stiffness of the soil surrounding it. While the original concept of arching was based on Marston's application of the Janssen silo theory, similar arching factors can be calculated using elastic soil-pipe interaction analyses like those of Burns and Richard (1964) and Hoeg (1968). The VAF varies depending on the type of installation which influences the stiffness of the soil around the pipe. VAF is used in both Indirect and Direct Design and is outlined in Table 12.10.2.1-3 in the AASHTO LRFD Bridge Design Code and presented here in Table 2.

Table 2. Vertical arching factor from AASHTO LRFD Bridge Design Code Table 12.10.2.1-3

Installation Type	**VAF**
Type 1	1.35
Type 2	1.40
Type 3	1.40
Type 4	1.45

3.2.5 Indirect Design Method

The Indirect Design Method, the most commonly used approach for concrete pipe design (Erdogmus and Tadros, 2006), incorporates aspects of Marston and Spangler's research with modern changes implemented based on the work of Heger and his research collaborators. A standard positive projection embankment loading condition is used as it is conservative for every type of burial condition (AASHTO LRFD 12.10.2.1). The weight of soil above the pipe is then multiplied by the VAF and added to the fluid load carried by the pipe. The total live load is then calculated and kept separate. The two load totals are then divided by their respective bedding factors and summed. The bedding factors for circular pipes are given in Table 12.10.4.3.2a-1 of the AASHTO LRFD Bridge Design Code and presented here in Table 3. Additionally, there are also bedding factors specifically provided for live loads in Table 12.10.4.3.2c-1 of the AASHTO LRFD Bridge Design Code. Bedding factors quantify the relationship between three-edge bearing test loads and field loading behavior. As described in the American Concrete Pipe Design manual, modern bedding factors for Standard Installations are based in reinforced concrete design theory and on a parametric study performed using SIDD. The resulting total is then multiplied by a safety factor and divided by the pipe diameter as per Equation 1.

$$D_{Load} = \left[\left(\frac{W_E + W_F}{B_f}\right) + \frac{W_L}{B_{LL}}\right] \times \frac{F.S.}{D_i} \quad (1)$$

The resulting value, known as a D-Load, is then used to determine the class of pipe from tables in ASTM C76 (2011).

Table 3. Bedding Factors, Embankment Conditions, Bfe from AASHTO LRFD Bridge Design Code Table 12.10.4.3.2a-1

Pipe Diameter	Type 1	Type 2	Type 3	Type 4
12 in.	4.4	3.2	2.5	1.7
24 in.	4.2	3.0	2.4	1.7
36in.	4.0	2.9	2.3	1.7
72in.	3.8	2.8	2.2	1.7
144in.	3.6	2.8	2.2	1.7

There are five class types categorized into tables by 0.01in cracking capacity and ultimate capacity. Each table is used to determine the amount of reinforcing steel required for a specified pipe diameter, wall thickness and concrete strength to support the calculated loads.

ASTM C76 provides no specifications for shear reinforcement but the use of shear reinforcement is not common in pipe design, Erdogmus and Tadros (2006).

3.2.6 Direct Design Method

Introduction

As indicated earlier, the Direct Design Method was developed using the finite element analysis program SPIDA created by Heger and his colleagues in the 1970's. This research project also resulted in "ASCE 15-98: Standard Practice for Direct Design of Buried and Precast Concrete Pipe Using Standard Installation", which introduced the four standard installations as described earlier. The Direct Design Method uses the same approach as the Indirect Design Method specified by the American Association of State Highway and Transportation Officials (AASHTO) to select installation type, and then for a given pipe diameter and wall thickness, calculate vertical earth load, fluid load and live load. However, instead of using bedding factors and tables to determine the amount of reinforcing steel (the Indirect Design approach), the Direct Design Method requires thrust, shear and moment values to be determined and used to calculate steel requirements based on conventional theories for design of reinforced concrete to withstand flexure (Concrete Pipe Design Manual, 2011). A table of coefficients was developed and presented in ASCE 15-98 that simplify the calculation of the moment, thrust, and shear acting on the pipe. These coefficients are presented as C_{mi}, C_{ni}, C_vi (their use is discussed further in a subsequent section). Strength reduction factors are also included in the design including factors for flexure, diagonal tension, radial tension and limiting crack width.

Design for Flexure

After moment and thrust acting on the pipe are calculated they are used in Equation 2 to determine the amount of circumferential steel required.

$$A_s = g\varphi d - N_u - \frac{\sqrt{g[g(\varphi d)^2 - N_u(2\varphi d - h) - 2M_u]}}{f_y} \geq 0.07 \qquad 2$$

The AASHTO LRFD Bridge Design Code provides a ratio to determine the amount of outside steel needed from the amount of steel calculated for the inside layer. In addition, the code provides equations for minimal requirements of steel to withstand flexure and shear. The minimum amount of steel allowed for any case is 0.07in^2/ft.

Design for Shear

The AASHTO LRFD Bridge Design Code provides equations for design in shear both with and without stirrups. Pipe sections are investigated at the critical section where M_{nu} / V_u d =3.0. Factored shear resistance V_r, for shear without stirrups, is found using Equation 3 where V_n is found using Equation 4.

$$V_r = \varphi V_n \quad (3)$$

$$V_n = 0.0316bdF_{vp}\sqrt{f_c'}(1.1 + 63\rho)\left(\frac{F_d F_n}{F_c}\right) \quad (4)$$

The equations for variables in Equation 4 can be found in section 12.10.4.2.5 of the AASHTO LRFD Bridge Design Code, as well as additional equations for reinforcement requirements including expressions for flexural reinforcement and reinforcement for crack width control.

3.2.7 Pipe Loading

Dead Loading

For both Indirect and Direct Design, the methods for calculating fluid load and earth load are the same. The fluid load is calculated from the internal volume of the pipe per unit length and the density of water at 62.4 pcf as shown in Equation 5. The earth load is calculated from the soil column method originally developed by Marston (1913). A VAF based on installation type is selected and multiplied by the prism load of the soil column as shown in Equation 6. The pipe load is calculated for the direct design method per unit length, as shown in Equation 7, from the volume of concrete and density of concrete typically taken to be 150 pcf. However, the pipe load is not included in the Indirect Design Method as it is "approximately accounted for by the weight of the pipe acting in the 3-edge bearing test load condition" (Heger et al., 1985).

$$W_F = \pi r_i^2 \cdot \gamma_w \quad (5)$$

$$W_E = VAF \cdot PL = VAF \cdot \gamma_s[H + 0.0089D_0]\frac{D_0}{12} \quad (6)$$

$$W_P = \pi(r_0^2 - r_i^2) \cdot \gamma_c \quad (7)$$

Live Loading

The effect of live load on the buried pipe is calculated by using the "worst-case" scenario of: (i) a single dual wheel loading of the AASHTO design truck, (ii) two single dual wheels of AASHTO design trucks in passing mode at a distance of 4ft apart, (iii) or two single dual wheels of two alternate load vehicles in passing mode. The "worst-case" is dependent on the direction of vehicular travel, pipe diameter and depth of cover. The details of loading case selection are

shown in Table 4. The downward distribution of load governed by the Live Load Distribution Factor (LLDF) has been modified since the SIDD design method from 1.75 to 1.15. ASCE 15-98 originally specified a LLDF of 1.75 but it was later found that a more conservative value of 1.15 for select-granular and 1.00 for any other soil was more appropriate (Standard Practice for Direct Design of Buried and Precast Concrete Pipe Using Standard Installation, 1998) (Concrete Pipe Design Manual, 2011). In addition, the spacing between passing design trucks has been modified from 6ft in ASCE 15-98 to 4ft in the AASHTO LRFD Bridge Design Code (2011) creating a more critical loading case at shallower depths due to the interaction between load spread areas. The live load spreading for a single wheel load is illustrated in Figure 1a while the load spreading diagrams for multiple vehicles are given in Figures 1b and 1c. Very recently, the live load distribution factor was adjusted for concrete pipes as a result of the finite element analysis work of Petersen et al. (2010), so that for pipes of diameter less than 24 in., LLDF is 1.15, for pipes greater than 96 in, it is 1.75, and between 24 in. and 96 in. in diameter, it is expressed as a linear function of internal diameter D_i

$$LLDF = 0.00833.D_i + 0.95 \quad (8)$$

Although the ASCE 15-98 suggested that an impact factor (IM) not be used in live load calculations, it has been included in the AASHTO LRFD Bridge Design Code (2011). This factor accounts for the dynamic force of the moving design truck on the pipe (associated with the vehicle hitting a pothole or other pavement irregularity). Furthermore, a multiple presence factor (MPF) is outlined in the AASHTO LRFD Bridge Design Code, which is used to account for the magnitude of truck loads when one or multiple lanes are occupied. When designing for a single truck in one lane an MPF of 1.2 is used. This factor is reduced to 1.0 for two trucks passing as it is unlikely that two overloaded trucks pass at the same instant. The truckload is divided by the spread area, in Figure 1, to determine the full distribution of the load into the soil and increased by the factors accounting for truck movement and overloading. Finally, the load is multiplied by the lesser of the pipe diameter or the governing load length (Equations 9 and 10) to account for the load distributed directly to the pipe as indicated in Equation 11 (Petersen et al., 2010).

Table 4. Critical Wheel Loads and Spread Dimensions at the Top of the Pipe (ACPA, 2011)

Vehicle Traveling Perpendicular to Pipe					
	H, ft	**P, lbs**	**Spread a, ft**	**Spread b, ft**	**Figure**
Live Load Distribution of 1.15 x H for Select Granular Fill	$H + 1.15D_o < 2.05$	16,000	a + 1.15H	b + 1.15H	3
	$2.05 - 1.15D_o < H < 5.5$	32,000	a + 4 + 1.15H	b + 1.15H	4
	$5.5 < H$	50,000	a + 4 + 1.15H	b + 4 + 1.15H	5
Live Load Distribution of 1.0 x H for Other Soils	$H + 1.30D_o < 2.30$	16,000	a + 1.00H	b + 1.00H	3
	$2.30 - 1.30\ D_o < H < 6.3$	32,000	a + 4 + 1.00H	b + 1.00H	4
	$6.3 < H$	50,000	a + 4 + 1.00H	b + 4 + 1.00H	5
Vehicle Traveling Parallel to Pipe					
Live Load Distribution of 1.15 x H for Select Granular Fill	$H < 2.03$	16,000	a + 1.15H	b + 1.15H	3
	$2.03 < H < 5.5$	32,000	a + 4 + 1.15H	b + 1.15H	4
	$5.5 < H$	50,000	a + 4 + 1.15H	b + 4 + 1.15H	5
Live Load Distribution of 1.0 x H for Other Soils	$H < 2.33$	16,000	a + 1.00H	b + 1.00H	3
	$2.33 < H < 6.3$	32,000	a + 4 + 1.00H	b + 1.00H	4
	$6.3 < H$	50,000	a + 4 + 1.00H	b + 4 + 1.00H	5

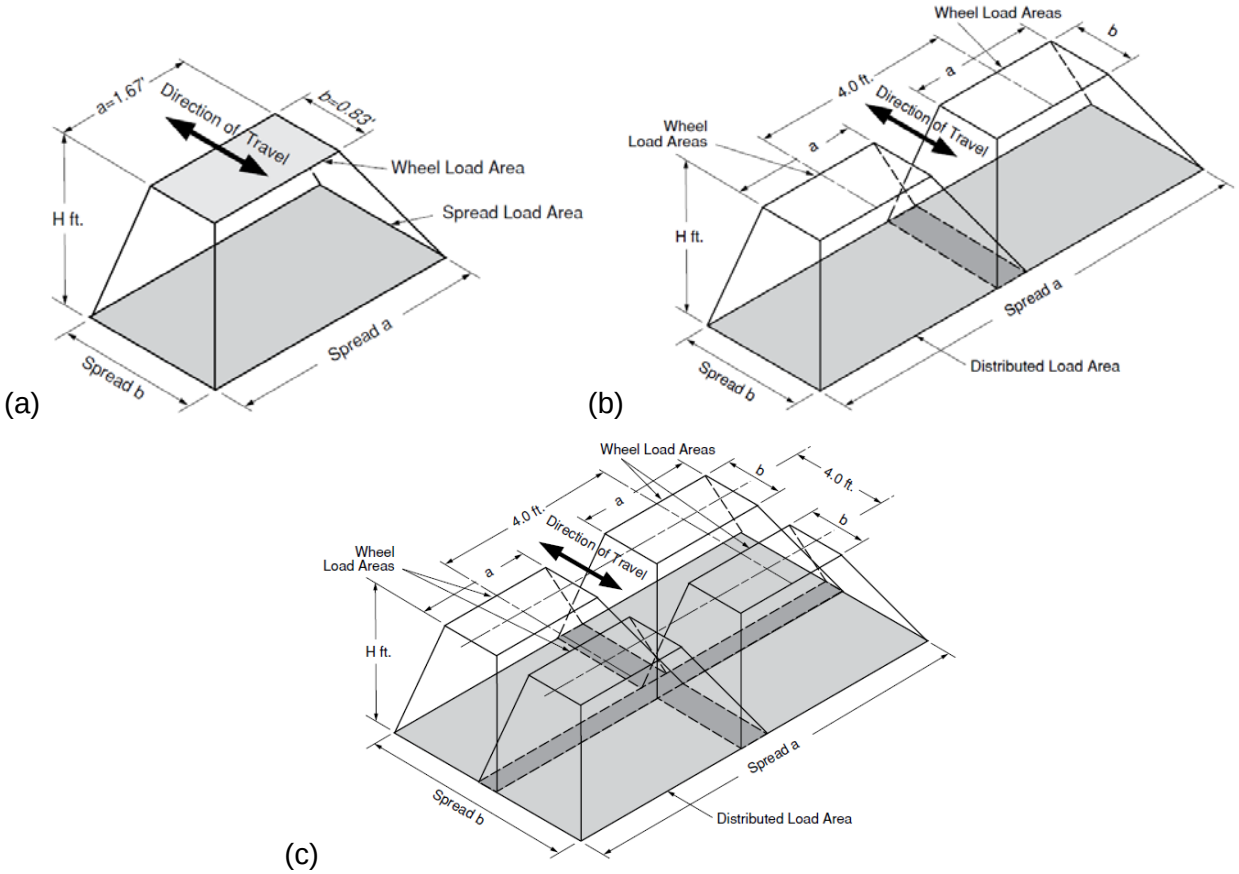

Figure 1: Spread Load Area - (a) Single Dual Wheel (b) Two Single Dual Wheels of AASHTO Design Trucks in Passing Mode (c) Two Single Dual Wheels of Two Alternate Loads in Passing Mode (ACPA, 2011)

$$L_{t_{gov}} = \frac{l_t}{12}; for\ H < 0.833 \quad (9)$$

$$L_{t_{gov}} = \frac{l_t}{12} + LLDF_i \cdot H; for\ H \geq 0.833 \quad (10)$$

$$W_L = MPF \cdot (1 + IM) \cdot \left[\frac{P}{(1.67+1.15H)(0.83+1.15H)}\right] \cdot \min\left(\frac{D_i}{12}, L_{t_{gov}}\right) \quad (11)$$

Design Forces

After determining the dead load, live load, fluid load and pipe load, the loads in combination with the installation coefficients, given in the ASCE 15-98, are used to find the moment, thrust and shear in the pipe at the crown, invert, springlines and critical shear locations as per Equations 12 to 14.

$$M_i = \sum \frac{Cm_i W_i D_i}{2} \quad (12)$$

$$N_i = \sum Cn_i W_i \quad (13)$$

$$V_i = \sum Cv_i W_i \quad (14)$$

The loading coefficients (Cm_i, Cn_i, Cv_i) used to calculate the moment, thrust and shear on the pipe in Equations 12 to 14 are based on the pressure distributions developed by Heger in his research studies (Heger, 1988).

3.2.8 Pressure Distributions

In the concrete pipe design software package PIPECAR, there are additional pressure distribution options that have been previously used in Direct Design: (i) the Paris distribution, and (ii) the Olander distribution. The uniform pressure distribution presented by Paris (1921) uses different uniform pressures along the top, sides and bedding of the pipe. The method also requires a soil-structure interaction and lateral pressure coefficient as well as bottom reaction widths for soil, water and live loading as well as pipe weight loading conditions (Simpson Gumpertz & Heger Inc., 2004). The radial pressure distribution presented by Olander (1950) uses two pressure bulbs to represent the pressure distribution on the pipe. Both these pressure distributions can be used in place of the pressure distribution by Heger in PIPECAR when analyzing loading on the pipe. As described in the AASHTO LRFD Bridge Design Code Section C12.10.4.2.1, the design equations are applied after the moment, thrust and shear are determined, and so design is not limited to any one assumed pressure distribution and any one of the acceptable pressure distributions can be used.

PIPECAR also employs a modified version of live load spreading, where LLDF=1.15 to the pipe crown, and then by LLDF=1.75 to a depth of ¾ of the way to the pipe invert. As a result, Direct Design calculations performed using PIPECAR satisfy neither the 2007 or 2013 versions of the AASHTO LRFD Bridge Design Specifications.

3.2.9 Comparison of Indirect and Direct Design

Erdogmus and Tadros (2006) present a comparison between Indirect and Direct Design outlining both the more conservative and less conservative nature of the two design methods as illustrated in Figure 2. Performing a parametric study for 48-in diameter pipes, they work to establish governing failure types, flexure, crack control and shear, similar to the controlling criteria summarized by Figure 3 from ASCE 15-98. The steps seen in the Indirect Design represent the changes in pipe class from Class II at the lowest step to Class V at the highest; each step signifying an increase in D-load of the pipe. Erdogmus et al. (2010) also state that Direct Design provides a unique and conservative design. Indirect Design is an empirical method where required steel reinforcement does not vary progressively with depth of cover, but instead increases in finite steps.

Erdogmus and Tadros (2009) indicate that when buried, both the inner and outer reinforcement layers in the pipe are in tension which is not reflected in the Direct Design method, leading to over-conservatism in some cases. Also, the differences become more evident in pipes smaller than 36in where there is only a single cage of reinforcement and behavior becomes more complex.

The Direct Design Method allows the inputs to be varied (concrete strength, steel reinforcement and crack control factor) in order to develop an optimum design. Erdogmus and Tadros (2006) found that varying the steel strength had almost no effect on the capacity of the pipe where flexure controls and none where cracking and shear govern (based on the assumption that stirrups are not considered part of normal pipe design and thus were not present). The crack control factor presented in Section 12 of the AASHTO LRFD Bridge Design Code indicates the probability of a crack of a specified maximum width occurring. By changing the crack control factor from between acceptable levels of 0.7 to 1.3 it was found that between the generally used factor of 0.9 and a more conservative 1.3 there was little difference in the design of the pipe (though when crack control is the governing limit state, an increase in the factor will decrease steel area requirements). Erdogmus and Tadros (2006), performing an investigation for the

Nebraska Department of Roads (NDOR), found that NDOR's pipe design policy relies on interdependence between the Direct Design program PIPECAR and the indirect design based ASTM C76 tables, resulting in some discrepancies in design.

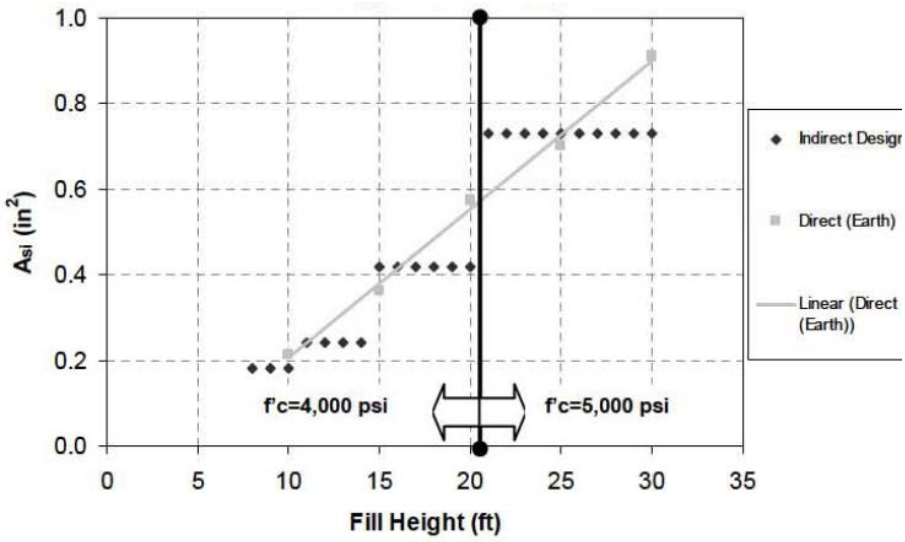

Figure 2: Comparison of inner cage area as function of fill height based on Indirect and Direct Design (Erdogmus and Tadros, 2006)

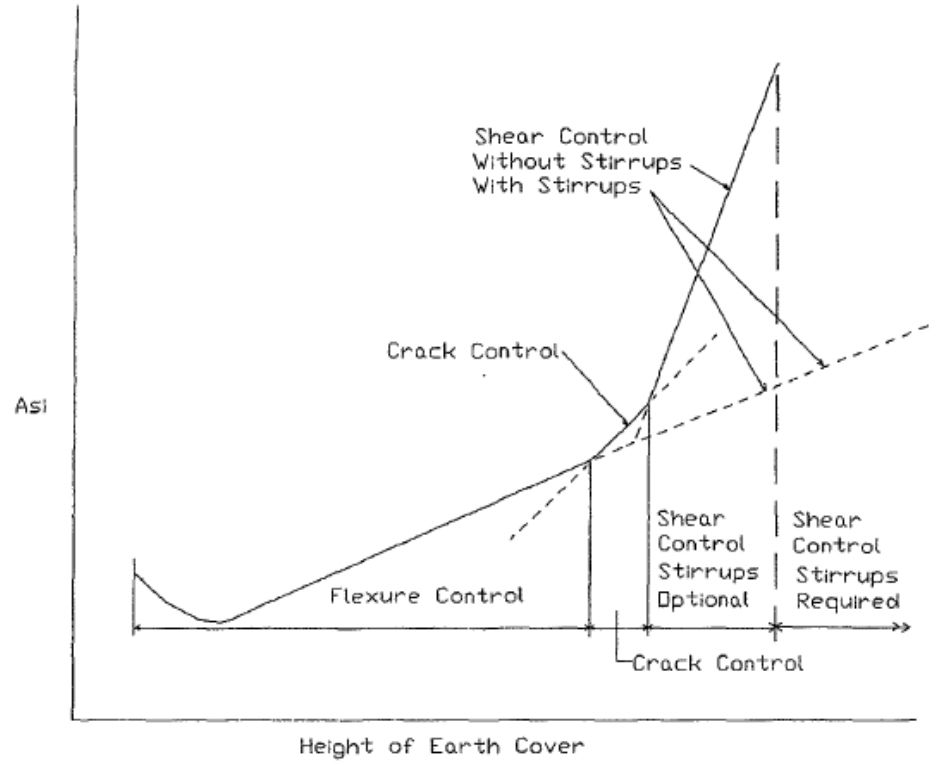

Figure 3: Plot of Required Inside Reinforcing Area versus Design Height of Earth Cover for Typical Design with Surface Wheel Loads ASCE 15-98

In the second phase of their research, Erdogmus and Tadros (2009) conclude that, from a designer's perspective, the Direct Design Method should be used and that three edge bearing tests and the 0.01-in crack control limit should no longer be observed. This conclusion was based on the observation that three edge bearing tests do not represent an accurate simulation of how pipes behave in the ground (they discount the ability of bedding factors to capture the effect of burial). Additionally, they conclude that the crack control limit of 0.01-in has no discernible technical origins and should be removed as a limit state. They argue that by limiting the direct design method by using the results of three edge bearing tests and ASTM C76, which was developed for Indirect Design, the potential of the Direct Design Method is unnecessarily limited. They suggest that the Direct Design Method has room for improvement by better accommodating material behavior and adjusting limit states. Erdogmus and Tadros (2009) suggest that, due to the complex behavior of small diameter (<36-in) singly-reinforced pipe, the Direct Design Method provides more conservative results than the Indirect Design Method and should be re-evaluated to better represent the "true" behavior of these pipes.

Now, it is well established in reinforced concrete analysis that the tensile strength of concrete is very low, to the point of being almost negligible, and that the reinforcing steel is not engaged until the concrete cracks. Therefore the cracking of concrete does not constitute failure but is necessary for the reinforced concrete system to function as designed. The same applies to reinforced concrete pipes. Cracks developed in concrete pipes, even up until the 0.01-inch crack width limit, do not therefore indicate that the pipe has reached its ultimate load capacity (ACPA, 2007). As stated in the ASTM C76-06: “the 0.01-inch crack is a test criterion for pipe tested in the three-edge-bearing test and is not intended as an indication of overstressed or failed pipe under installation conditions”. The acceptance criterion of a 0.01-inch crack width was suggested by Professor W.J. Schlick of Iowa State University to provide a consistency in quality control of pipes, not as a performance criterion (according to ACPA, 1978). The number was arbitrarily selected and is still used as an ASTM acceptance criterion (Heger and McGrath, 1984). Three-edge-bearing tests have shown that the pipe continues to perform beyond the development of 0.01-inch width cracks (ACPA, 1976), and the industry maintains that even in corrosive conditions the development of 0.01-inch crack does not lead to significant corrosion of the reinforcement (ACPA, 1971). Heger and McGrath (1984) developed the crack control factor, currently used in the Direct Design method, which indicates the probability that a specific size crack will occur; this included cracks smaller and larger than the 0.01-inch crack.

3.2.10 Experimental evidence of earth pressures or bending moments

Some recent work has been reported to examine the performance of buried concrete pipe, augmenting earlier tests that influenced the work of Marston, Spangler, Heger and others.

Wong et al. (2006) examined four installations of shallow buried reinforced concrete pipe using Type 4 bedding. Pipe diameters ranged from 24 in. to 36 in., and burial depths ranged from 4.7 to 5.6 ft (1.4 to 1.7m). Conventional earth pressure cells were used to measure radial earth pressure on the pipe, and these were compared to the Heger distributions. Bending moments were not measured, but they noted that the current values of horizontal stresses produce conservative calculations of design moment.

Becerril Garcìa (2012) (see also Moore et al., 2012) tested 24 in. and 48 in. diameter pipes at burial depths of 2ft and 3ft, responding to single wheel pairs loaded with the fully factored loads associated with a single axle AASHTO Design Truck. Strains and deformations were measured in the pipe barrel, and these were used to calculate the moments at crown and invert. While that

work primarily focused on the structural response of the pipe joints, data of this kind may be useful for assessing the effectiveness of moment estimates during direct design.

Lay (2012) tested 24-in diameter, Class V, reinforced concrete pipes under single design truck axle load with 1ft, 2ft, and 3ft cover to determine the capacity of the pipe and compare the observed behavior to the calculated results. He used measurements of wall strain to calculate moments at the critical sections (crown, springlines and invert). It was found that the pipe did not crack under working loads at the minimum burial depth of 1ft. Cracking occurred at fully factored loads for the minimum burial depth of 1 ft, however the crack width limit was not reached. At larger burial depths no cracks developed in the pipe under loads of up to 500kN (more than the fully factored axle load). As expected, at the fully factored load, crown moments and tensile strains decreased as the cover was increased. These results show that expected load resistance of the pipe far exceeded the factored loads, and suggests there is significant conservatism in design.

3.2.11 Advantages and disadvantages of Indirect Design and Direct Design

The pros and cons of the two design procedures can be assessed as follows. The advantages of Indirect Design include:

- the simple manner by which the procedure incorporates considerations of soil-structure interaction (the effect of soil support for different burial conditions is incorporated in the bedding factors), including separate consideration of the soil-structure associated with earth loading and surface (vehicle) loading;
- the ability to measure pipe strength using a straightforward laboratory test (the three edge bearing test), so pipe capacity (D-load) can be readily measured and compared with a project's requirement;
- steel quantities, wall thicknesses, and steel locations that are prescribed in standards (e.g. ASTM C76) so there is minimal need for engineering design, and the resulting pipes can be readily checked against the amounts required for a specific project;
- design based on crack width which seeks to include considerations of durability on pipe performance (though further work is needed to demonstrate the relationship between allowable crack width and service life);
- crack measurement is at the surface of the concrete (rather than at the level of the reinforcing steel), making it more readily obtained;

- the use of an actual test of moment capacity (i.e. D-load) which implicitly includes the effect of multiple steel bars, nonlinear steel and concrete behavior and other factors on the pipe strength.

Indirect Design has disadvantages which include:

- the need to perform tests on all sizes of pipe, including large diameter pipe structures that require high capacity, specialized equipment;
- the use of bedding factors that were originally based on small segments (arcs) of pipe, and which may never have been verified for large diameter structures using buried pipe tests;
- more recently adjustments to bedding factors that are based on analysis which relied on the conservative, simplifying assumptions associated with Direct Design;
- bedding factors that neglect issues like moisture in the soil;
- cracking loads during three edge bearing tests that feature compressive thrusts that are much lower than those that apply to the pipe when it is buried;
- the expense of testing pipe samples to confirm that they have the required capacity (instead of relying on a calculation based on geometry and material properties);
- no adjustment of the crack width requirement (0.01 inches) to account for the complexities of the environment (soil and groundwater acidity) and the detailed geometry and materials properties of the pipe (wall thickness, number of steel layers, depth of cover to the steel, cement chemistry);
- no explicit consideration of failure modes associated with shear and radial tension.

The advantages of Direct Design include:

- design flexibility which permits calculation of steel requirements for pipes of a wide range of different diameters, wall thicknesses, steel strengths, and concrete strengths;
- its explicit consideration of soil-structure interaction during development of the moment, shear, and thrust factors that are in common use;
- its explicit consideration of different failure modes, rather than reliance on the single focus of Indirect Design (crack width);
- its inclusion of considerations of crack width based on empirical data (measurements taken during three edge bearing tests);
- the use of elastic ring theory, and the availability of simple coefficients to facilitate estimation of expected values of moment, thrust and shear using a spreadsheet or other simple procedure.

The disadvantages of Direct Design include:

- its development of moment, shear and thrust factors based on 2D finite element analyses, whereas response to vehicle load is strongly three dimensional;
- its use of elastic ring theory to estimate moment, thrust and shear whereas the pipe behavior is nonlinear once cracking initiates
- its use of a single location at the maximum moment capacity (where a 'plastic hinge' develops), neglecting the need for a number of plastic hinges before the pipe reaches its load capacity and collapses
- its reliance on software provided by third parties that may not necessarily satisfy the AASHTO standards, or investments needed in development of in-house analyses (spreadsheets or other) that may be challenging for DOTs and other stakeholders;
- its treatment of crack width using semi-empirical procedures based on data from three edge bearing tests; crack widths are likely very different when the pipe is buried;
- the limited evaluations performed against measurements of actual pipe behavior (the actual moments that develop, and the actual moment capacities);
- the current equation used to calculate ultimate moment examines only one layer of reinforcement, and relies on other simplifications such as ductile plasticity after yield (it neglects the possible strengthening effects of strain hardening);
- has been subject to very limited field evaluations of expected moment and moment capacity, and may require recalibration when changes are made to procedures for estimating expected moment (such as the recent changes to live load spreading under wheel and axle loads, for pipes with diameter exceeding 24 inches).

3.2.12 Conclusions

It is concluded that work is warranted to investigate factors that have not been assessed by other researchers, or which have not been explained fully:

a. The degree to which the current bedding factors used in Indirect Design reflect actual buried pipe performance (i.e. the level of conservatism of Indirect Design assessments of buried pipe strength)
b. The level of moment that develops in buried concrete pipe tests compared to the moment demands (expected values) estimated during Direct Design (based on two dimensional finite element analysis and the Heger Pressure Distributions), considering

performance of those Direct Design calculations for both shallow buried and deeply buried pipes

c. The failure modes predicted during Direct Design compared to those observed in buried reinforced concrete pipe tests, and the level of conservatism of Direct Design assessments of buried pipe strength
d. The potential benefits of using Modified Compression Field theory to determine the strength limits for reinforced concrete pipe during Direct Design (the moment and shear capacities) instead of the design approximations for flexural and shear strength currently employed; this includes consideration of both layers of reinforcing steel (for structures with more than one) and more sophisticated treatment of shear strength
e. The level of conservatism that results when the effect of strain hardening in reinforcing steel is neglected during Direct Design
f. The manner in which pipe diameter influences each of the aforementioned factors and their influence on the relative performance of Direct and Indirect Design.

The remainder of this report presents the results of the investigation into issues a to f listed above. It starts with details of the buried pipe tests that were performed.

3.3 Laboratory tests on small and medium sized reinforced concrete pipes

3.3.1 Introduction and Objectives

To develop a better understanding of how reinforced concrete pipes respond to both surface and soil loading and the performance of the Indirect Design and Direct Design methods, full-scale buried reinforced concrete pipe tests were performed on specimens with varying (1) inner diameters, (2) reinforcement levels, (3) wall thicknesses, (4) cover depths, and (5) loading regimes. The goals of this work were:

i. To measure how moments develop in shallow buried pipes responding to vehicle loads;
ii. To measure how moments develop in deeply buried pipes for different levels of overburden pressure (equivalent to the effect of earth loads at various burial depths);
iii. To conduct ultimate limit state tests to bring the pipes to their performance limits and to determine their capacities;
iv. To evaluate the effect of pipe diameter on both the moments that develop and the moment capacity;

v. To evaluate the effect of reinforcement level and pipe strength on both the moments that develop and the moment capacity;
vi. To evaluate the effect of wall type on both the moments that develop and the moment capacity;
vii. To obtain data for pipe response in the three edge bearing test to support the Indirect Design calculations.

The measurements are used in Section 3.4 to evaluate the effectiveness of both Indirect Design and Direct Design in capturing these behaviors (involving comparisons between the experiments and the design calculations).

The following sections outline the experimental program, the pipe specimens, the instrumentation, and the test set-up. The results of the testing program are then presented and discussed.

3.3.2 Experimental Program

Test matrix

Table 5 summarizes the complete test matrix. The goals outlined in the previous section were addressed by subdividing the work into four test programs. The first, referred to as Program A, investigated the impact of two different reinforcement levels (i.e. D-load capacities) on the demand and resistance of buried 24 in. diameter pipes. The second, referred to as Program B, examined 48 in. diameter pipes with different wall thicknesses but the same target strength (capacity in a D-load test) to determine how the capacity of the buried pipes were affected. The third, referred to as Program C, investigated the effects of deep burial on 24 in. diameter pipes. The fourth, referred to as Program D, involved performing D-Load tests on the 48 in. diameter pipes to complement measurements of strength in three-edge bearing for the 24 in. pipes obtained from other sources (the manufacturer and as part of an earlier research project at Queen's).

Programs A and B examining pipes under shallow cover were conducted in the West half of the large buried infrastructure test pit at Queen's (as described by Moore, 2012). This permits simulation of vehicle loads using a servo-controlled testing system supported by a reaction frame anchored to the underlying rock, to apply vertical loads onto steel loading pads placed on the ground surface (representing the contact areas associated with standard wheel pairs).

Program C was conducted using the Biaxial test cell, which simulates overburden pressures that result during deep burial (Brachman et al., 2000, 2001). Program D was conducted using the laboratory's servo-controlled testing system to apply three-edge bearing loads onto the pipes. Programs A and B involved examining the pipes at three different burial depths, while Program C simulated a range of burial depths by increasing overburden pressures up to failure.

Table 5. Test matrix

Test program	Facility	Diameter (in.)	Loading type	Depths (ft)	Goals
A	West test pit	24	Earth & simulated vehicle	1, 2, and 4	i, iii, iv, v
B	West test pit	48	Earth & simulated vehicle	1, 2, and 4	i, iii, iv, vi
C	Biaxial cell	24	Earth load (deep burial)	1 to 152[E]	ii, iii
D	Load frame	48	Three edge bearing	Unburied	vii

Note – E: equivalent depth of burial for soil of density 130 pcf.

Instrumentation

All the test pipes had similar instrumentation to measure the strains, deflections, and longitudinal crack development within the pipe during loading. The following sections describe the use of strain gages and Particle Image Velocimetry. Diameter change measurement using linear potentiometers and string potentiometers is described subsequently.

Strain Gages

Concrete surface strain gages manufactured by Vishay Micro-Measurements Co. were used to measure the circumferential strain around the pipe. To ensure that the strains being measured represented average strains rather than localized strains across an individual piece of aggregate, the size of the strain gage was specifically chosen to be at least three times larger than the largest aggregate size. The gages used were 2-inches in length with a resistance of 120 Ω ($\pm 0.2\%$). Each pipe had 8 strain gages to measure circumferential strain around a cross-section of the pipe. Strain gages were located at the crown, invert, and springlines on both the inner and outer surfaces of the pipe to capture the extreme fiber strains.

It is explained in a subsequent subsection how these measurements of surface strain were used to calculate the curvatures and average strains that developed in the reinforced concrete pipe

wall during the pseudo-elastic (i.e. pre-cracking) phase of the concrete pipe response (curvatures are subsequently used in Section 3.4 to estimate the experimental moments at crown, springlines and invert, for comparison to the elastic moment estimates obtained during Direct Design).

Strain measurement on the surface of reinforced concrete pipes has been used successfully in other projects to determine strain, thrust and moment (e.g. Moore et al., 2012). However, another approach is to measure strains directly on the steel reinforcing bars (e.g. Sargand et al., 1995). That involves placing gages on the reinforcing steel prior to pipe manufacture, and so prevents the use of pipes obtained directly from manufacturers, and raises questions regarding whether the bond between the steel and concrete is degraded or enhanced. Strain gages placed on the steel reinforcement do provide measurements beyond the point where the concrete on the tensile face cracks (when surface gages generally cease to function), but it is difficult or impossible to obtain reliable estimates of curvature from these strains, since non-uniform strain distributions then develop along the reinforcing steel which depend on the somewhat random location of the cracks in the concrete and local stress transfer to or away from the rebar. This means that neither surface gages nor those placed on the reinforcement can be used to provide reliable estimates of curvature after cracking, and surface gages were used since these avoid the other issues mentioned earlier.

Particle Image Velocimetry

Digital cameras were used with a remote camera operation program (*DSLR Remote Pro*) from Breeze Systems to take digital images of the crown and invert at five to ten second intervals throughout the loading of the pipes. The images were processed using Particle Image Velocimetry (PIV) to track the movement of subsets and from these movements the width of longitudinal cracks could be determined. A texture was applied to the surface of the concrete using spray paint to create a difference in color for the program to detect (White and Take, 2002). A linear potentiometer was installed below the support of the camera to detect any out of plane movements of the camera. This movement was then factored into the analysis. Crack width interpretation using PIV is explained in further detail in Appendix C.

Test Program A

Test Specimens

To investigate the effect of different reinforcement levels, two 24-inch diameter pipes were used in Test Program A: a 24-inch, Wall C, Class IV-equivalent pipe and a 24-inch, Wall C, Class V-equivalent pipe. All the pipes used in the testing program were manufactured in accordance with ASTM C655M so references to pipe strength classes throughout this report represent equivalent classes (i.e. they do not have the steel reinforcing specified in ASTM C76, but provide minimum D-loads the same as those for C76 pipes). Both the Class IV and Class V-equivalent pipes had an internal diameter of 24-inches with a wall thickness of 3.75-inches and a length of 8ft, including the bell but excluding the spigot. The pipes were manufactured by M-CON Products Ltd. of Ottawa, Ontario. The Class IV pipe was circumferentially reinforced with a single layer of reinforcement centered in the pipe wall with a wire gage of W2.5 (0.025 in^2) at 3-inch spacing. This pipe had a concrete strength (f'_c) of 10200psi and the reinforcement steel had yield strength (f_y) of 86300 psi and an ultimate strength of 90600 psi. The Class V pipe was circumferentially reinforced with a single layer of reinforcement centered in the pipe wall with a wire gage of D4 (0.04 in^2) at 2.7-inch spacing. This pipe had a concrete strength (f'_c) of 9600 psi and the reinforcement steel had a yield strength (f_y) of 84800 psi and a ultimate strength of 86600 psi. A summary of all test pipe specimen material properties is given in Table 6.

Arrangement in the Test Pit

Test Program A was conducted using an embankment installation within a 25-foot by 25-foot by 10-foot deep test pit, Figure 4 (the West pit at Queen's, Moore, 2012). The pipes were oriented north to south with the Class IV-equivalent pipe in the north position and the Class V-equivalent pipe in the south position. To prevent interaction with the rigid boundary condition represented by the concrete floor of the test pit, soil bedding that was 36 inches deep was prepared, with an additional four inches of loose bedding to help prevent voids at the haunches. The pipe was then buried in six to twelve inch lifts to a maximum cover depth of four feet (details of the backfill soil and its compaction are described in a subsequent section).

Table 6. Description of Pipes Specimens

Pipe Inner Diameter	Wall Type	Wall Thickness	Class Equivalent	f'_c	f_y	f_u	Wire Gage	Spacing	in^2/ft

in		in		ksi			in^2	in	Inside	Outside
24	C	3.75	IV	10.1	86.3	90.6	0.025	3.0	0.100	n/a
24	C	3.75	V	9.6	84.8	86.6	0.04	2.7	0.179	n/a
48	B	5	III	8.4	70.3	79.8	0.04	2.0	0.239	0.239
48	C	5.75	III	8.4	70.3	79.8	0.04	2.7	0.179	0.179

a. Pipes placed before burial; b. Ultimate wheel pair load test

Figure 4. Testing of the 24 in. test pipes in the West test pit at the GeoEngineering Laboratory.

Instrumentation Layout

Before burial, each of the 24-inch pipes was instrumented with eight strain gages, four around the outside circumference and four around the inside circumference, at the crown invert and springlines. The strain gages were located at the cross section of the pipe located directly beneath the steel loading pad (simulating a wheel pair).

Four linear potentiometers (LPs) were installed in the 24-inch pipes to measure changes in horizontal and vertical diameter (conventionally called 'pipe deflections') at two locations in the pipe. One pair of LPs was installed within 1-inch of the strain gages, under the wheel pad, and 37 inches from the joint connecting the North and South test pipes. The other pair of LPs was located equidistant (37 inches) from the other end of the pipe (the North end of the North pipe or the South end of the South pipe). In the Class IV pipe the pair of LPs under the wheel pad was identified as LP1 and the pair opposite was identified as LP2. In the Class V pipe the pair of LPs under the wheel pad was identified as LP2 and the pair opposite was identified as LP1. Linear potentiometer measurements are accurate to 0.006 inches.

Two cameras were mounted in each pipe to monitor longitudinal crack development at the crown and invert. The cameras were mounted near the wheel pad loading point, one camera facing the crown and one camera facing the invert. A photo of the mounting system is shown in Figure 5. The cameras were operated remotely using the DSLR Remote Pro Multi-Camera software which permits pairs of photos to be taken simultaneously at five to ten second intervals throughout the test.

Figure 5. SLR Camera mounting system to monitor crack widths during loading

Burial Conditions

A Topcon RL-H3C self-levelling laser level was used to ensure that lifts were consistent and did not exceed 12 inches. A CPN MC-1DR-P Portaprobe nuclear densometer (ASTM D6938-08a) was used to gather density, percent water content, and percent standard Proctor maximum dry density (SPMDD) readings within each lift to ensure that the entire burial was consistent and achieved minimum required soil density. Table 7 presents details of the level of compaction achieved. Lougheed (2008) and Lay (2012) report that for this test soil, dry density measured with the nuclear densometer ranged from 14% lower to 8% higher than density obtained using the sand cone method (ASTM D1556-07), with mean dry density about 6% lower.

The pipes for Program A were installed using sandy gravel denoted GP-SP in the Unified Classification System and A-1-a material by AASHTO, in accordance with Type 2 burial conditions as per AASHTO (2009) to a minimum of 90 percent standard Proctor (i.e. 90% of the maximum dry unit weight achieved for this soil using a standard Proctor test). The soil was compacted in approximately 8-inch lifts using both small and large vibrating plate compacters to

achieve the required soil conditions. The average soil properties for the pipe burial are described in the following table.

Table 7. Average Soil Compaction Properties for 24-inch Pipe Burial

	24-inch Class IV Pipe Burial			24-inch Class V Pipe Burial		
	Dry Density (pcf)	Water Content (%)	Standard Proctor (%)	Dry Density (pcf)	Water Content (%)	Standard Proctor (%)
Bedding	130	3.2	91	129	2.9	91
Sidefill	128	3.0	90	128	3.2	90
Cover	129	4.1	91	130	4.2	92

Loading Regime

The pipes in test Program A were tested in eight stages involving cover depths of four feet, two feet, and then one foot, and tested as summarized in the top eight loading stages listed in Table 8. The wheel pair configuration associated with the AASHTO design truck was applied at the ground surface above the buried pipes using a steel axle frame with steel wheel pads loaded by a 200-tonne (450 kips) hydraulic actuator. The actuator is supported over the test pit by a reaction frame anchored into the underlying rock, and was aligned to apply a vertical load above the centerline of the pipe. The steel wheel pads were 10-inches by 20-inches as specified by AASHTO (2012) and were loaded by a steel axle frame that separated the wheel pads by 6ft (again, in accordance with the standard). The axle frame transferred the load to the wheel pads through spherical bearings to ensure there was negligible moment transfer. The axle frame was aligned over the longitudinal axis of the pipe to simulate a truck travelling perpendicular across the pipe's longitudinal axis. To limit bearing failure of the soil under the loading pads during the ultimate limit states test (test stages 4 and 8 presented in Table 8), enlarged wooden bearing pads of length 37.4 in. and width 14.6 in. were placed below the steel pads to better distribute the load. At each load stage, for four, two and one-foot cover, the loads were cycled three times to ensure the soil beneath the load pads was compacted and that the results were obtained for first loading (where permanent as well as recoverable deformations can be expected), and second and third load cycles where recoverable (elastic) deformations dominated.

Test Program B

Test Specimens

To investigate the performance of larger diameter pipes, as well as the effects of different wall thicknesses, two 48-inch diameter pipes were used in Test Program B: a 48-inch, Wall B, Class III-equivalent pipe and a 48-inch, Wall C, Class III-equivalent pipe. The Wall B pipe had a wall thickness of 5-inches and the Wall C pipe had a wall thickness of 5.75-inches. Both pipes had an internal diameter of 48-inches with a length of 8ft, including the bell but excluding the spigot. The pipes were manufactured by Hanson Pipe and Precast of Cambridge Ontario. The Wall B pipe was circumferentially reinforced with a double layer of reinforcement with an average cover of 1-inch and a wire gage of D4 ($0.04in^2$) at 2-inch spacing. This pipe had a concrete strength (f'_c) of 84800psi and the reinforcement steel had yield strength (f_y) of 70300psi and an ultimate strength of 79800psi. The Wall C pipe was circumferentially reinforced with a double layer of reinforcement with an average cover of 1-inch and a wire gage of D4 ($0.04in^2$) at 2.7-inch spacing. This pipe had a concrete strength (f'_c) of 84800psi and the reinforcement steel had yield strength (f_y) of 70300psi and an ultimate strength of 79800psi. Table 6 summarizes the material properties of these test pipes.

Arrangement in the Test Pit

Test Program B was conducted using a similar embankment installation to Test Program A within the same 25-foot by 25-foot by 10-foot deep test pit. The 48 in. (1.2m) diameter pipes were oriented east to west with the Wall C pipe in the east position and the Wall B in the west position. A compacted soil foundation of 25 inches was prepared on top of the rigid concrete floor with an additional three inches of loose bedding. Figures 6 and 7 illustrate pipe location and surface loading.

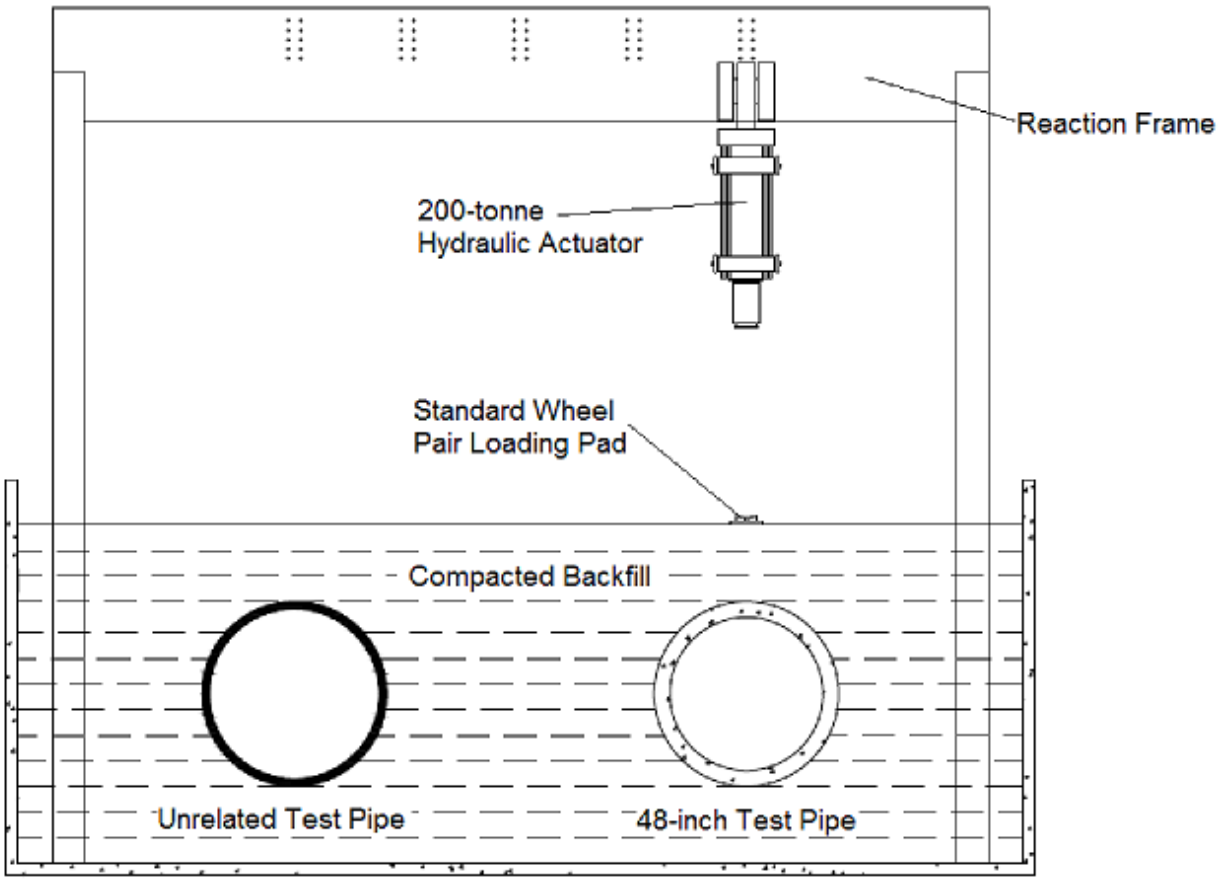

Figure 6. Testing of the 48 in. test pipe in the West test pit at the GeoEngineering Laboratory.

Figure 7. Service load testing under the standard AASHTO wheel pair over the 48 in. test pipes in the West test pit at the GeoEngineering Laboratory.

Table 8. Stages of the Buried Pipe Tests

Test Program	Test stage	Pipe Inner Diameter (in)	Wall Type	Class Equivalent	Burial Depth (ft)	Load Type	Max. Applied load (kips)	Type
A	1	24	C	IV	4	SLS	25	Wheel
	2	24	C	IV	2	SLS	24	Wheel
	3	24	C	IV	1	SLS	25	Wheel
	4	24	C	IV	1	Max	101	Wheel
	5	24	C	V	4	SLS	25	Wheel
	6	24	C	V	2	SLS	24	Wheel
	7	24	C	V	1	SLS	25	Wheel
	8	24	C	V	1	Max	101	Wheel
B	9	48	B	III	4	SLS	25	Wheel
	10	48	B	III	2	SLS	24	Wheel
	11	48	B	III	1	SLS	25	Wheel
	12	48	B	III	1	Max	135	Wheel
	13	48	C	III	4	SLS	25	Wheel
	14	48	C	III	2	SLS	24	Wheel
	15	48	C	III	1	SLS	25	Wheel
	16	48	C	III	1	Max	146	Wheel
C	17	24	C	V	120[C]	Max	102 (psi)	Surface Pressure

Notes

SLS: service load test

Max: test to an ultimate limit state of the pipe or the soil under the surface load pads

C: Burial depth equivalent to maximum overburden pressure assuming soil density of 130 pcf.

Instrumentation Layout

Each of the 48-inch pipes was fitted with eight strain gages, four around the outside circumference and four around the inside circumference, at the crown, invert, and springlines.

The strain gages were located at the cross section of the pipe located directly beneath the wheel loading pad.

Four string potentiometers were installed in the 48-inch pipes to measure changes in horizontal and vertical diameter at two locations in the pipe. One pair of string potentiometers was installed within 1-inch of the strain gages while the other pair was located at the other end of the pipe, the same distance from the end of the pipe as the first pair of LPs. In the Wall B pipe the pair of LPs under the wheel pad was identified as SP2 and the pair opposite was identified as SP1. In the Wall C pipe the pair of LPs under the wheel pad was identified as SP1 and the pair opposite was identified as SP2. Strings potentiometers are accurate to 0.0005 inches.

Two cameras were mounted in each pipe to monitor longitudinal crack development at the crown and invert in the same configuration as in the 24-inch pipes.

Burial Conditions

The burial process for the 48 in. pipes was identical to that used for the smaller diameter specimens. The soil properties for the 48-inch pipe burial are shown in Table 9.

Table 9. Average Soil Compaction Properties for 48-inch Pipe Burial

	48-inch Wall B Pipe Burial			48-inch Wall C Pipe Burial		
	Dry Density (pcf)	Water Content (%)	Standard Proctor (%)	Dry Density (pcf)	Water Content (%)	Standard Proctor (%)
Bedding	133	2.7	93	133	2.4	93
Sidefill	131	3.9	90	129	3.9	90
Cover	124	3.7	87	131	3.8	92

Loading Regime

The test Program B pipes were buried with cover depths of four feet, two feet, and then one foot and tested in accordance with testing stages 9 to 16 shown in Table 8. The same AASHTO design truck load geometries were employed at the ground surface above the buried pipes using the steel axle frame with steel wheel pads loaded by the hydraulic actuator. Bearing failure under the loading pads was again delayed during the Ultimate Limit States tests by using wooden wheel pads under the steel pads, during loading stages 12 and 16 in Table 8. At each

loading stage, the loads were again cycled three times to gather information during the initial load cycle and two subsequent 'elastic' load cycles.

Test Program C

Test Specimens

To investigate the behavior of pipes under deep burial and create a comparison to shallow burial pipe, a 24-inch, Wall C, Class V-equivalent pipe was loaded under simulated deep burial. The pipe had an internal diameter of 24-inches with a wall thickness of 3.75-inches and a length of 8ft, including the bell but excluding the spigot. The pipe was manufactured by M-CON. This pipe was circumferentially reinforced with a single layer of reinforcement centered in the pipe wall with a wire gage of D4 (0.04 in^2) at 2.7-inch spacing. This pipe had a concrete strength (f'_c) of 9600 psi and the reinforcement steel and a yield strength (f_y) of 84800 psi and a ultimate strength of 86600 psi. The pipe specimen material properties are summarized in Table 6.

Biaxial Test Cell

Test Program C was conducted in the biaxial test cell. This is a 6.6-foot by 6.6-foot by 5.2-foot deep steel box with a rubber bladder under the lid that was used to apply a uniform pressure on the ground surface over the 24-inch pipe to simulate deep burial. The pipe was horizontally centered in the cell, with 24 inches between the wall of the pipe specimen and the edge of the cell on each side, and 8 inches of soil under the pipe invert. A double layered friction treatment was applied to each wall of the cell to reduce the effects of friction between the soil in the cell and the cell wall. A single layer of polyethylene sheeting was attached to the four vertical walls of the biaxial cell, lubricated with specially selected silicon grease, and then covered in a second sheet of polyethylene without securing it to the cell walls in any other way. This creates a boundary with very low friction values to reduce vertical load transfer through shear to the side boundaries. In addition, lines were marked on both layers of friction treatment to assess the movement between the two sheets after testing. Further description of the friction treatment within the biaxial cell is provided by Tognon et al. (1999). Two settlement plates were placed below and on either side of the pipe within the first soil lift, to monitor settlement and therefore vertical strain in two short columns of test soil near the base of the test system. These measurements can be used subsequently to estimate the modulus of the test soil.

a. Pipe segment being lowered into the biaxial cell.

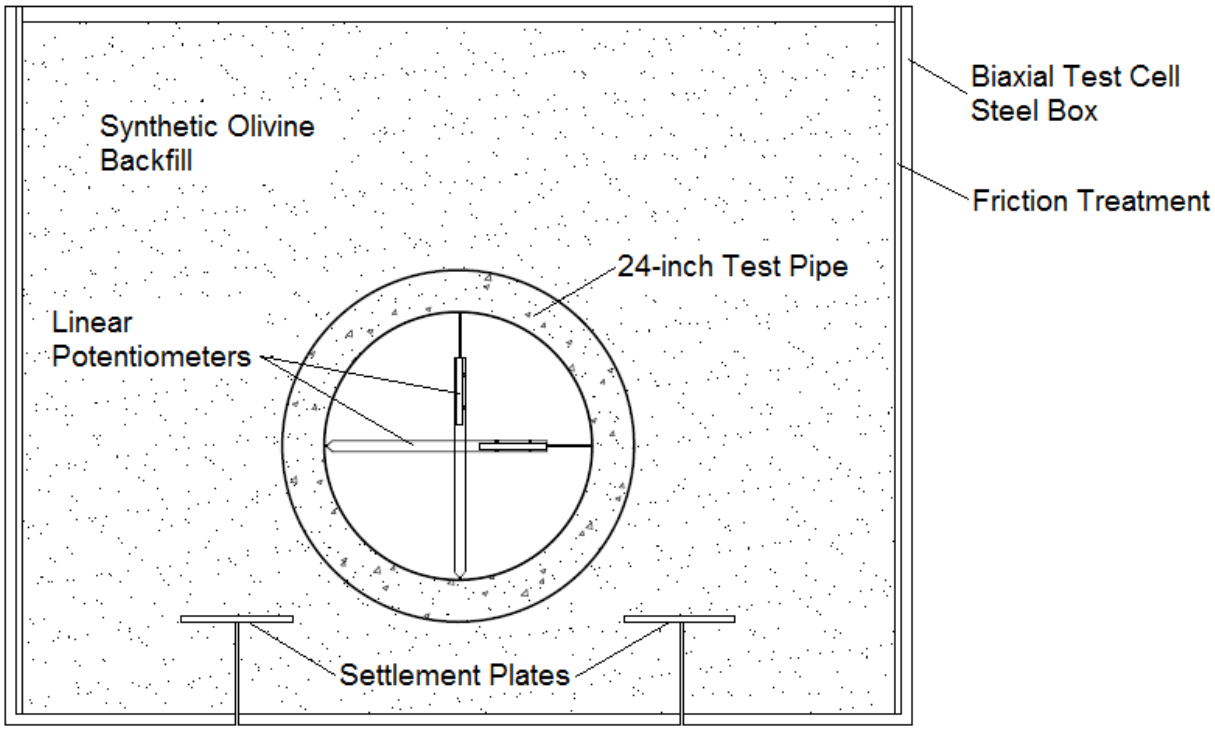

b. Vertical section showing pipe location, linear potentiometers, and settlement plates

Figure 8. Configuration of the deeply buried pipe test.

Instrumentation Layout

The 24-inch pipe was outfitted with eight strain gages, four around the outside circumference and four around the inside circumference, at the crown, invert, and springlines. The strain gages were located at the center cross section of the pipe. Two linear potentiometers were installed within 1-inch of the strain gages to measure changes in horizontal and vertical pipe diameter at the center of the pipe. SLR cameras were installed to monitor crack development at the crown and invert. Two settlement plates buried within the first lift of the soil had shafts extending through the base of the biaxial cell and attached to two linear potentiometers. These linear potentiometers can be used to estimate vertical strains and therefore the modulus of the soil.

Burial Conditions

A Topcon RL-H3C self-levelling laser level was used to ensure that lifts were consistent and did not exceed 12 inches. A CPN MC-1DR-P Portaprobe nuclear densometer was used to gather density, percent water content, and percent standard Proctor maximum dry density (SPMDD) readings within each lift to ensure that the entire burial was consistent and achieved minimum required percent standard Proctor density. The pipe was then buried in 4 to 10-inch lifts. The pipe in Test Program C was buried in the biaxial cell within synthetic olivine sand (a material classified as SP by the unified classification system). Compaction details are shown in Table 10.

Table 10. Average Compaction Properties for 24-inch Deep Burial in Synthetic Olivine Sand

	24-inch Class V Pipe Burial		
	Dry Density (pcf)	Water Content (%)	Standard Proctor (%)
Bedding	101	0.5	71

Loading Regime

Test Program C was conducted within the biaxial cell using compressed air applied on the top of the rubber bladder placed on the soil surface over the pipe (the bladder is very compliant and remains in full contact with the soil surface). The pressure in the cell was steadily increased at a rate of approximately 5.1psi/min (7.6ft cover/min). The test was run to a maximum pressure of 102 psi, approximately equivalent to a burial depth of 145 ft in the synthetic olivine backfill, or 113 ft of material with density of 130 pcf.

Test Program D

Pipe samples were tested in three edge bearing to determine D-Load, so comparisons can be made between the response when buried and under three-edge bearing. Manufacturer data showed that the 48-inch pipes were loaded until the required service limit, however the samples showed no signs of cracking. To be able to compare 0.01-inch crack loads between three-edge bearing loading and cracking performance when buried, the 48-inch pipes were tested in three edge bearing until they reached the maximum allowable crack width (0.01 in.). The 24-inch Class IV pipe was provided with D-Load data by the manufacturer up to the 0.01-inch crack width. The D-Load data for the 24-inch Class V pipe was determined from previous testing performed on another sample of the same pipe (manufactured at the same time and place as the test pipe).

Instrumentation Layout

Two LPs were placed at the center of the pipe, one to measure change in vertical diameter and the other to measure change in horizontal diameter. Two SLR cameras were set up to record the development of cracks at the crown and invert during the experiment. The load cell attached to the actuator recorded the amount of load being applied to the pipe.

Loading Regime

Following the ASTM C497-13 standard, the pipes were supported by two strips of wood which were mounted on a steel I-beam. A flat piece of wood approximately ½-inch thick and a steel I-beam were placed on top of the pipe to apply a line-load along the top of the pipe. The top I-beam was loaded by the 200-tonne (450 kip) actuator.

3.3.3 Results and Discussion

Calculation of moment and thrust

To assess the impact of cover depth on the buried pipes, the strain readings were used to calculate the curvature and average strain in the pipes to investigate how each pipe behaved under loading. Using PIV technology, the development of cracks was monitored during loading to monitor the occurrence of the critical crack of width 0.01-inches. The curvature of the pipe wall was found using the strain readings and the wall thickness employing Equation 15.

$$\varphi = \frac{\varepsilon_{inside} - \varepsilon_{outside}}{Wall\ Thickness} \quad (15)$$

The average strain in the pipe wall was found using the strain readings and Equation 16.

$$\varepsilon_{average} = \frac{\varepsilon_{inside} + \varepsilon_{outside}}{2} \quad (16)$$

Test Program A

The purpose of this test program is to investigate the effects of live loading at shallow cover on the service load response and the capacity of the 24 in. diameter pipes. For service load testing at a burial depth of four, two and one foot, the pipes remained within the elastic limit. The results of the moments calculated from those curvatures are presented in Section 3.4 where they are compared to elastic design calculations.

Testing at one foot burial was undertaken to higher load levels, and established the capacity of the pipe. The results for that Ultimate Limit States (ULS) test are presented in detail in the following subsections.

Diameter Change

Both the Class IV and Class V pipe experienced minimal vertical diameter changes under maximum loading at one foot burial depth as presented in Figure 8. The Class IV pipe underwent 0.043-inches of vertical diameter decrease nearest the ‘wheel pair’ loading pad (LP1) and 0.031-inches at the position further from the loading pad (LP2). The Class V pipe experienced 0.064-inches of vertical diameter decrease nearest the ‘wheel pair’ loading pad (LP1) and 0.027-inches at the location further from the loading pad (LP2).

Up to the service loads, the pipe behavior is linear and experiences only very small change in diameter. After cracking occurs at approximately 60 kips, the change in diameter begins to increase more significantly and becomes distinctly nonlinear. Before cracking occurs, the vertical diameter decrease in both pipes is almost the same. However, immediately after cracking the Class IV pipe experiences greater vertical diameter changes than the Class V pipe. This is as expected since the Class V pipe has a greater area of steel to resist the bending moments.

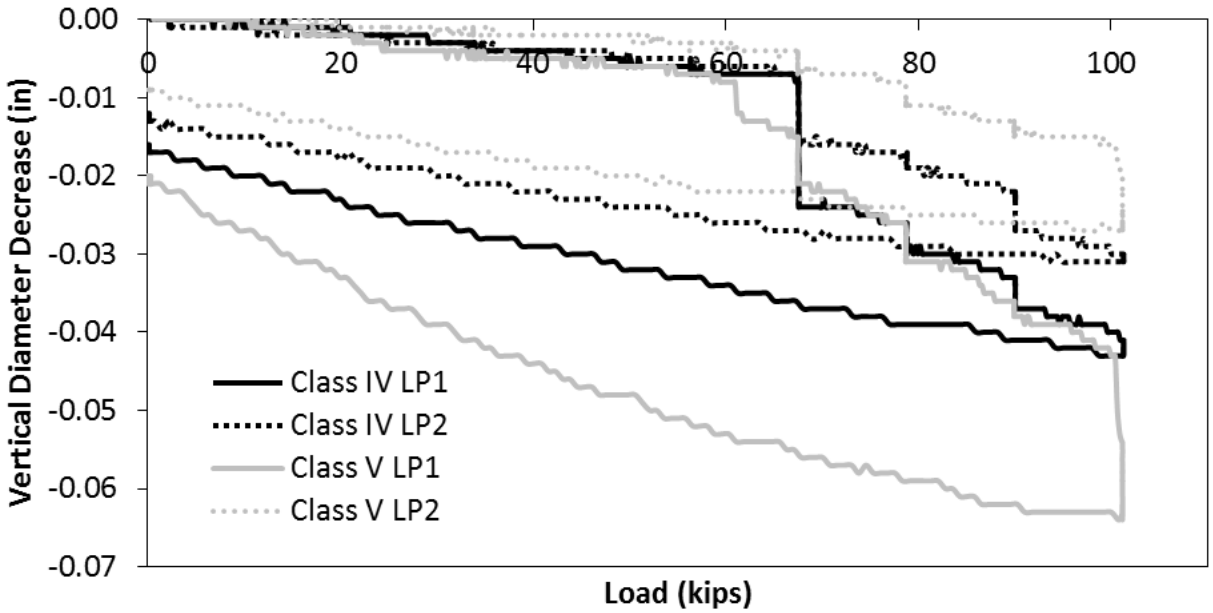

Figure 8: Vertical diameter decrease of Class IV and Class V pipes during the Ultimate Limit State test

Strain Behavior

The concrete strain gages present the strain behavior of the pipe up until the pipe begins to crack. After cracking, the strain gages can no longer be relied on to provide accurate results since cracking interferes with the strain measurements on the tensile side of the pipe wall, and the stiffness of the wall is no longer uniform through its cross section. As can be seen in Figure 9 (where curvature changes calculated using strains are presented), cracking is associated with discontinuities in the curves. Some strain gages continued to provide data after cracking though this data is only included to highlight the non-linear behavior of the pipe after cracking (the values of strain are unreliable). The strain gage located at the outside crown of the Class IV pipe was damaged early in the maximum load test and therefore curvature in the pipe at the crown is only shown up to 34 kips.

Figure 9 shows that curvature changes in both the Class IV and Class V pipe developed almost linearly with load, and were nearly equal to one another before cracking occurred. Additionally, the curvature changes at the crowns of both pipes are greater than those at the inverts. These results are as expected; at shallow burial the crown would develop the greatest curvature due to the closer proximity to the surface load being applied (three dimensional load spreading

produces greater load attenuation at the inverts). The curvature changes are almost the same for the two pipes before cracking since both pipes have the same outer diameter so should attract the same moments in the elastic range. Given that they have the same wall thickness and their flexural rigidities (EI values) are largely dependent on the concrete, their elastic stiffnesses should be almost identical (concrete strengths f'_c for the two pipes are 6% different), and therefore lead to almost the same curvatures.

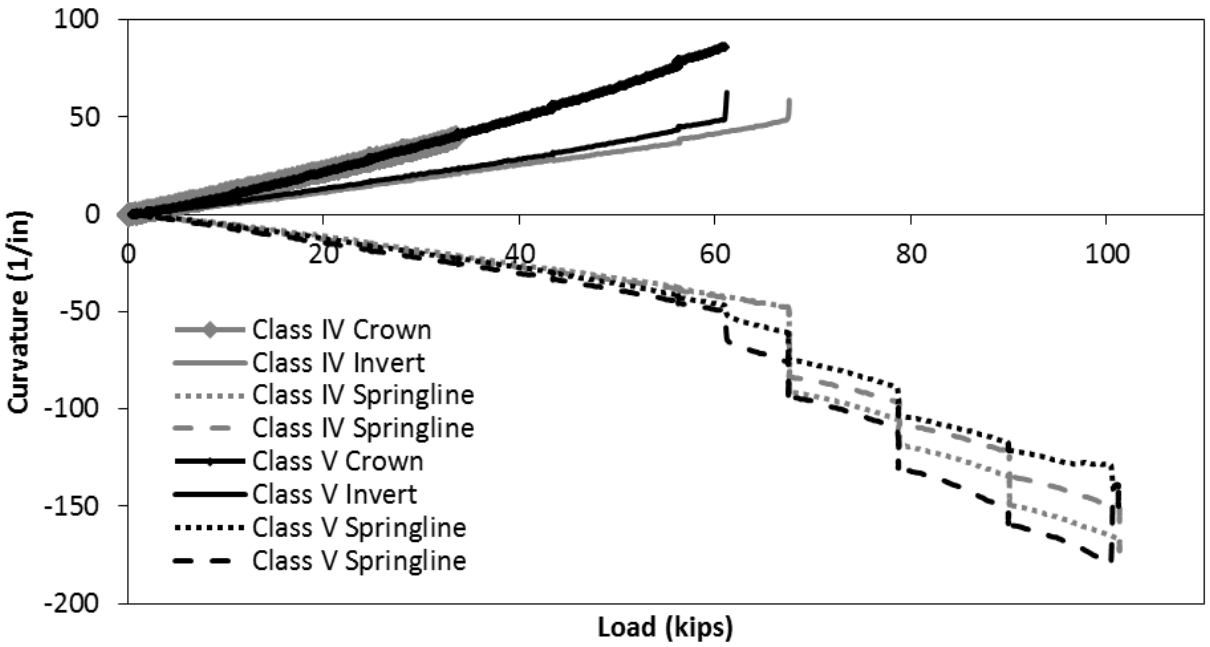

Figure 9. Curvature changes in the 24-inch diameter pipe during the Ultimate Limit States test

Figure 10 shows the average strain in both pipes developed linearly with load and were almost the same prior to cracking. Again, these results are as expected; the outside diameters are identical, so thrusts should be the same, and average strains would therefore be almost identical.

Crack Widths

Figure 11 shows crack widths monitored during the ultimate limit states tests on the 24 in. diameter pipes. The first sign of visible cracking occurred in the Class V pipe at the crown at approximately 56 kips and was shortly after followed by cracking at the invert at approximately 67 kips. The first sign of visible cracking in the Class IV pipe occurred at the crown at approximately 67 kips and was later followed by cracking at the invert at approximately 90 kips.

In both cases, cracking first occurred at the crown followed by cracking at the invert. This is as expected due to the greater load attenuation at the invert.

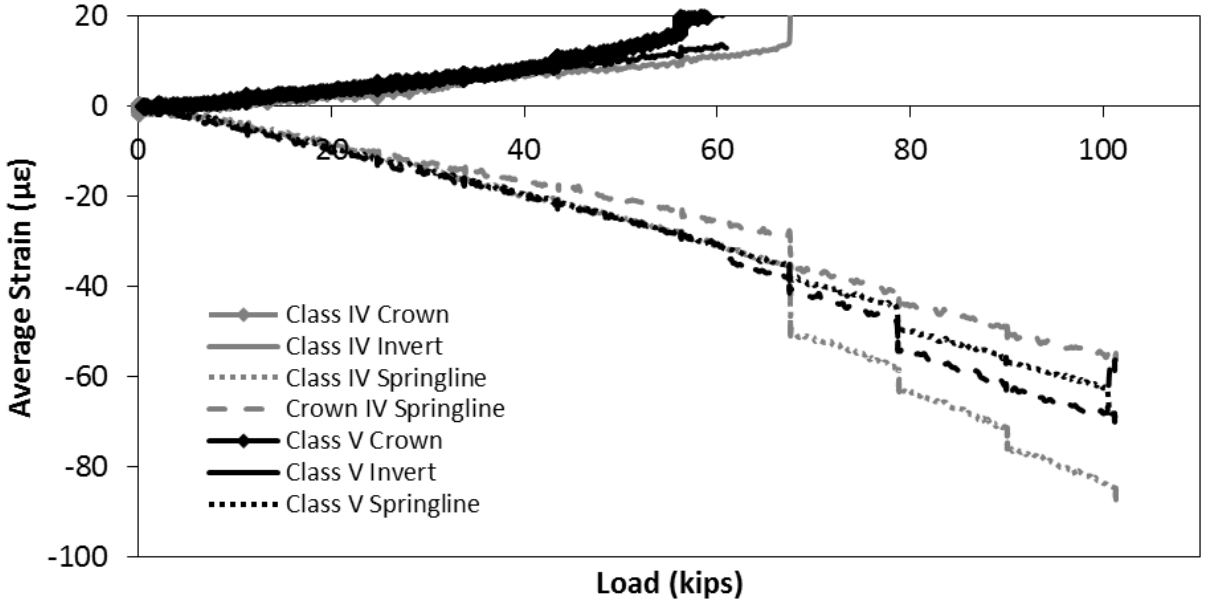

Figure 10. Average strain increase with load for the 24-inch Diameter Classes IV and V pipes during the ultimate limit state tests

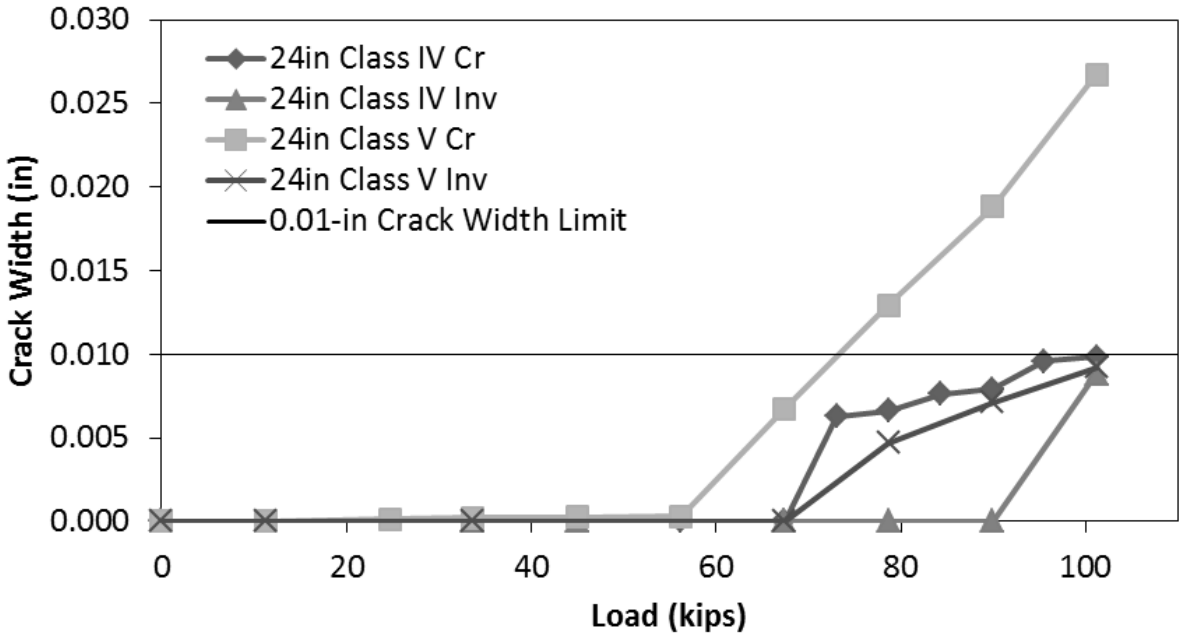

Figure 11. Crack width development in 24-in diameter pipes during the ultimate limit state test

Performance of Class IV and Class V Pipe

As mentioned previously, pipes are designed to resist both a serviceability limit state and an ultimate limit state. The serviceability of the pipe is governed by a maximum crack width of 0.01-inches following development of the tensile cracking strain. The ultimate limit state of the pipe is defined by the development of ultimate moment capacity at one location around the pipe circumference.

The 0.01 in. design crack in the Class V-equivalent pipe developed at a surface load of 73 kips. This crack width required a surface load of 101 kips for the pipe equivalent to Class IV, though crack width reached 0.007 in. in the Class IV-equivalent pipe at 71 kips and crack growth slowed dramatically beyond this load. Likely these variations are evidence of the inherent variability of cracking behavior for brittle, non-homogenous materials like concrete.

According to the AASHTO LRFD loading conditions, pipes buried at 1-foot should be able to resist a live wheel-pair load of 16 kips, factored by an impact factor of 1.289 and a multiple presence factor of 1.2, resulting in a service load of 25 kips, and further factored by a live load factor of 1.75, resulting in an ultimate load of 43 kips. No visible crack developed at any locations until after both the service live load requirement and ultimate live load requirement, as defined by AASHTO (2013) had been exceeded. The buried test pipes did not reach their service live load limit requirements until loads 4.0 and 3.0 times greater than the calculated 0.01-inch crack load limit of the pipe, for the pipes equivalent to Class IV and V, respectively.

Test Program B

Introduction

The 48 in. diameter pipes loaded under four foot, two foot, and one foot burial at service loads remained within the elastic zone and experienced no significant deflections or cracking. The moments that developed during these service load tests are examined in Section 3.4 and only the ultimate limit state test results are presented in the following section.

Diameter Change

Both the Wall B and Wall C pipes underwent minimal vertical diameter decrease under maximum loading at one foot burial depth as can be seen in Figure 12. The Wall B pipe

underwent 0.250-inches of vertical diameter decrease nearest the wheel loading pad (SP2) and 0.136-inches of vertical diameter decrease at the position further from the 'wheel pair' loading pad (SP1). The Wall C pipe underwent 0.140-inches of vertical diameter decrease nearest the loading pad (SP1) and diameter decrease of 0.097-inches at the position further from the loading pad (SP2). The pipe behavior was linear and stiff (with small changes in diameter recorded) until between 25 to 30 kips where the rate of diameter change increased and became nonlinear.

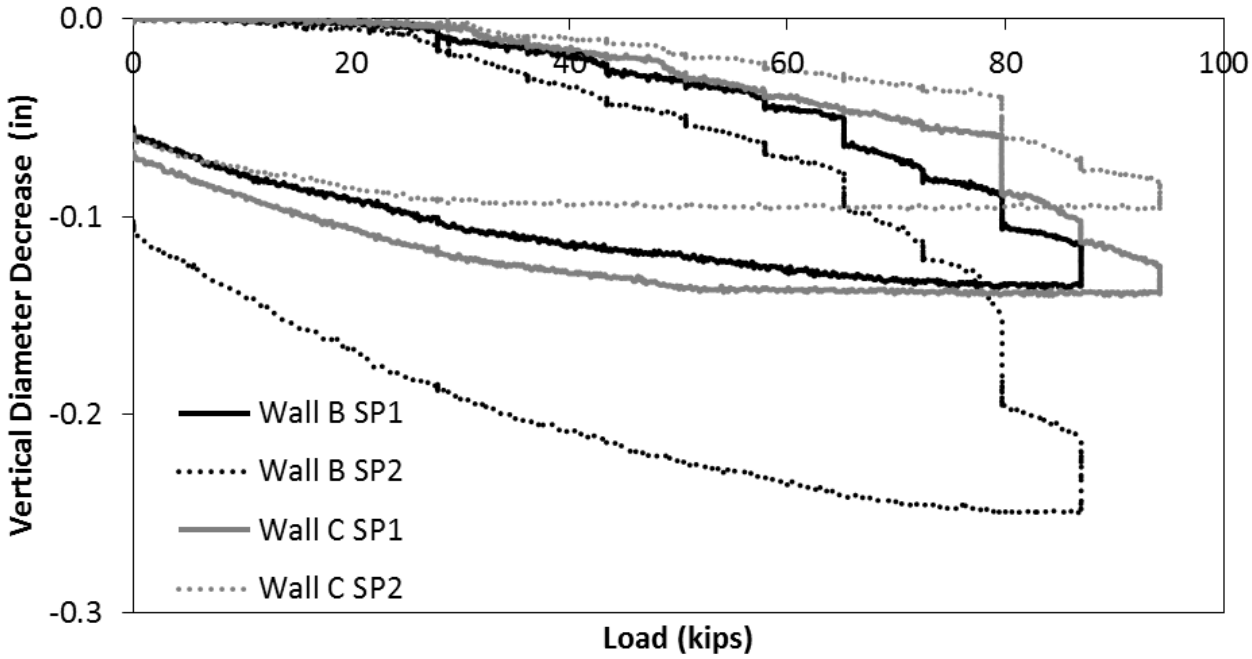

Figure 12. Vertical diameter decreases for wall B and wall C pipes during the ultimate limit states tests.

Strain Behavior

As mentioned previously, concrete strain gages present the strain behavior of the pipe only up until the pipe begins to crack. The Wall B pipe has a smaller wall thickness than the Wall C pipe, but has more reinforcement. Both wall types are designed to have similar flexural capacity and it is interesting therefore to determine whether they develop similar curvatures and crack widths. In both pipes, the curvature at the crown exceeds the curvature at the invert which is to be expected due to the proximity of the applied load, as can be seen in Figure 13. The curvature developed linearly until cracking occurred between approximately 30 and 50 kips. The curvature

for the Wall B pipe exceeds that of the Wall C pipe for each measured location of the pipe. This is also expected since the lower flexural rigidity of the thinner pipe will lead to greater curvatures when the moments are the same.

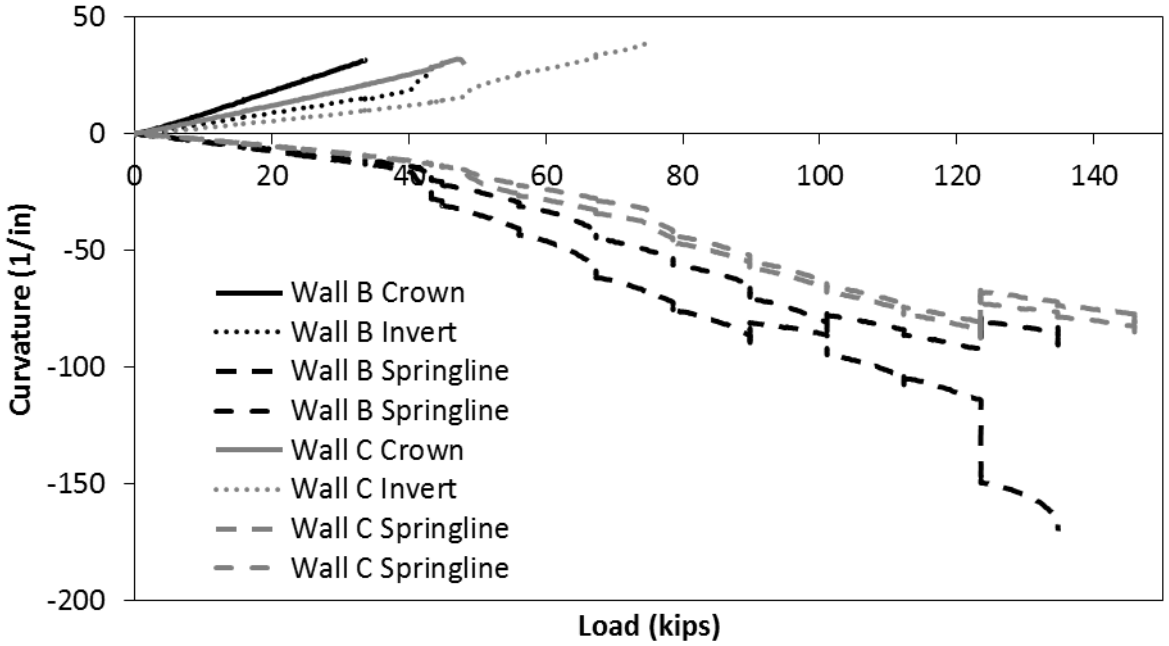

Figure 13. Comparison of changes in curvature in the 48-in wall B and wall C pipes during the ultimate limit states test.

The average strains for the Wall B and Wall C pipes are presented in Figure 14. These average strains developed linearly with load before cracking occurred, with the Wall B pipe developing higher strain than the Wall C Pipe as might be expected (given the smaller wall thickness). Wall C developed, on average, only 37% of the average strain of Wall B at the crown. Though thrust should be slightly different (since outside diameters are not quite the same), if the thrusts and concrete moduli for the two pipes were equal, then average strain at the springline of the Wall C pipe should be 5/5.75 times (i.e. 87% of) that in the Wall B pipe. However, the Wall C pipe developed, on average, only 77% of the strain observed in the Wall B pipe.

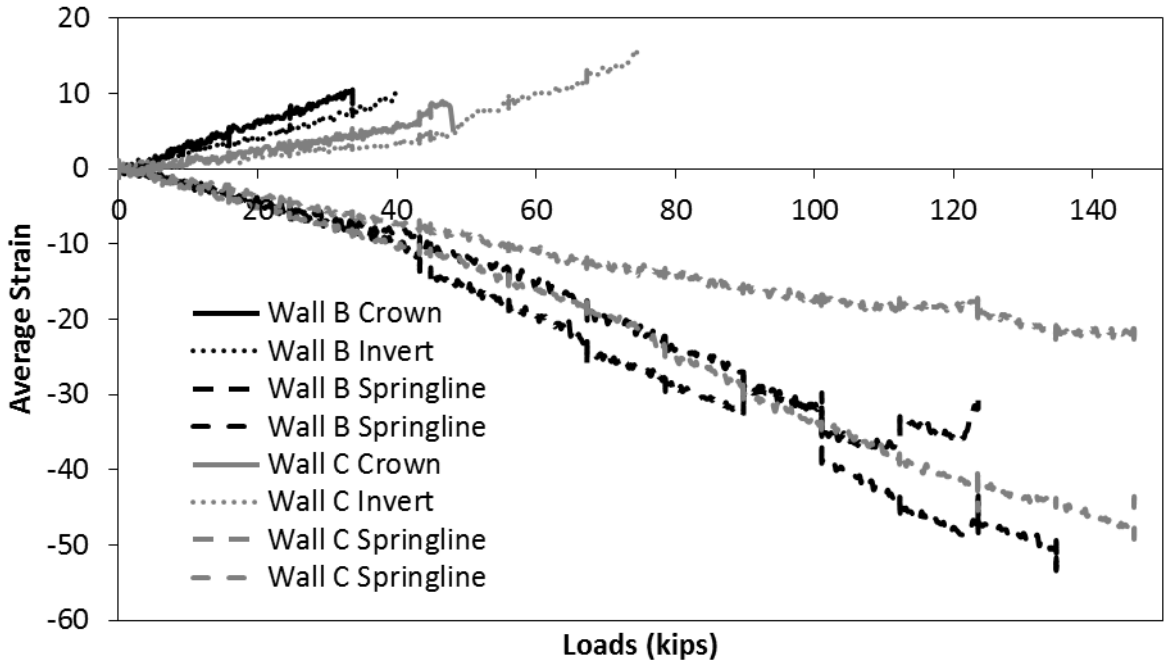

Figure 14. Comparison of average strain in the 48-in wall B and wall C pipes during the ultimate limit states test

Crack Width

Crack widths monitored during the ultimate limit states tests are presented in Figure 15. The first sign of visible cracking occurred in the Wall B pipe at the crown at approximately 25 kips and was followed by cracking at the invert at approximately 45 kips. The first sign of visible cracking in the Wall C pipe occurred at the crown at approximately 45 kips and was later followed by cracking at the invert at approximately 67 kips. In both cases, cracking first occurred at the crown followed by cracking at the invert. This is as expected due to higher dimensional load attenuation (spreading) at the invert. Cracking developed first in the Wall B pipe as expected due to the lower thickness (strain associated with elastic bending in a flexural element is proportion to moment divided by modulus times thickness squared). If moments and concrete modulus are the same at the same value of surface load, strain to induce cracking should occur in the Wall B pipe at loads $(5/5.75)^2$ or 76% of those for the Wall C pipe. The ratio seen above is 25/45 = 56%. Possible explanations for this difference between observed and calculated differences may be because of differences in the concrete moduli, initial strains resulting from earth loading and the prior loading history, or soil support provided to the two different pipes.

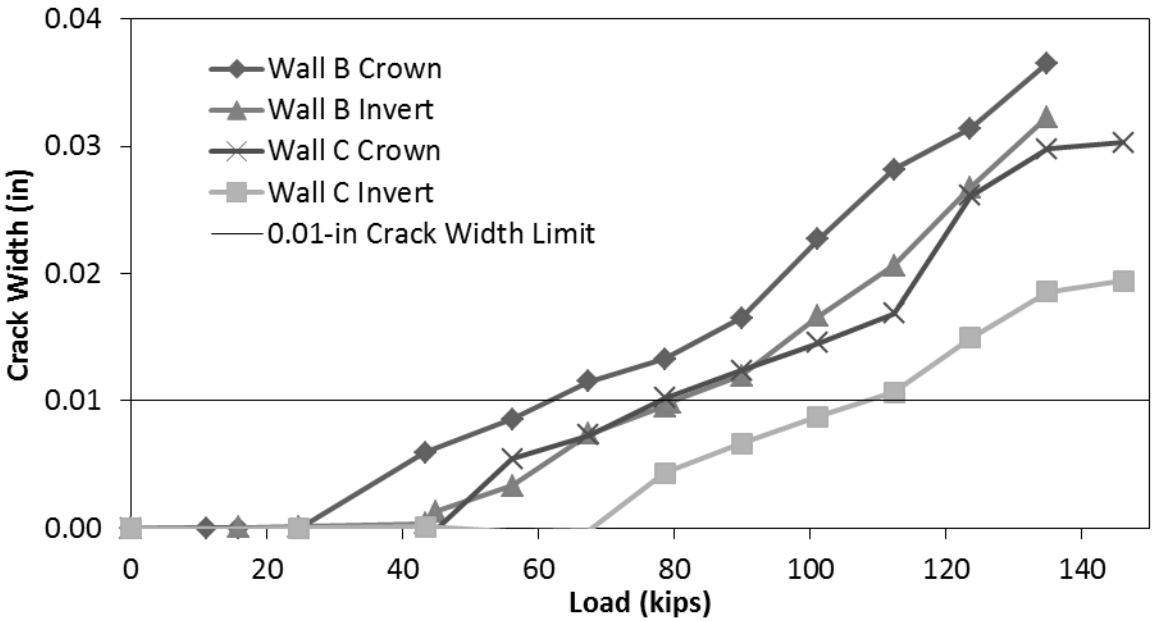

Figure 15. Development of crack width in 48 in. diameter pipe during ultimate limit states test

Performance of Wall B and C

As mentioned previously, pipes are designed to resist both a serviceability limit state and an ultimate limit state. As can be seen in Figure 15, at the full service load of 25 kips the Wall B pipe has just begun to crack and there is no visible cracking in the Wall C pipe. At the ultimate load of 43 kips, the Wall C pipe has begun to show a visible crack; however it is still below the crack width limit of 0.01-inch. The pipes first reach the 0.01-inch cracking limit at loads of 61 kips and 75 kips, for Walls B and C, respectively.

Test Program C

Introduction

A 24-inch reinforced concrete pipe was tested to determine the response under deep burial. The pipe was loaded in the biaxial test cell to a maximum pressure of 102 psi, equivalent to a burial depth of approximately 145 ft in that synthetic olivine backfill, or 113 ft for backfill with density of 130 pcf.

Diameter Change

The pipe responded linearly with respect to overburden pressure until a surface pressure of 40 psi (approximately 45 feet of equivalent burial under soil of unit weight 130 pcf), where the rate of diameter decrease began to increase nonlinearly due to cracking in the pipe. The pipe reached a deflection of 0.16 inches at an overburden pressure of 102 psi, as shown in Figure 16.

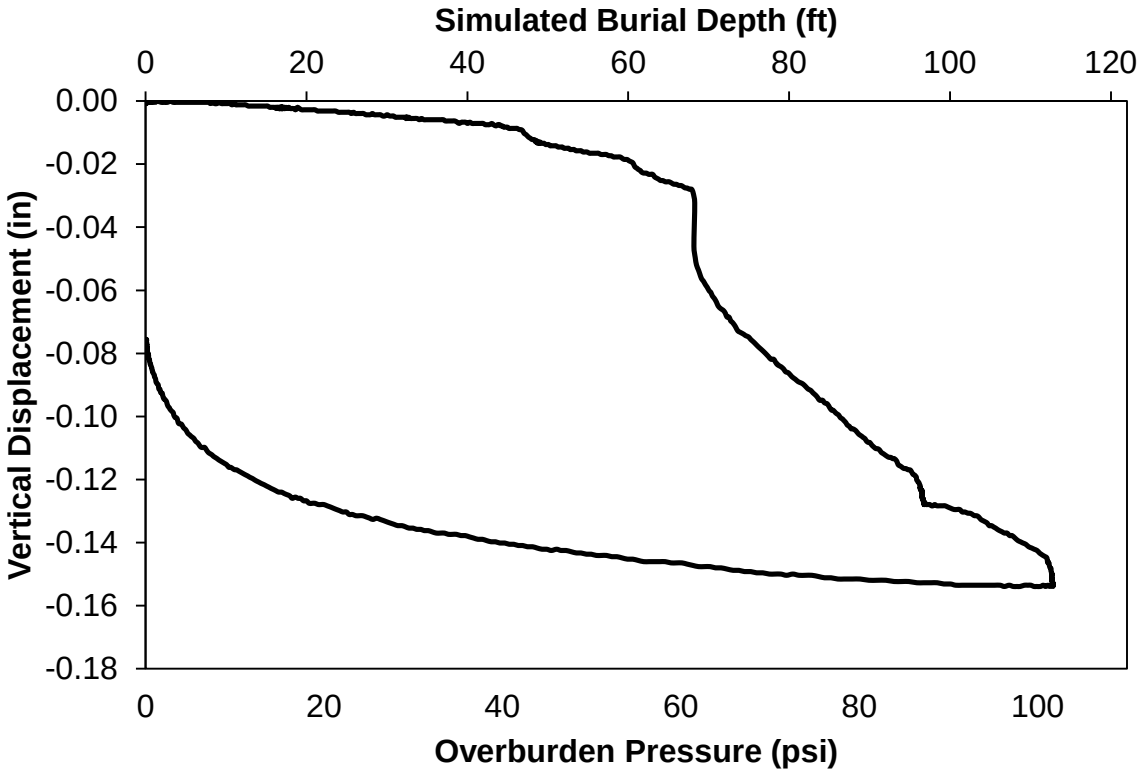

Figure 16. Deflection of 24-in Class V, Wall C pipe under simulated deep burial

Strain Behavior

As opposed to the shallow buried tested pipes which had maximum curvature at the crown, this simulated deep buried pipe had maximum curvature at the invert. The pipe behaved linearly until cracking began at between 38 to 43 psi of overburden pressure, as shown in Figures 17 and 18.

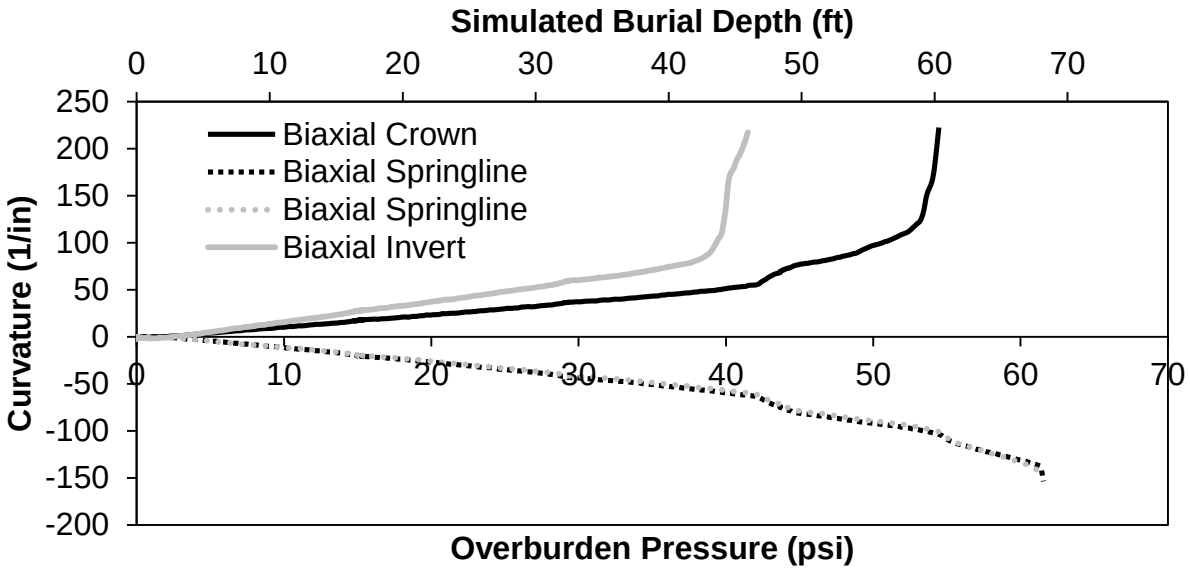

Figure 17. Curvature in 24-in class V, wall C pipe under simulated deep burial

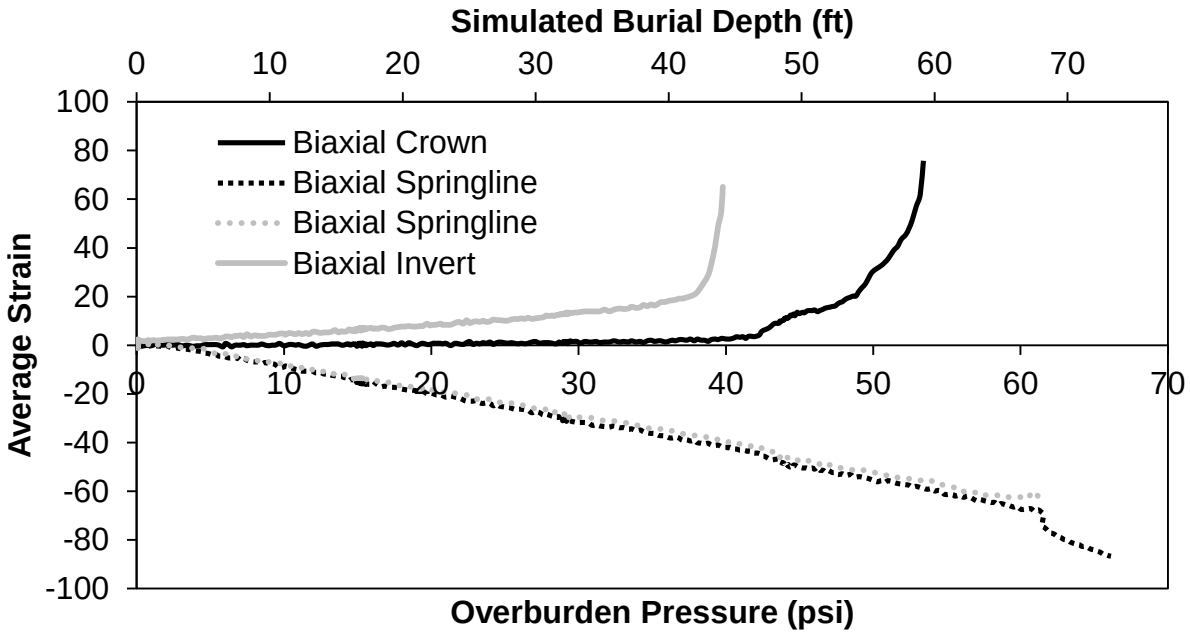

Figure 18. Average strain in 24-in class V, wall C pipe under deep burial

Crack Width

Crack widths monitored during the test of the 24 in. diameter pipe under simulated deep burial are presented in Figure 19. The first sign of visible cracking occurred at the invert at approximately 36 psi of overburden pressure and was followed by cracking at the crown at approximately 51 psi of overburden pressure. This was as expected due to the development of higher curvature at the invert.

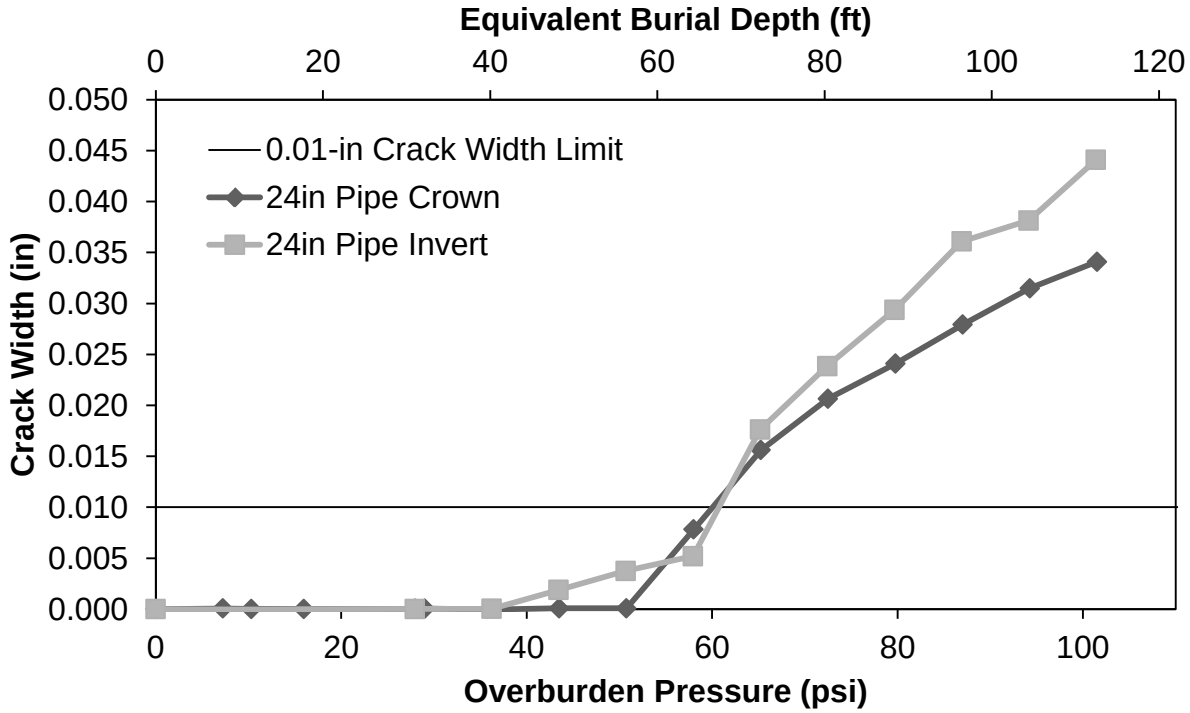

Figure 19. Crack width development in 24-in class V, wall C pipe under deep burial

Behavior of Deeply Buried Pipes

As mentioned previously, pipes are designed to resist both a serviceability limit state and an ultimate limit state. The pipe first reached the 0.01-inch cracking limit at an overburden pressure of approximately 60 psi.

Test Program D

Three edge bearing tests

D-Load data was provided by the manufacturer for the 24-inch Class IV pipe. A Class IV pipe according to the ASTM C76 tables can support a D-Load up to 2000 pounds per foot length of

pipe per foot inner diameter (lbs/ft/ft) while producing a maximum crack width of 0.01 inches. The 24-inch Class IV pipe used for Test Program A reached a D-Load of 3004lbs/ft/ft with a crack width of 0.012-inch (0.3mm crack limit according to CSA A257-2009) and an ultimate failure at a D-load of 3326lbs/ft/ft, according to the manufacturer's data. The D-Load data for the 24-inch Class V pipe was based on load tests performed by David Becerril on previous pipe samples.

The manufacturer provided three edge bearing data for the 48-inch pipes, for test Program B, showing that the pipe did not develop a crack larger than the limiting crack width at the required load for the 48-inch, Class III-equivalent, Wall B and Wall C pipe. However, the manufacturer did not go beyond this load to show at what load the limiting crack width did occur. Therefore additional D-load tests were conducted to determine under what D-load the limiting crack developed.

Diameter Change

Both pipes did not deflect significantly until approximately 40 kips where the rate of deflection began to increase nonlinearly due to cracking in the pipe. The Wall B pipe reached a deflection of 1.10 inches at a load of 121 kips and the Wall C pipe reached a deflection of 0.84 inches at a load of 100 kips, as shown in Figure 20.

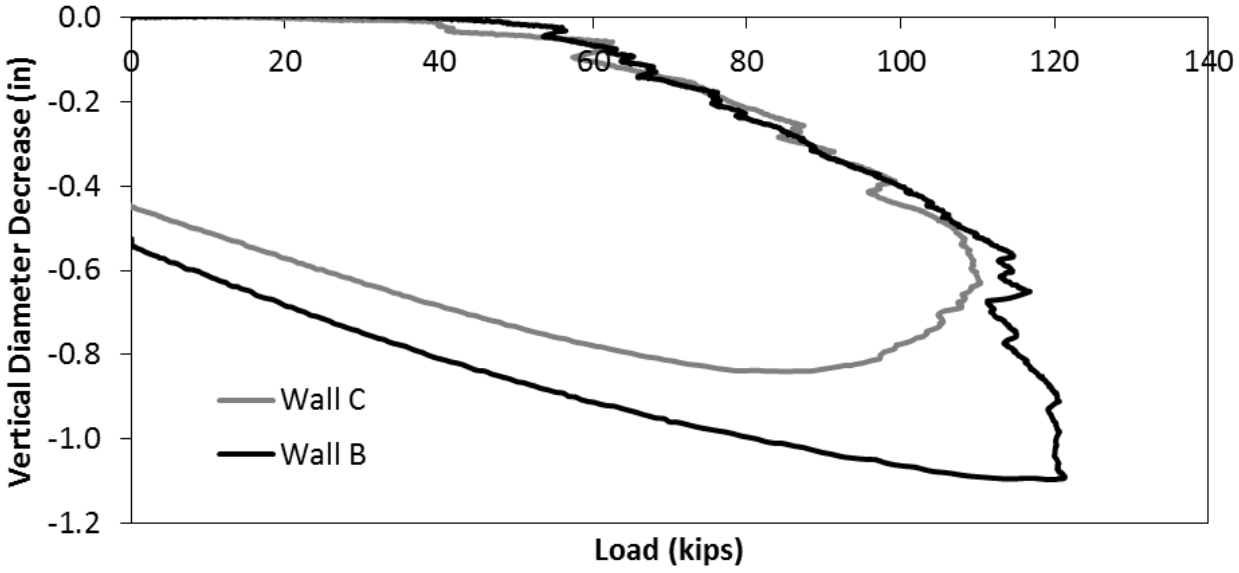

Figure 20. Vertical diameter decrease in 48-in wall B and C pipes during the three edge bearing tests (including pipe responses during unloading).

Crack Width

Crack widths monitored during the D-load tests on the 48 in. diameter pipes are presented in Figure 21. The first sign of visible cracking in the Wall C pipe occurred at the invert and crown at the same load of approximately 34 kips. The first sign of visible cracking in the Wall B pipe occurred at the invert at a load of approximately 45 kips followed shortly after by cracking at the crown at a load of 56 kips.

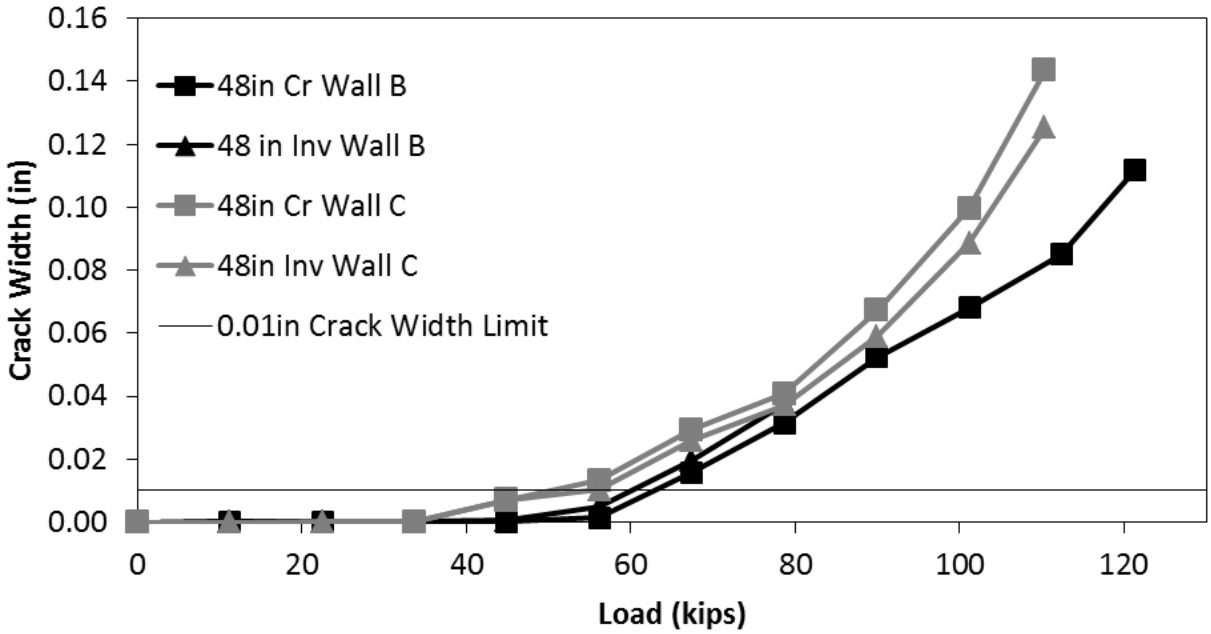

Figure 21. Development of crack width for 48-in wall B and C pipes during D-Load testing.

A Class III pipe according to the ASTM C76 tables can support a D-Load up to 1350lbs/ft/ft while producing a maximum crack width of 0.01 inches. The Wall B pipe used in the test reached a D-Load of 1862lbs/ft/ft to achieve a cracking limit of 0.01-inch cracking limit and the Wall C pipe reached a D-Load of 1581lbs/ft/ft to achieve a cracking limit of 0.01-inch cracking limit. This means both exceeded the load requirements equivalent to Class III pipe.

3.4 Comparison of experimental results and design calculations

3.4.1 Introduction

This section provides details of the comparisons made between test measurements and design calculations. These comparisons are made to examine the performance of the Direct Design and Indirect Design methods. In particular, these comparisons:

- provide evidence of the performance of the procedures available for estimating expected moments resulting from live load during Direct Design
- provide evidence of the performance of the procedures available for estimating expected moments resulting from earth load during Direct Design
- provide evidence of the performance of the moment capacity models available for use in Direct Design
- provide evidence of the performance of load capacity estimation using Indirect Design

3.4.2 Live load moment

Experimental measurements of live load moment

Two sets of buried pipe tests were conducted to examine the performance of buried pipes, as summarized in Table 11. Two 24 inch diameter pipes and two 48 inch diameter test pipes were provided by Hanson and M Con by arrangement with the Ontario Concrete Pipe Association. The pipes were tested at four different depths (1ft, 2 ft and 4ft) after burial within sandy gravel backfill (an A-1-a material compacted to at least 90% of maximum dry unit weight determined from a standard Proctor test). These tests were described in detail in Section 3.3.

Details of the steel and concrete for the four different test pipes employed are given in Table 12 (the pipe used for Test 3 was identical to 1B).

In each case, strains were measured on the inside and outside of the pipes at the crown, springlines and invert. These measured strains have been used to determine the changes in curvature at a specific value of surface load (a 24.7 kip force applied to a steel plate with standard dimensions of a wheel pair). Modulus and thickness of each of the test pipes were then used to calculate the test moments from the curvatures. A total of 36 such measurements were made (3 locations around the pipe circumference for 4 test pipes tested at 3 different burial depths).

Calculation of elastic moments due to surface loads in Direct Design

Three currently available methods for calculating the effect of live loads are examined. Each procedure uses the concept of load spreading under a rectangular area where load is applied at the ground surface. For surface contact area of length L_0 and width W_0 the applied load P_L is

assumed to spread out according to a live load distribution factor (*LLDF*) to apply pressure p_L across all or part of the outside diameter of the concrete

$$p_L = \frac{P_L}{(L_0 + LLDF.H)(W_0 + LLDF.H)} \quad 17$$

The surface area examined during design is that which provides the highest increases in vertical pressure on the pipe considering the AASHTO design truck featuring i. a single wheel pair, ii. a single axle (two wheel pairs), and iii. a tandem axle loading. For the comparisons being made here to the moment values observed in the test pipes, the single wheel pair configuration of 20 inch length and 10 inch width is used, since that is the loading geometry that was used in the experiments.

The procedures for approximating live load spreading with depth are as follows:

a) AASHTO (2007) specifies *LLDF*=1.15 for the granular test soil used in this project, and indicates that *H* is the depth to the top of the pipe; this procedure will be subsequently denoted 'LRFD 2007';
b) AASHTO (2013) was published towards the end of this project; the revised specification defines *LLDF* to be a function of inside pipe diameter; for pipes with diameter 24 inch or less, *LLDF*=1.15; for pipes with diameter 96 inches or more, *LLDF*=1.75; structures in between these diameters feature intermediate values of *LLDF*; for the calculations presented in this report, linear interpolation was used to give *LLDF*=1.35 for the 48 inch diameter pipes; as with the previous AASHTO procedure, burial depth was defined to the top of the pipe; this procedure will subsequently denoted 'LRFD 2013'; it is identical to LRFD 2007 for the 24 inch test pipes, but results in greater live load spreading (and smaller moments) for the 48 inch test pipes;
c) ASCE (1998) specifies use of *LLDF*=1.15 to the top of the pipe, and then distribution factor of 1.75 to a depth of *H*+0.75 *OD*; this procedure is implemented in program PipeCar developed for the American Concrete Pipe Association, and will be subsequently denoted 'PipeCar'.

Total force per unit length along the pipe is calculated as p_L multiplied by the lesser of W_0 or *OD*, where the vehicle is considered to be driving directly across the culvert (not along). This takes account of the spreading dimension relative to the pipe size (if it is less than OD, then all of the applied load is applied; if it is more, then only a portion of the load acts on the pipe). In the

tests being examined, the short dimension of the surface loading place was oriented parallel to the pipe diameter, consistent with vehicles driving directly across the culvert.

Once total force per unit length along the pipe W_i is determined, it is used to calculate moment based on two dimensional analysis that considers the pipe burial conditions and the soil-pipe interaction. The procedure generally used is the procedure based on two dimensional finite element analysis of an elastic ring outlined by ASCE (1998), where moments are given as moment factors:

$$M = C_{mi}\, W_i\, (ID+OD)/4 \qquad 18$$

where coefficients C_{mi} are given at three locations (crown, spring and invert) for five different loading cases (pipe weight, earth loads, fluid loads, and deeply or shallow buried surface loadings). Linear interpolation is used for burial depths between 1 ft (where factors WL2 apply) and 1.75 OD (beyond which factors WL1 apply). For the type two burial conditions used in the tests, the moment factors for live loading and earth loading are given in Table 13.

Table 14 summarizes the 36 values of moment obtained in the tests, as well moments obtained by the three procedures described above. These results are also presented in Figure 22. Another set of calculations is presented in the table and figure (denoted LRFD 2013+). These results will be explained and discussed later in this section.

These comparisons indicate that:

- measured moment (i.e. moment evaluated from measured strains) is always substantially lower than the calculated values
- moments measured at the crown are distinctly higher than those at the invert, whereas the calculation provide invert moments that are much closer to those at the crown

To quantify the differences between ‘measured moments’ (moments obtained from measured strains) and calculated values, ratios of calculated to test moment have been included in Table 14 and these are also shown in Figure 23. A perfect calculation procedure would provide a ratio of 1. Given the need for safety in design, a ratio exceeding one is desirable, but perhaps not higher than 2. The actual ratios vary widely, and many exceed 2 by a considerable margin. Table 15 summarizes the means and standard deviations for the ratios:

- moments obtained using the LRFD 2007 approach are between 2.9 and 11.7 times higher than the measured values, with an overall mean of 5 and a standard deviation of 2.2
- moments obtained using the LRFD 2013 approach are between 2.9 and 10.3 times higher than the measured values, with an overall mean of 4.7 and a standard deviation over 1.9
- moments obtained using PipeCar (the ASCE, 1998) approach are between 1.5 and 15 times higher than the measured values, with an overall mean of 5.1 and a standard deviation of over 3.

None of the procedures, therefore, are very effective at providing the moments resulting from application of surface load (at least for these shallow buried pipes subjected to the actions of a wheel pair). If the surface was paved, the discrepancies between calculated and test values would be even higher. Furthermore, the recent change to the live load spreading approach specified by AASHTO in 2013 did little to improve the calculations relative to the 2007 guidelines.

Values for individual cases in Figures 22 and 23 are summarized separately in Table 15 using means and standard deviations of moment ratios for the crown, springline and invert positions. These show that the discrepancies are substantially greater at the springline and invert, than at the crown. This is due to the additional live load spreading (or load attenuation) that develops at these greater depths, and this is the reason for the ASCE (1998) and PipeCar procedures for using an additional depth of 0.75 OD with LLDF = 1.75 (to capture load spreading through the pipe). It may also explain the reasons for the recent modifications to live load spreading published by AASHTO in 2013, since this provides somewhat better moment estimates at the invert, where moment is often most critical (those changes were based on three dimensional analyses presented by Petersen et al., 2010). However, the use of a single effective pressure in calculations of moment at all three positions (crown, springline and invert) does not address the significant differences in distance from the ground surface to these three different locations – a difference that is very substantial for large diameter pipes at shallow cover. For example, the 48 inch diameter pipe at 1 ft of cover has depth to invert that is five times higher than depth to crown.

Therefore, to address this issue further, it is possible to use the different depths to each of these locations in calculations of load spreading. A fourth set of calculations are therefore included in Table E-4 and shown in Figures 22 and 23, where depth to:

- Crown is set as H (so values remain the same as those for LRFD 2013);
- Springline is set as H + OD/2; and
- Invert is set as H + OD.

These calculations are denoted 'LRFD 2013+' or 'LRFD+' in Figures 22 and 23, and Tables 14 and 15. This modified approach provides much more consistent estimates of moment at the three circumferential locations, with mean of 2.6 and standard deviation of 1.2 Figure 23 shows that except at five cases out of the 36, the ratios of calculated to test moment are between 1 and 4, with more than 2/3 being below 2.5. Instead of having invert moment ratios in Figure 23 almost all exceeding a value of 4 (just two of the LRFD 2007 and LRFD 2013 calculations fall below this value), with one exception the LRFD+ calculations all fall below 4.

Calculation of elastic moments due to earth loads in Direct Design

The deeply buried test on the pipe of 24 inch diameter also included measurements of circumferential strains on the inner and outer surfaces of the pipe, at crown, springline and invert. These have also been used to estimate moments during the test, for comparison with calculated values. Table 16 provides a summary of the test measurements of curvature at an overburden pressure of 37.6 psi. These have been used to calculate test moments using pipe modulus 5576 ksi and second moment of area 52.7 in^4/ft. Also included are calculations using the coefficients given in ASCE (1998). The ratios of design moment to test moment are 1.9, 1.6 and 1.5 at the crown, springline and invert, respectively. These ratios are similar to those discussed in the previous section for live load using the procedure 'LRFD 2013+' (the current AASHTO procedure modified to account for the increased burial depths to the springline and invert).

3.4.3 Limit States Tests

In addition to undertaking six sets of service load testing under surface loads, five different ultimate limit states tests were conducted on the buried concrete test pipes:

1A. 24 inch Class IV-equivalent test pipe at 1 ft of cover using an enlarged wheel pair
1B. 24 inch Class V-equivalent test pipe at 1 ft of cover using an enlarged wheel pair
2A. 48 inch Wall B test pipe at 1 ft of cover using an enlarged wheel pair
2B. 48 inch Wall C test pipe at 1 ft of cover using an enlarged wheel pair
3. 24 inch Class V-equivalent test pipe in the biaxial cell, increasing surface pressures (representing overburden stresses)

In each case, the surface pressure representing the weight of a wheel pair (tests 1A to 2B) or the overburden pressure (test 3) were increased progressively until a limit state was reached. Cracking was monitored using digital images so that the crack widths could be measured using particle image velocimetry and the applied loads which induce a 0.01 in. crack determined (see Appendix C for explanation of crack width monitoring).

None of the pipes reached an ultimate strength limit, and so comparisons with design estimates made in Tables 17 and 18 are for the surface loads (force in kips for the shallow buried tests or pressure in psi for the simulation of deep burial) required to induce that 0.01 inch crack during each of the limit states tests.

In the test on pipe 1A, after initial cracking the crack width increased rapidly up to approximately 0.007 inches, but crack growth then slowed dramatically, and finally passed the 0.01 inch mark at a load over 100 kips. This is the only test where rate of crack growth was so irregular. To relate that specific measurement to the other tests, a load limit of 73 kips was estimated based on extrapolating its initial rate of crack width growth up to the 0.01 inch limit, and this additional load limit is included in Table 17 in parentheses, for reference in the subsequent discussion.

3.4.4 Comparisons to Design Estimates

Table 17 shows the experimental measurements of limiting loads discussed in the previous section, as well as D-load values for each pipe (expressed as total force on the pipe) and estimates of the surface load that induces 0.01 in. cracks obtained using Indirect Design. These show that the Indirect Design Method is providing estimates of the load limits for these test pipes that are between 54% and 81% of the observations. This level of safety is likely reasonable given the simplified nature of Indirect Design.

Table 18 shows the limiting loads measured in the experiments and the Direct Design estimates of the surface loads to induce moment equal to the ultimate moment capacity of the pipe at 1ft of cover. Also shown are the percentages of calculated load limit to the measured value. Since most of the applied loads for these buried pipes result from the surface forces or applied surface pressures, these ratios are a useful measure of the level of safety associated with the design calculations. The percentages vary a great deal for the four shallow buried pipe experiments, with pipes 1B and 2B having Direct Designs strength estimates 47% and 51% of the measured

values, pipe 1A having design strength of 19% of the measured value, and 2A having direct design strength 71% of the measured value. Test 3 (the deep burial test on the same pipe type as that used in 1B) featured calculated strength of 77% of the observed value.

The very low value of calculated to measured load limit in Test 1A may be partly a result of the nonlinear crack growth with load observed in that test, which delayed development of the 0.01inch crack until load of 101 kips (see Figure 19). If the alternative value discussed earlier was adopted, the calculated load capacity would have been 26% of the observed value.

These differences between calculated and observed load limits result from various causes. Potential causes are,

a. Direct Design is based on the conservative use of elastic analysis of maximum expected moment, where this is equated to the ultimate moment; the load limit observed in the tests was the serviceability limit (the 0.01 in. crack) not ultimate moment
b. Conservative estimates of expected moment result from use of the AASHTO LRFD procedures – as discussed in previous sections; the ratios of observed to calculated moments are included in Table 17 (they appeared earlier in Table 14); however, these ratios of calculated to measured moment are reasonably consistent (approximately 3 for the shallow buried pipes and 2 for the deeply buried pipe), whereas the ratios of observed load limits to the calculated values are far more variable.

Table 18 has been augmented to included calculations of the surface load limits made considering the moment reduction factor being proposed for use in design of these thick-walled pipes. The modified values of the surface loads that induce the ultimate moment capacity are then about 5% higher, and this brings all of the calculated load limits somewhat closer to those observed in the tests.

The current project involved testing of pipes of 24 in. and 48 in. diameter in Type 2 installations, and additional testing is recommended to examine the performance of the Indirect Design and Direct Design Methods for large diameter pipes and for other installation types. In particular, buried pipe tests in the laboratory for pipes of 60 in. and 72 in. diameter would enable the levels of safety associated with the existing design methods to be directly evaluated for these important structures.

Table 11. Summary of tests performed and pipes employed.

Test	**Diameter**	**Wall**	**Burial** ft	**Test cell**
1A	24 in.	C	1, 2, 4	West pit
1B	24 in.	C	1, 2, 4	West pit
2A	48 in.	B	1, 2, 4	West pit
2B	48 in.	C	1, 2, 4	West pit
3	24 in.	C	1 to 185[B]	Biaxial

[A]: Pipes were fabricated in accordance with ASTM C655M so these are equivalent classes.

[B]: Simulated by applying overburden pressures

Table 12. Summary of materials and geometry of the test pipes.

Test	**Diameter** in.	**Asi** in^2/ft	**Inner Cover** in.	**Aso** in^2/ft	**Outer Cover** in.	**Thick**. in.	f'_c ksi	f'_y ksi	E_c ksi	I in^4/ft
1A	24	0.100	1.88	None	1.88	3.75	10.2	86.3	5461	53
1B, 3	24	0.179	1.88	None	1.88	3.75	9.6	84.8	5302	53
2A	48	0.239	1	0.239	1	5	8.4	70.3	4953	125
2B	48	0.179	1	0.179	1	5.75	8.4	70.3	5260	190

Table 13. Moment calculation factors for the test pipes; Installation Type 2 (ASCE, 1998).

Invert				Springline				Crown			
WL1	WL2	We	W_p	WL1	WL2	We	W_p	WL1	WL2	We	W_p
0.107	0.189	0.122	0.227	-0.078	-0.16	-0.09	-0.091	0.08	0.241	0.094	0.079

Table 14. Moments in the elastic range (curvature □units: $in^{-1}x10^{6}$); 24.7 kips on a wheel pair

		#	Type	Depth	□	Test	PipeCar	Ratio	LRFD 2007	Ratio	LRFD 2013	Ratio	LRFD+	Ratio
Crown	24 in diameter	1	IV	4	7.8	2.4	6.1	2.57	5.8	2.5	5.8	2.5		
		2	IV	2	17.1	6.0	9.5	1.58	17.0	2.8	17.0	2.8		
		3	IV	1	28.2	9.3	16.9	1.82	29.4	3.2	29.4	3.2		
		4	V	4	7.2	2.2	6.1	2.82	5.8	2.7	5.8	2.7		
		5	V	2	18.8	6.0	9.5	1.58	17.0	2.8	17.0	2.8		
		6	V	1	35.8	10.8	16.8	1.55	29.4	2.7	29.4	2.7		
	48 in diameter	7	B	4	7.8	5.2	12.8	2.46	18.4	3.5	16.4	3.1		
		8	B	2	15.9	10.4	22.9	2.21	36.3	3.5	33.0	3.2		
		9	B	1	27.0	17.7	41.4	2.34	56.1	3.2	52.4	3.0		
		10	C	4	5.6	5.3	13.3	2.53	18.9	3.6	16.8	3.2		
		11	C	2	11.6	11.6	23.6	2.03	36.9	3.2	33.5	2.9		
		12	C	1	18.5	17.9	42.4	2.36	56.9	3.2	53.1	3.0		
Springline	24 in diameter	13	IV	4	-6.3	-1.8	-6.7	3.70	-5.0	2.8	-5.0	2.8	-3.4	1.9
		14	IV	2	-15.3	-4.4	-10.6	2.41	-11.9	2.7	-11.9	2.7	-6.7	1.5
		15	IV	1	-23.8	-6.0	-17.4	2.91	-19.5	3.3	-19.5	3.3	-10.3	1.7
		16	V	4	-4.4	-1.3	-6.7	5.11	-5.0	3.8	-5.0	3.8	-3.4	2.6
		17	V	2	-12.8	-4.0	-10.4	2.64	-11.9	3.0	-11.9	3.0	-6.7	1.7
		18	V	1	-25.7	-6.5	-17.2	2.63	-19.5	3.0	-19.5	3.0	-10.3	1.6
	48 in diameter	19	B	4	-4.2	-2.7	-14.2	5.23	-13.3	4.9	-11.8	4.3	-6.4	2.4
		20	B	2	-7.7	-5.0	-24.2	4.85	-24.6	4.9	-22.4	4.5	-10.5	2.1
		21	B	1	-10.2	-6.6	-37.0	5.60	-37.2	5.6	-34.8	5.3	-13.9	2.1
		22	C	4	-4.2	-3.7	-15.7	4.31	-13.6	3.7	-12.0	3.3	-3.1	0.8
		23	C	2	-7.3	-7.1	-24.9	3.49	-25.0	3.5	-22.7	3.2	-10.6	1.5
		24	C	1	-8.8	-8.5	-37.9	4.46	-37.8	4.4	-35.3	4.1	-14.0	1.6
Invert	24 in diameter	25	IV	4	5.3	1.7	9.3	5.66	6.6	4.0	6.6	4.0	4.0	2.4
		26	IV	2	10.8	4.3	14.1	3.31	14.4	3.4	14.4	3.4	5.3	1.2
		27	IV	1	14.6	5.7	21.9	3.84	23.0	4.0	23.0	4.0	7.6	1.3
		28	V	4	3.8	1.1	9.4	8.58	6.6	6.1	6.6	6.1	4.0	3.6
		29	V	2	9.9	3.4	14.1	4.22	14.4	4.3	14.4	4.3	5.3	1.6
		30	V	1	21.6	6.5	21.6	3.30	23.0	3.5	23.0	3.5	7.6	1.2
	48 in diameter	31	B	4	3.7	3.0	21.1	7.06	16.3	5.5	14.5	4.9	5.2	1.7
		32	B	2	8.8	6.0	32.6	5.48	29.4	4.9	26.7	4.5	7.5	1.3
		33	B	1	12.6	8.2	47.0	5.72	44.0	5.4	41.1	5.0	9.3	1.1
		34	C	4	3.8	3.5	22.2	6.44	16.7	4.8	14.8	4.3	1.7	0.5
		35	C	2	6.9	6.8	34.0	4.99	29.9	4.4	27.2	4.0	7.5	1.1
		36	C	1	9.5	9.3	48.5	5.22	44.6	4.8	41.7	4.5	9.3	1.0

Table 15. Summary of performance of four different procedures for estimating elastic moments in a buried concrete pipe; means and standard deviations for ratio of calculated moments relative to the 36 different 'measured' values (moments calculated from measured strains).

	Crown		Springline		Invert		Overall	
Moment Analysis Method	Mean	Standard Deviation	Mean	Standard Deviation	Mean	Standard Deviation	Mean	Standard Deviation
LRFD 2007	3.07	0.35	3.80	0.93	4.59	0.77	3.82	0.95
LRFD 2013	2.92	0.22	3.60	0.77	4.37	0.69	3.63	0.85
LRFD 2013+	2.92	0.22	1.80	0.44	1.50	0.78	2.07	0.81
PipeCar	2.16	0.42	3.94	1.08	5.32	1.50	3.81	1.70

Table 16. Summary of performance of the Direct Design procedure for estimating elastic moments in a deeply buried concrete pipe; overburden pressure 37.6 psi, pipe modulus 5576 ksi, and I = 52.7 in^4/ft.

Location	Crown	Springline	Invert
Curvature ($in.^{-1}$) x 10^6	47.0	-53.9	78.8
M_{Test} in.kips/ft	13.8	-15.8	23.2
M_{LRFD} in.kips/ft	26.0	-24.9	33.7
M_{LRFD}/M_{Test}	1.9	1.6	1.5

Table 17. Summary of tested strength and strength calculations using Indirect Design

Test	Diameter	Test load	D-load	ID load	ID/test
1A	24 in.	101 kips (73 kips)	48 kips	54.8 kips	54%
1B	24 in.	73 kips	50 kips	56.9 kips	78%
2A	48 in.	61 kips	62 kips	49.6 kips	81%
2B	48 in.	75 kips	64 kips	51.3 kips	68%
3	24 in.	60 psi	50 kips	34 psi	57%

Table 18. Summary of test loads and Direct Design calculations.

Test	Diameter	Test load 0.01 in. crack	Direct Design load limit[+]	DD load limit considering thickness correction	M_{Calc}/M_{Test}
1A	24 in.	101 kips (73 kips)	19.2 kips (19%)	20.3 kips (20%)	3.2
1B	24 in.	73 kips	34.0 kips (47%)	35.9 kips (49%)	2.7
2A	48 in.	61 kips	43.4 kips (71%)	45.1 kips (74%)	3.0
2B	48 in.	75 kips	37.9 kips (51%)	39.7 kips (53%)	3.0
3	24 in.	60 psi	46.2psi (77%)	49.2 psi (84%)	1.9

Note: [+] While the Direct Design load limit was based on ultimate moment capacity, the limit seen in the test was the 0.01 in. crack.

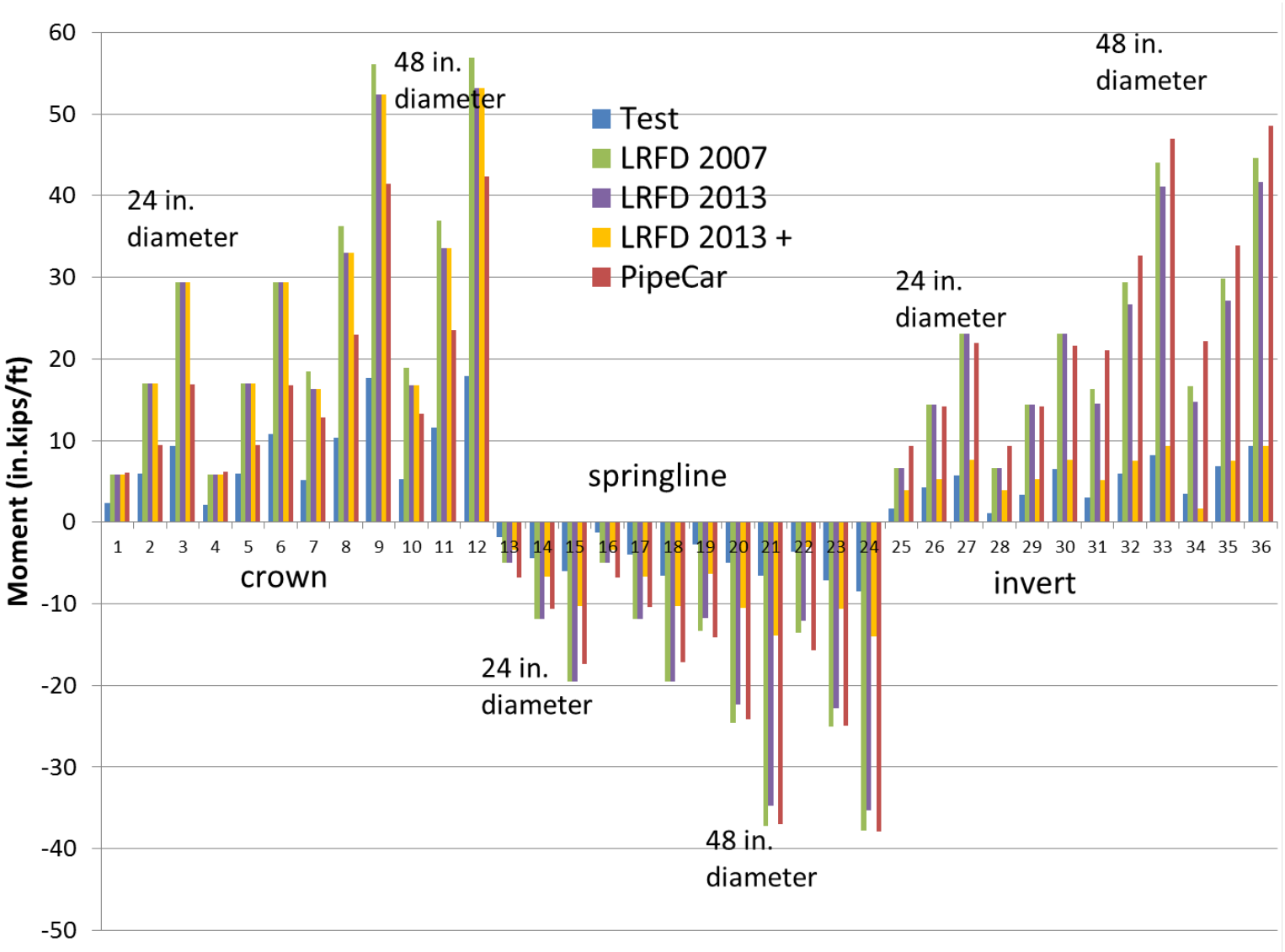

Figure 22. Comparison of 36 measured and calculated moments at the crown, springlines, and invert of the test pipes; four calculation procedures.

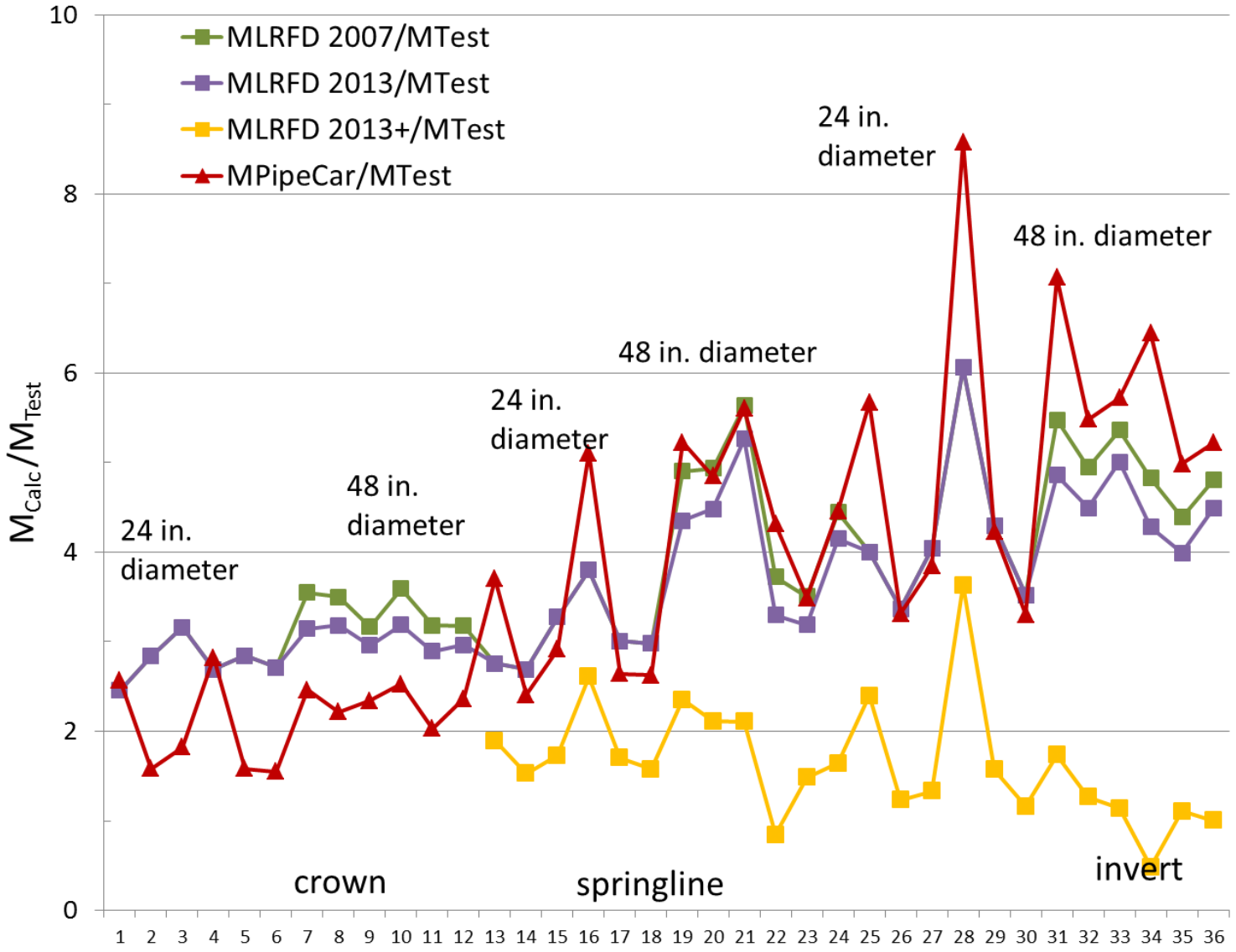

Figure 23. Ratio of calculated to measured moments at crown, springline, and invert of the test culverts; four calculation procedures.

3.5 Potential changes to Direct Design procedures

3.5.1 Pipe geometries considered during the parametric study.

This section provides details of the input variables and results for various calculations of moment capacity. Table 19 summarizes the geometry and properties of the pipes that were used in the calculations.

Each of the moment capacity calculations detailed here are based on Type 2 installation, and for a specific choice of wall type. The calculations are for pipes buried between 9ft and 30ft. These are sufficiently remote from the ground surface to be unaffected by vehicle loads, and thus avoid problems with ongoing changes in treatment of live load effects during design (discussed earlier in the report).

While the required steel areas for other installation types or shallow buried structures responding to the influence of vehicles will be different, the way the steel area requirements for specific levels of ultimate moment are influenced by the calculation procedures will be largely the same (changes in thrust values at different levels of required moment could change the impact of the different calculation methods somewhat).

3.5.2 PipeCar calculations

PipeCar (2010) uses the AASHTO (2007) procedure (equation 12.10.4.2.4a-1) for estimating moment capacity as a function of f'_c (concrete strength), f_y (yield strength of the reinforcing steel), d (distance of the compression face to the centroid of tension reinforcement), h (wall thickness of pipe), M_u (moment due to factored loads), N_u (thrust due to factored loads) and ϕ (resistance factor for flexure). That equation simplifies the behavior by not explicitly considering the compatibility of strains between the various components of the reinforced concrete cross-section, with

- consideration of only the layer of steel closest to the extreme fiber placed in tension (it neglects the impact of any other flexural steel);
- an approximation for the impact of compressive axial force on the strains and stresses in the reinforced-concrete cross-section;

- a simplified lever arm between the concrete and the steel which is taken as a fixed proportion of the total wall thickness;
- yield stress in the steel, rather than any higher stresses that might result from strain hardening of the steel up to an ultimate stress; this is the conventional approach to design of reinforced concrete elements, since the development of strain-hardening in the steel generally requires strains that are associated with unacceptably large deflections;
- an approximation for the total compressive thrust carried by the concrete part of the composite structure as a function of f'_c.

Choices made in this analysis for concrete and steel material strength (f'_c and f_y) are consistent with those associated with pipes prescribed in ASTM C76 based on Indirect Design. This includes concrete strength of 4000 psi at lower levels of moment, rising to 6000 psi when pipes of greater moment capacity are required (corresponding to larger D-loads in ASTM C76). Other choices could of course be made when undertaking Direct Design, in accordance with the specific materials being considered for manufacture of the reinforced concrete pipe, however using the same material strengths enabled a direct comparison of the two approaches. Details of the key input variables are provided in Tables 20 to 24 for pipes of 24 in., 36 in., 48 in., 60 in., and 72 in. diameter, respectively.

Tables 20 to 24 also provide minimum required areas of inner steel at the pipe invert (A_{si}) calculated using PipeCar with two different values of steel yield stress. The results presented in column (3) are for f_y = 70 ksi. A second set of calculations, for f_y = 76 ksi, are presented in column (4). This was performed to obtain an estimate for the potential impact of strain-hardening of the steel on the ultimate moment that might be calculated. This higher stress is based on using peak rather than yield strength of the steel bars, which inherently assumes imposed levels of curvature and average axial strain associated with applied moments and thrusts that lead to strain levels for the inner steel sufficient to generate this higher level of strength in the steel. Any combination of moment and thrust that leads to lower levels of strain would produce less enhancement in the ultimate moment, and the design would then require a greater amount of steel (an amount between the calculated values based on 70ksi and 76 ksi).

The comparison of solutions from PipeCar based on 70ksi and 76 ksi steel indicates the potential level of enhancement in moment capacity (i.e. reductions in area of inner steel) that might be achieved if a strain-compatibility calculation were undertaken considering the strain-

hardening characteristics of the steel (although such a strain compatibility approach is not used by PipeCar).

To illustrate those comparisons graphically, Figures 23 to 28 have been prepared showing minimum area of steel $\underline{A_{si}}$ for pipes of 24 in., 36 in., 48 in., 60 in., and 72 in., respectively. Four sets of solutions are provided in each figure – two undertaken with PipeCar and two others that are explained in subsequent subsections.

Inspection of Figures 24 to 28 indicates that:

- steel requirements for the smallest (24 in.) diameter pipe are set to the minimum permitted in the standard (0.07 in^2/ft) when moments are small (at burial depths below 13ft);
- if the beneficial effects of thrust are neglected, the required steel area calculated using equation 12.10.4.2.4a-1 is inversely proportion to steel yield stress; for the combinations of thrust and moment for all these design cases, the increase in steel yield stress from 70 ksi to 76 ksi has a maximum potential to reduce required steel by about 7%;
- when design is controlled by shear (rows marked in yellow on Tables 22 to 24 where results are presented), then the steel yield stress has no influence on required area of steel; these zones of shear force limit state are delimited on the Figures by sudden changes in the slope of steel area as function of burial depth, or by a discontinuity in the steel requirements and details of those changes to the ultimate limit state can also be identified directly in the tables.

To capitalize on the potential benefits of strain hardening, a calculation of moment capacity that is considerably more complex would be needed, requiring explicit consideration of compatibility between the steel reinforcement and the rest of the concrete. It is concluded that the additional complexity of that calculation is not justified by the potential reductions in steel required. However, the potential for incorporating that additional complexity into the calculation of moment capacity is included in the proposed changes to the AASHTO LRFD Bridge Design specifications drafted in Appendix D.

3.5.3 Calculations using RESPONSE

Overview of the program

While it was possible to obtain an upper bound estimate of the effects of steel strain hardening on moment capacity using equation 12.10.4.2.4a-1, it is not possible to consider other aspects

of the moment capacity calculation to be evaluated using this simplified equation. Therefore, a more advanced calculation procedure for the capacity of reinforced concrete moments is now introduced.

The program RESPONSE (Bentz, 2000) forces strain-compatibility between steel and concrete, and has therefore been used to evaluate the influence of some of the simplifying approximations used in the development of equation 12.10.4.2.4a-1. It has been used with steel modeled as an elastic-perfectly plastic material, so as to eliminate the potential impact of strain hardening of the steel (considered in the previous section) relative to other effects investigated in the remaining subsections.

RESPONSE forces strain-compatibility between steel and concrete using an iterative calculation procedure, with area of steel selected after a sequence of trials illustrated in Figure 29, based on a solution tolerance *tol*. Tables 20 to 24 feature both the moment requirements (column 8) and the ultimate moment obtained from RESPONSE after the iterative procedure (columns 13 and 16). These values match because the iterative process has converged with a tolerance sufficiently low to have most moments match to two significant figures.

Imposition of strain-compatibility and use of nonlinear stress block for concrete

Since RESPONSE forces strain-compatibility between the steel and concrete, and uses a nonlinear stress-block for the concrete (based on a more advanced stress-strain curve for concrete), a comparison can be made between the A_{si} requirements obtained from PipeCar and those from RESPONSE, to reveal the impact of these issues on the estimated values of ultimate moment (or the area of inner steel required to obtain a specific moment capacity).

Calculated values of a single layer of steel obtained using RESPONSE are given in column (13) in Tables 20 to 24. These are plotted together with the PipeCar results on Figures 24 to 28.

With the exception of the steel requirements at low cover for the 24 in. diameter pipes and those where shear governs (discussed further below), the steel areas obtained from RESPONSE fall just below those from PipeCar with the same steel yield stress (70 ksi). Differences are greatest for the small diameters pipes: calculated steel requirements are from 5 to 8% lower for the 24 in. diameter pipe, 2 to 4% lower for 48 in. diameter pipes, and 2 to 3% lower for the 72 in. diameter pipes.

Effect of a second layer of steel on calculations of inner steel requirements

Calculations for required area of inner steel at the invert have also been made considering two layers of steel in RESPONSE, and these are included in Figures 24 to 28. These results are based on the assumption that the outer steel area is equal to that used for the inner steel. These were the proportions used in the 48 in. pipes tested for this project, though lower areas of outside steel are prescribed in ASTM C76 for the pipes defined there for use with Indirect Design.

Consideration of the second layer of steel makes a significant difference to steel area requirements for small diameter pipes, with a reduction in A_{si} of from 24 to 28% for 24 in. pipes buried at depths of 13 ft or more, a reduction of from 18 to 22% for 36 in. diameter pipes, a reduction of from 11 to 16% for the 48 in. diameter pipes, and reductions less than 12% and 8% for 60 in. and 72 in. diameter pipes, respectively. It appears that there may be significant benefit in these more complex calculations of moment capacity based on two layers of steel reinforcing.

3.5.4 Modified compression field theory for estimation of shear capacity

The program RESPONSE also includes calculations of shear capacity based on use of the Modified Compression Field Theory (Vecchio and Collins, 1986). The Modified Compression Field Theory (MCFT) brings together material models for the concrete and steel with equilibrium and compatibility considerations to model cracked reinforced concrete. The MCFT uses average strain behavior and the material models to calculate the principal stresses, which are typically composed of both compressive and tensile components. Unlike its predecessor, the Compression Field Theory (Collins, 1978), the MCFT includes the tensile contribution of the concrete through a careful consideration of aggregate interlock at the crack interface as well as the tensile strength of the concrete between the cracks. The material models were initially developed based on a series of panel tests (Vecchio and Collins, 1986) but the MCFT has since been verified through extensive experimental testing. The MCFT forms the basis for the shear design provisions of the Canadian Concrete Design Code (CSA, 2004), the Canadian Highway Bridge Design Code (CSA, 2006) and the AASHTO bridge design manual (2013).

Importantly, in addition to imposing the strain-compatibility required to permit consideration of nonlinear concrete behavior and more than one layer of reinforcing steel during calculations of ultimate moment capacity, it includes more advanced estimates of shear capacity.

The potential effect of using this model on reducing steel requirements for shear can be seen by examining zones where shear capacity controls design on Figures 24 to 28. For example, Figure 27 shows A_{si} requirements for 60 in. diameter pipes between 18 and 22 ft of burial. The RESPONSE calculations provide much lower steel areas, whether one or two layers of steel reinforcing are considered. These improvements are also, however, a function of the strength of the concrete being used, and whether or not stirrups are employed, and such choices influence A_{si} considerably. For example, at burial depths greater than 28 ft for 72 in. pipe, the mandatory use of stirrups is considered in PipeCar, and so the flexural steel requirements to control shear strength drop dramatically. The RESPONSE calculations in this range are for the case where stirrups are not employed, so the magnitude of A_{si} is larger.

3.5.5 Possible inclusion of strain-compatibility calculations in PipeCar

As indicated by the discussion above, the accuracy of PipeCar is limited by its use of equation 12.10.4.2.4a-1, although the steel area estimates from this equation appear to be conservative. To include the more accurate analysis discussed previously would require the implementation of the Modified Compression Field Theory within PipeCar. This can be done by using a layered approach to analyze the cross section as detailed in Collins and Mitchell (1997) whereby an initial strain state is assumed, and using the material models and the equations of the Modified Compression Field Theory, the resultant forces acting on the section are determined. If the resultant forces acting on the section are not in equilibrium (with the applied loads), a new assumption about the strain state is made until equilibrium is achieved. In the current implementation a second trial and error approach is used to determine the optimum amount of steel to resist the applied loads determined from the Direct Design elastic analysis (as discussed above). However, if this approach were implemented into PipeCar, the area of steel could be solved for directly since moment equilibrium could be checked at the same time. The output of the program would be the optimum area of steel required to resist the given loading case as determined from the structural analysis.

The development of RESPONSE by Bentz was his doctoral research project, and the inclusion of these much more complex calculations into a specialized concrete pipe analysis program such as PipeCar would require considerable effort and the costs and potential benefits of that work would need to be considered carefully.

Table 19. Pipe geometries.

Pipe diameter	24in	36in	48in	60in	72in
Wall thickness	3.75in	4.75in	5.75in	6.75in	7.75in
Outer diameter	31.5in	45.5in	59.5in	74in	88in

Table 20. Details of moment and shear capacity calculations for 24 in. diameter pipes

		f_y=70 ksi	f_y=76 ksi	Ultimate Moments/Thrusts						Single			Double		
f'_c	Cover	A_{si}	A_{si}	M	N	V	N	M	V	A_s.iter.	M (min. A_s)	A_{si}	A_s.iter.	M (min.A_s)	A_{si}
ksi (1)	ft (2)	in^2/ft (3)	in^2/ft (4)	in.kips/ft (5)	kips/ft (6)	kips/ft (7)	kN/ft 8)	kNm/ft (9)	kN/ft (10)	mm^2/ft (11)	kN.m (12)	in^2/ft (13)	mm^2/ft (14)	kN.m (15)	in^2/ft (16)
4	9	0.070	0.070	10.83	0.633		2.816	1.2		32	1.2	0.05	24	1.2	0.04
4	10	0.070	0.070	11.81	0.707		3.145	1.3		34	1.3	0.05	26	1.3	0.04
4	11	0.070	0.070	12.78	0.782		3.479	1.4		36	1.4	0.06	28	1.4	0.04
4	12	0.070	0.070	13.75	0.856		3.808	1.6		42	1.6	0.07	30	1.6	0.05
4	13	0.070	0.070	14.73	0.931		4.141	1.7		46	1.7	0.07	34	1.7	0.05
4	14	0.078	0.071	15.70	1.005		4.470	1.8		48	1.8	0.07	38	1.8	0.06
4	15	0.082	0.076	16.67	1.080		4.804	1.9		50	1.9	0.08	40	1.9	0.06
4	16	0.087	0.081	17.65	1.154		5.133	2.0		54	2	0.08	42	2.0	0.07
4	17	0.092	0.085	18.62	1.232		5.480	2.1		56	2.1	0.09	44	2.1	0.07
4	18	0.097	0.090	19.60	1.303		5.796	2.2		58	2.2	0.09	46	2.2	0.07
4	19	0.102	0.094	20.57	1.378		6.130	2.3		62	2.3	0.10	48	2.3	0.07
4	20	0.107	0.099	21.55	1.452		6.459	2.4		64	2.4	0.10	50	2.4	0.08
4	21	0.112	0.103	22.52	1.527		6.792	2.5		66	2.5	0.10	52	2.5	0.08
4	22	0.117	0.108	23.50	1.601		7.122	2.7		72	2.7	0.11	56	2.7	0.09
6	23	0.120	0.111	24.47	1.676		7.455	2.8		76	2.8	0.12	58	2.8	0.09
6	24	0.125	0.115	25.44	1.750		7.784	2.9		76	2.9	0.12	60	2.9	0.09
6	25	0.130	0.120	26.42	1.825		8.118	3.0		80	3	0.12	62	3.0	0.10
6	26	0.135	0.124	27.39	1.899		8.447	3.1		82	3.1	0.13	64	3.1	0.10
6	27	0.140	0.129	28.37	1.974		8.781	3.2		84	3.2	0.13	66	3.2	0.10
6	28	0.145	0.133	29.34	2.048		9.110	3.3		88	3.3	0.14	68	3.3	0.11
6	29	0.150	0.138	30.31	2.123		9.44	3.4		90	3.4	0.14	70	3.4	0.11
6	30	0.155	0.142	31.29	2.197		9.773	3.5		94	3.5	0.15	72	3.5	0.11

Table 21. Details of moment and shear capacity calculations for 36 in. diameter pipes.

		f_y=70 ksi	f_y=76 ksi	Ultimate Moments/Thrusts/Shears						Single			Double		
f'_c	Cover	A_{si}	A_{si}	M	N	V	N	M	V	A_s.iter.	M (min.A_s)	A_{si}	As.iter.	M (min.A_s)	A_{si}
ksi (1)	ft (2)	in^2/ft (3)	in^2/ft (4)	in.kips/ft (5)	kips/ft (6)	kN/ft (7)	kN/ft (8)	kNm/ft (9)	kN/ft (10)	mm^2/ft (11)	kN.m (12)	in^2/ft (13)	mm^2/ft (14)	kN.m (15)	in^2/ft (16)
4	9	0.091	0.084	24.54	0.870		3.87	2.8		56	2.8	0.087	46	2.8	0.071
4	10	0.098	0.091	26.60	0.978		4.35	3.0		60	3.0	0.093	50	3.0	0.078
4	11	0.106	0.098	28.67	1.093		4.86	3.2		64	3.2	0.099	54	3.2	0.084
4	12	0.114	0.105	30.73	1.193		5.31	3.5		70	3.5	0.109	58	3.5	0.090
4	13	0.121	0.112	32.80	1.301		5.79	3.7		74	3.7	0.115	60	3.7	0.093
4	14	0.129	0.119	34.86	1.409		6.27	3.9		78	3.9	0.121	66	3.9	0.102
4	15	0.137	0.126	36.93	1.516		6.74	4.2		84	4.2	0.130	72	4.2	0.112
4	16	0.145	0.133	38.99	1.624		7.22	4.4		88	4.4	0.136	74	4.4	0.115
4	17	0.153	0.14	41.06	1.732		7.70	4.6		92	4.6	0.143	78	4.6	0.121
4	18	0.16	0.148	43.13	1.839		8.18	4.9		100	4.9	0.155	84	4.9	0.130
4	19	0.168	0.155	45.19	1.947		8.66	5.1		104	5.1	0.161	88	5.1	0.136
4	20	0.176	0.163	47.26	2.054		9.14	5.3		108	5.3	0.167	92	5.3	0.143
4	21	0.184	0.170	49.32	2.162		9.62	5.6		114	5.6	0.177	98	5.6	0.152
4	22	0.193	0.177	51.39	2.270		10.10	5.8		118	5.8	0.183	102	5.8	0.158
6	23	0.196	0.181	53.45	2.377		10.57	6.0		120	6.0	0.186	100	6.0	0.155
6	24	0.204	0.188	55.52	2.485		11.05	6.3		126	6.3	0.195	106	6.3	0.164
6	25	0.212	0.195	57.58	2.593		11.53	6.5		130	6.5	0.202	110	6.5	0.171
6	26	0.22	0.202	59.65	2.700		12.01	6.7		134	6.7	0.208	114	6.7	0.177
6	27	0.227	0.21	61.71	2.808		12.49	7.0		140	7.0	0.217	120	7.0	0.186
6	28	0.235	0.217	63.78	2.915		12.97	7.2		144	7.2	0.223	124	7.2	0.192
6	29	0.243	0.224	65.84	3.023		13.45	7.4		148	7.4	0.229	128	7.4	0.198
6	30	0.251	0.231	67.91	3.131		13.93	7.7		156	7.7	0.242	134	7.7	0.208

Table 22. Details of moment and shear capacity calculations for 48 in. diameter pipes.

		f_y=70 ksi	f_y=76 ksi	Ultimate Moments/Thrusts/Shear						Single			Double		
f'_c	Cover	A_{si}	A_{si}	M	N	V	N	M	V	A_s.iter.	M (min.A_s)	A_{si}	A_s.iter.	M (min.A_s)	A_{si}
ksi (1)	ft (2)	in^2/ft (3)	in^2/ft (4)	in.kips/ft (5)	kips/ft (6)	kips/ft (7)	kN/ft (8)	kNm/ft (9)	kN/ft (10)	mm^2/ft (11)	kN.m (12)	in^2/ft (13)	mm^2/ft (14)	kN.m (15)	in^2/ft (16)
4	9	0.133	0.123	45.016	1.080		4.80	5.09		84	5	0.130	72	5.1	0.112
4	10	0.144	0.132	48.578	1.221		5.43	5.49		90	5.5	0.140	78	5.5	0.121
4	11	0.154	0.142	52.139	1.362		6.06	5.89		96	5.9	0.149	84	5.9	0.130
4	12	0.165	0.152	55.701	1.514		6.74	6.29		102	6.3	0.158	92	6.3	0.143
4	13	0.175	0.161	59.262	1.644		7.31	6.70		110	6.7	0.171	97	6.7	0.150
4	14	0.186	0.171	62.824	1.795		7.99	7.10		116	7.1	0.180	104	7.1	0.161
4	15	0.197	0.181	66.385	1.925		8.56	7.50		122	7.5	0.189	110	7.5	0.171
4	16	0.208	0.191	69.947	2.066		9.19	7.90		130	7.9	0.202	116	7.9	0.180
4	17	0.218	0.201	73.508	2.207		9.82	8.31		136	8.3	0.211	124	8.3	0.192
4	18	0.229	0.211	77.070	2.347		10.44	8.71		142	8.7	0.220	130	8.7	0.202
4	19	0.24	0.221	80.631	2.488		11.07	9.11		150	9.1	0.233	138	9.1	0.214
4	20	0.252	0.232	84.193	2.629		11.69	9.51		156	9.5	0.242	144	9.5	0.223
4	21	0.277	0.277	87.755	2.770	4.82	12.32	8.44	21.53	187	8.4	0.290	190	8.4	0.295
4	22	0.325	0.325	91.316	2.921	5.03	12.99	8.79	22.38	203	8.8	0.315	208	8.8	0.322
6	23	0.278	0.256	94.878	3.051		13.57	10.72		174	10.7	0.270	156	10.7	0.242
6	24	0.289	0.266	98.439	3.192		14.20	11.12		180	11.1	0.279	162	11.1	0.251
6	25	0.3	0.276	102.001	3.333		14.83	11.52		186	11.5	0.288	169	11.5	0.262
6	26	0.31	0.286	105.562	3.474		15.45	11.93		194	11.9	0.301	176	11.9	0.273
6	27	0.321	0.299	109.124	3.614		16.07	12.33		200	12.3	0.310	182	12.3	0.282
6	28	0.332	0.321	112.685	3.755		16.70	12.73		206	12.7	0.319	190	12.7	0.295
6	29	0.355	0.355	116.247	3.896	6.36	17.33	11.24	28.28	274	11.4	0.425	294	11.2	0.456
6	30	0.393	0.393	119.808	4.037	6.55	17.96	11.93	29.13	295	12.2	0.457	310	11.5	0.481

Notes: Orange cells – capacity is controlled by shear.

Table 23. Details of moment and shear capacity calculations for 60 in. diameter pipes.

		f_y=70 ksi	f_y=76 ksi	Ultimate Moments/Thrusts/Shear						Single			Double		
f'_c	Cover	A_{si}	A_{si}	M	N	V	M	N	V	A_s.iter.	M (min.A_s)	A_{si}	A_s.iter.	M (min.A_s)	A_{si}
ksi (1)	ft (2)	in^2/ft (3)	in^2/ft (4)	in.kips/ft (5)	kips/ft (6)	kips/ft (7)	kN.m/ft (8)	kN/ft (9)	kN/ft (10)	mm^2/ft (11)	kN.m (12)	in^2/ft (13)	mm^2/ft (14)	kN.m (15)	in^2/ft (16)
4	9	0.181	0.166	73.19	1.263		8.3	5.618		114	8.3	0.177	103	8.3	0.160
4	10	0.194	0.179	78.65	1.437		8.9	6.392		122	8.9	0.189	111	8.9	0.172
4	11	0.207	0.191	84.11	1.611		9.5	7.166		130	9.5	0.202	119	9.5	0.184
4	12	0.221	0.204	89.58	1.785		10.1	7.940		138	10.1	0.214	127	10.1	0.197
4	13	0.235	0.216	95.04	1.959		10.7	8.714		146	10.7	0.226	135	10.7	0.209
4	14	0.248	0.229	100.50	2.132		11.4	9.484		156	11.4	0.242	145	11.4	0.225
4	15	0.262	0.241	105.96	2.306		12.0	10.258		164	12.0	0.254	154	12.0	0.239
4	16	0.276	0.254	111.43	2.480		12.6	11.032		172	12.6	0.267	163	12.6	0.253
4	17	0.290	0.267	116.89	2.654		13.2	11.806		180	13.2	0.279	172	13.2	0.267
4	18	0.334	0.334	102.49	3.667	5.552	11.6	16.312	24.70	220	11.6	0.341	228	11.7	0.353
4	19	0.396	0.396	107.18	3.878	5.790	12.1	17.250	25.76	234	12.1	0.363	240	12.1	0.372
4	20	0.459	0.459	111.88	4.088	6.027	12.6	18.184	26.81	248	12.6	0.384	254	12.6	0.394
4	21	0.521	0.521	116.57	4.298	6.265	13.2	19.118	27.87	268	13.2	0.415	274	13.2	0.425
4	22	0.584	0.584	121.27	4.508	6.502	13.7	20.053	28.92	286	13.7	0.443	292	13.7	0.453
6	23	0.365	0.347	149.67	3.713		16.9	16.516		228	16.9	0.353	215	16.9	0.333
6	24	0.379	0.374	155.13	3.872		17.5	17.224		236	17.5	0.366	223	17.5	0.346
6	25	0.412	0.412	135.36	4.045	7.215	15.3	17.993	32.09	312	15.3	0.484	314	15.3	0.487
6	26	0.462	0.462	140.05	5.349	7.452	15.8	23.794	33.15	322	15.8	0.499	324	15.8	0.502
6	27	0.512	0.512	144.75	5.559	7.69	16.4	24.728	34.21	337	16.2	0.522	344	16.4	0.533
6	28	0.562	0.562	149.44	5.769	7.927	16.9	25.662	35.26	349	16.5	0.541	374	16.9	0.580
6	29	0.612	0.612	154.14	5.979	8.164	17.4	26.596	36.32	377	17.4	0.584	416	17.4	0.645
6	30	0.662	0.662	158.83	6.19	8.402	17.9	27.534	37.37	396	17.9	0.614	438	17.9	0.679

Notes: Orange cells – capacity is controlled by shear.

Table 24. Details of moment and shear capacity calculations for 72 in. diameter pipes.

		f_y=70 ksi	f_y=76 ksi	Ultimate Moments/Thrusts/Shear						Single			Double		
f'_c	Cover	A_{si}	A_{si}	M	N	V	M	N	V	A_s.iter.	M (min.A_s)	A_{si}	A_s.iter.	M (min.A_s)	A_{si}
psi (1)	ft (2)	in^2/ft (3)	in^2/ft (4)	in.kips/ft (5)	kips/ft (6)	kips/ft (7)	kN.m/ft (8)	kN/ft (9)	kN/ft (10)	mm^2/ft (11)	kN.m (12)	in^2/ft (13)	mm^2/ft (14)	kN.m (15)	in^2/ft (16)
4	9	0.233	0.215	109.97	1.418		12.4	6.31		146	12.4	0.226	138	12.4	0.214
4	10	0.249	0.23	117.74	1.625		13.3	7.23		157	13.3	0.243	148	13.3	0.229
4	11	0.266	0.245	125.51	1.832		14.2	8.15		168	14.2	0.260	159	14.2	0.246
4	12	0.282	0.26	133.27	2.039		15.1	9.07		178	15.1	0.276	170	15.1	0.264
4	13	0.299	0.275	141.04	2.246		15.9	9.99		187	15.9	0.290	180	15.9	0.279
4	14	0.312	0.288	148.81	2.453		16.8	10.91		196	16.8	0.304	186	16.8	0.288
6	15	0.329	0.303	156.58	2.660		17.7	11.83		207	17.7	0.321	198	17.7	0.307
6	16	0.345	0.318	164.35	2.867		18.6	12.75		217	18.6	0.336	208	18.6	0.322
6	17	0.362	0.333	172.12	3.074		19.4	13.67		227	19.4	0.352	218	19.4	0.338
6	18	0.379	0.366	179.89	3.281		20.3	14.60		237	20.3	0.367	229	20.3	0.355
6	19	0.42	0.42	156.90	4.568	7.15	17.7	20.32	31.81	288	17.7	0.446	307	17.2	0.476
6	20	0.489	0.489	163.58	4.818	7.433	18.5	21.43	33.06	306	18.5	0.474	320	18.7	0.496
6	21	0.579	0.579	168.91	5.115	7.799	19.1	22.75	34.69	324	19.1	0.502	336	19.3	0.521
6	22	0.457	0.457	210.97	4.109		23.8	18.28		277	23.8	0.429	268	23.8	0.415
6	23	0.534	0.534	182.17	5.619	8.372	20.6	25.00	37.24	346	20.6	0.536	358	20.8	0.555
6	24	0.597	0.597	188.79	5.871	8.658	21.3	26.12	38.51	366	21.3	0.567	373	21.3	0.578
6	25	0.661	0.661	195.42	6.123	8.945	22.1	27.24	39.79	386	22.1	0.598	430	22.1	0.667
6	26	0.723	0.723	202.05	6.376	9.231	22.8	28.36	41.06	408	22.8	0.632	454	22.8	0.704
6	27	0.786	0.786	208.68	6.628	9.518	23.6	29.48	42.34	478	23.6	0.741	524	23.6	0.812
6	28	0.849	0.849	215.31	6.88	9.804	24.3	30.60	43.61	502	24.3	0.778	552	24.3	0.856
6	29	0.688	0.688	221.94	7.132	10.09	25.1	31.73	44.88	547	25.1	0.848	638	25.1	0.989
6	30	0.721	0.707	228.56	7.384	10.38	25.8	32.85	46.16	616	25.8	0.955	670	25.8	1.039

Notes: Orange cells – capacity is controlled by shear; Red cells – stirrups become mandatory.

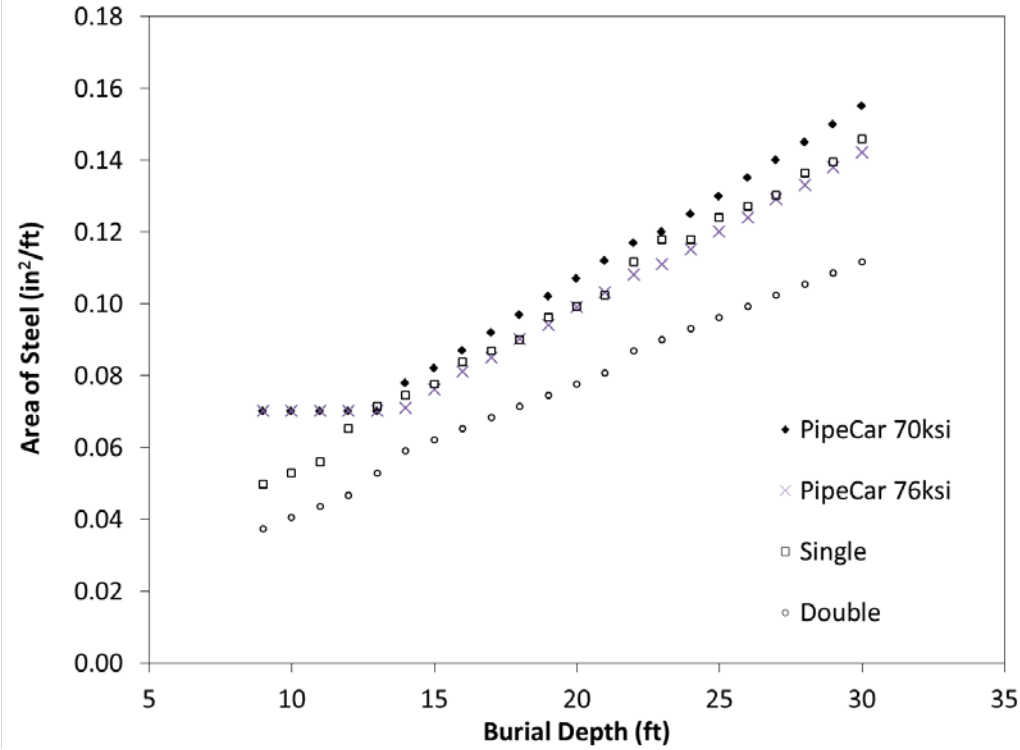

Figure 24. Comparison of inner steel requirements for 24 in. diameter reinforced concrete pipe based on four different methods of calculation; Type 2 installation.

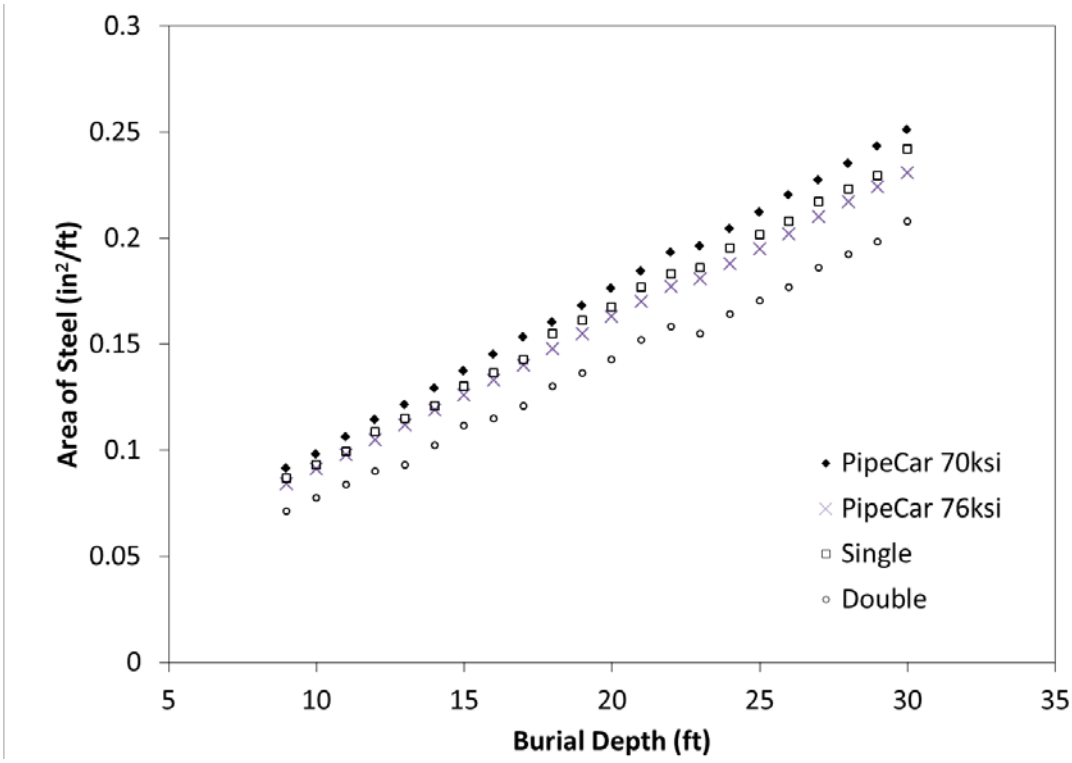

Figure 25. Comparison of inner steel requirements for 36 in. diameter reinforced concrete pipe based on four different methods of calculation; Type 2 installation.

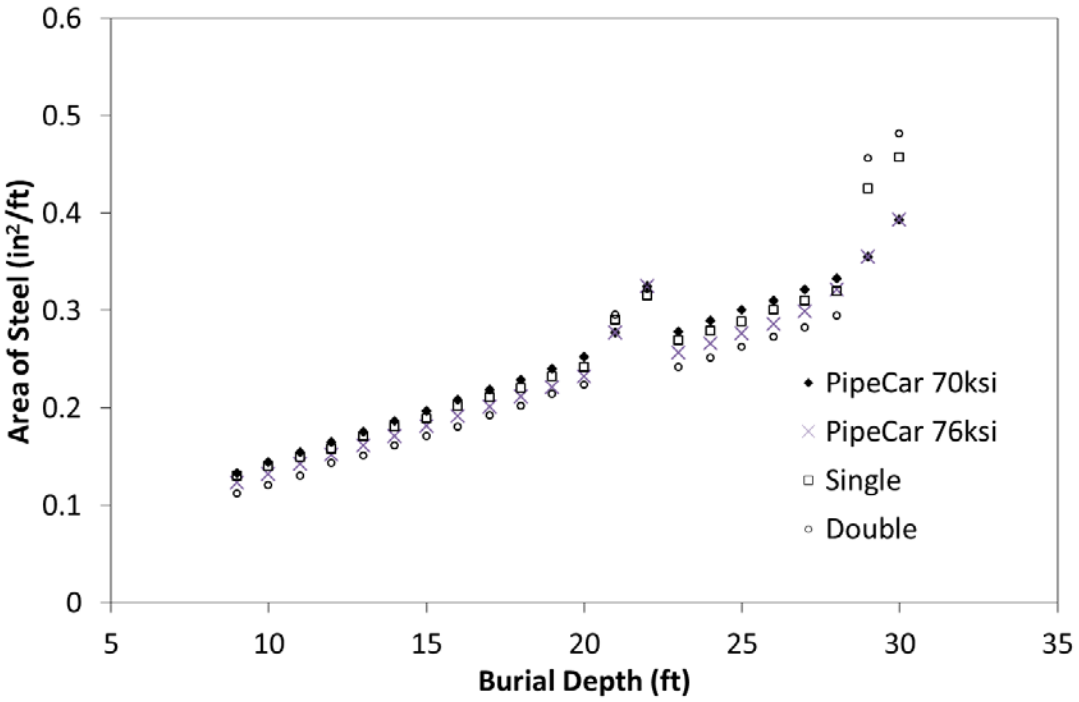

Figure 26. Comparison of inner steel requirements for 48 in. diameter reinforced concrete pipe based on four different methods of calculation; Type 2 installation.

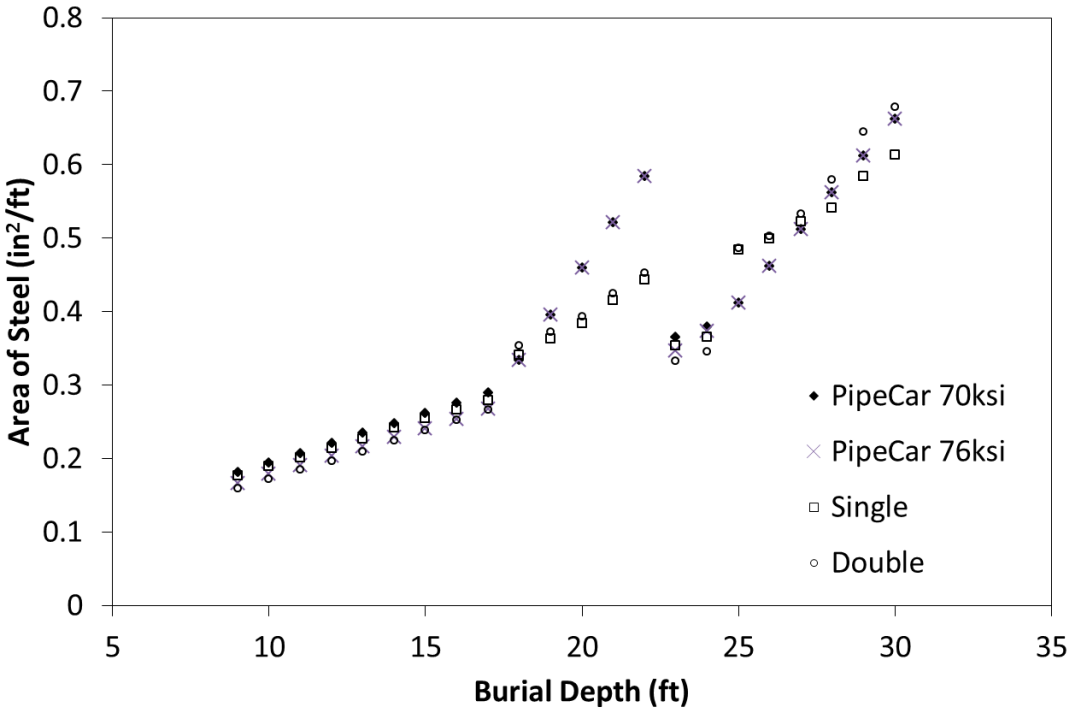

Figure 27. Comparison of inner steel requirements for 60 in. diameter reinforced concrete pipe based on four different methods of calculation; Type 2 installation.

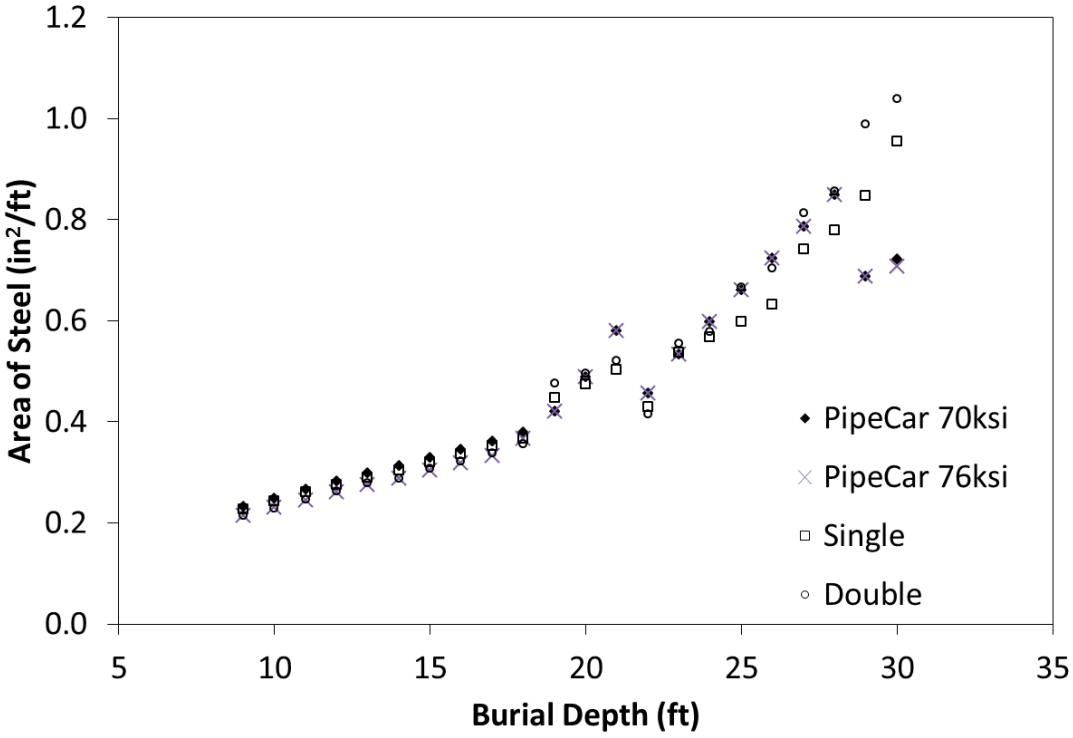

Figure 28. Comparison of inner steel requirements for 72 in. diameter reinforced concrete pipe based on four different methods of calculation; Type 2 installation.

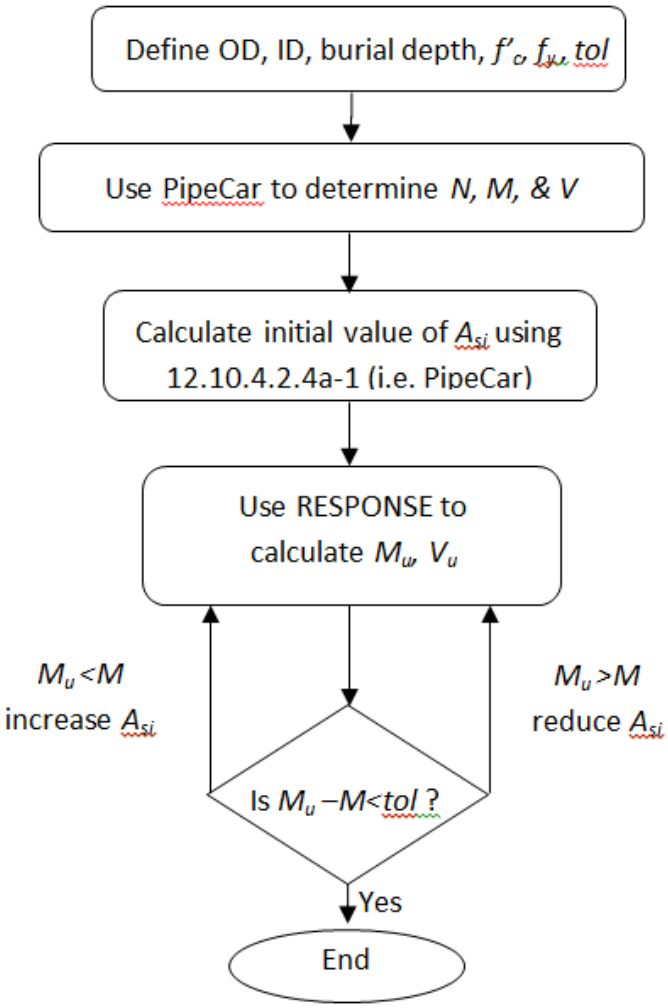

Figure 29. Flowchart explaining calculation procedure for A_{si} using RESPONSE (2000).

3.5.6 Adjustment of expected moments to account for thick ring theory

Moment calculations during Direct Design are based on the use of thin ring theory. However, the thickness of reinforced concrete pipes is typically greater than 10% of the radius of the pipe, and thin ring theory is conservative. Appendix A examines the implications of thick versus thin ring theory, and presents an adjustment factor that could be used to reduce moments at the crown or invert to account for the influence of the thick ring:

$$\left.\frac{M}{M_{thin}}\right|_{crown,invert} = 1 - 0.373\frac{t}{R} \qquad 18$$

where t is the pipe thickness, R its average radius, and M_{thin} is the moment estimate from Direct Design based on thin ring theory.

3.5.7 Potential consideration of plastic collapse mechanism

Direct Design evaluates the loads that induce the ultimate moment in the buried pipe by equating maximum expected moment from elastic ring theory to the ultimate moment capacity. However, pipe strength is not fully mobilized when moments reach the ultimate value at a single location on the pipe circumference. Instead, a plastic collapse mechanism for the pipe would involve four locations around the circumference reaching the ultimate moment capacity.

Therefore, use of plastic collapse analysis to determine the ultimate load capacity of buried concrete pipes has been examined in Appendix B.

This analysis approach would require additional research to determine the soil characteristics required in the analysis for different burial conditions. In particular, the earth pressure distributions currently used to estimate earth load effects would change, and may approach those associated with flexible pipes (the development of a collapse mechanism removes most of the flexural stiffness of the structure). However, the limiting load obtained during each of the five limit states tests was controlled by the service limit (the 0.01 in. crack), and none came close to generating the ultimate moment in the pipe. For that reason, the development and implementation of analysis based on a plastic collapse mechanism is not likely warranted, or should not be undertaken unless enhancements were made to permit effective estimates of the loads required to produce the limiting crack.

3.6 Comparison of Steel Requirements from the Indirect and Direct Design Methods

3.6.1 Introduction

Erdogmus et al. (2010) employed summary plots comparing the steel requirements determined using Indirect Design and Direct Design. These are very effective in illustrating the differences in outcomes from these two different design procedures, so are used here to illustrate:

- the current outcomes of Indirect Design and Direct Design (summarized in Table 25)
- the outcomes that would result if corrections for thick ring theory were included in Direct Design (summarized in Table 26)
- the outcomes that would result if the maximum potential benefits of steel strain hardening were achieved when undertaking Direct Design (summarized in Table 27)
- the outcomes that would result if Modified Compression Field Theory were used and two bars of steel were considered when undertaking Direct Design (summarized in Table 28)

All Indirect Design results are given for Wall C pipes defined in ASTM C76, since these have lower steel areas than Wall B pipes. All pipes are considered for a Type 2 installation. Details of the calculation procedures, the input variables and the results were given earlier.

3.6.2 Current differences for pipes under deep burial

Figure 30 shows the steel requirements associated with the existing design methods for pipes of diameters 24 inches to 72 inches and cover depths between 1ft and 30ft. The steel associated with Class II to Class V pipes defined in ASTM C76 are indicated, with maximum bedding depths calculated using the Indirect Design Method. Surface loading at shallow burial has been calculated based on AASHTO (2007) (not including modifications approved in 2013). Each of those pipes has a minimum burial depth associated with it also, set as one foot greater than the maximum limit of the previous pipe class (e.g. the maximum cover permitted for the Class IV pipe of 72 in. diameter is 21 ft, and so the minimum shown for the Class V pipe is 22 ft).

Direct Design employs equation 12.10.4.2.4a-1 from the AASHTO LRFD Bridge Design Specifications. This produces individual steel requirements for each burial depth, and the solid lines show those steel requirements for each of the five pipe diameters with each line color matching the symbol colors of the Indirect Design results. The calculations performed by PipeCar are for live load effects use the live load spreading approach recommended by the ACPA (1998), rather than the current or former AASHTO (2007, 2013) procedures. The objective with these plots is to illustrate differences between Indirect and Direct Design outcomes rather than the different approaches for treating surface live load, so the Direct Design estimates have been terminated at minimum burial depth of 8ft.

The performance of the existing design methods can, therefore, be evaluated by comparing the solid lines with the symbols. The ideal situation is when both design methods produce identical steel requirements. In that case, the solid lines would just touch the right hand end of each set of cover depths for a specific Indirect Design pipe Class. This is not generally the case however. For the largest diameter (72 in.) pipe results (shown in green), the Direct Design steel areas fall consistently below the Indirect Design areas, falling more progressively to the right as burial depth (or pipe Class) is increased.

For all of the smaller diameter pipes, the amounts of steel calculated using Direct Design have ranges of burial depth where their areas are greater than those for the pipe Classes associated with Indirect Design. This discrepancy is significant for 24 in. and 36 in. diameter pipes where Indirect Design indicates that a Class IV pipe should be employed (burial depths from 15 to 22 ft), with area of steel from Direct Design falling consistently above the results from Indirect Design.

It was shown in earlier sections of this report that both Indirect Design and Direct Design resulted in conservative strength estimates for a number of test pipes. However, one key objective of Project 20-07 Task 316 is to understand and reconcile the differences between Direct and Indirect Design. A follow-on objective might be to change design so that the areas of steel resulting from Direct Design are always less than or equal to Indirect Design i.e. bringing the solid lines on Figure 30 to touch the right hand end of

the symbols presenting the steel areas associated with Indirect Design. The outcomes associated with various potential modifications to Direct Design are examined in the subsections that follow.

In Figure 30 and the four figures that follow, the flexural steel requirements are shown, not the total steel employed. In some cases where Direct Design requires use of stirrups, the steel requirements for Direct Design may exceed those for Indirect Design even though the figure's focus on flexural steel might be misunderstood to imply that Direct Design requires less steel area.

3.6.3 Proposed modification to account for thick ring theory

Appendix A presents computational results that indicate that the use of thin elastic ring theory during Direct Design leads to conservative estimates of bending moment. That Appendix presented a correction factor that can be used to adjust moments obtained from the thin ring theory used in the calculations of soil-pipe interaction in PipeCar and most other procedures, so they become close to those that arise from thick ring theory.

Figure 31 therefore presents the steel requirements that result if the moment capacity needed during Direct Design is reduced to account for thick ring theory at the crown and invert (using the correction factor defined in Appendix A). The figure demonstrates that some of the discrepancy between Direct and Indirect design has been resolved, but the significant differences at burial depths between 15 and 22 ft remain. Further adjustment of Direct Design is required if the two design methods are to provide the same steel outcomes.

3.6.4 Possible modification to account for strain hardening of the reinforcing steel

An upper bound for the effects of strain hardening in the reinforcing steel has been estimated by setting yield stress of the steel to 76 ksi (replacing the 70 ksi value). Figure 32 shows the required areas of steel that result if strain-hardening of the steel reinforcing bars is sufficient to bring them to axial stresses of 76 ksi. Since these improvements are not sufficient to bring the Direct Design steel areas for small diameter pipes into alignment with Indirect Design values, and they assume steel efficiency that is greater

than or equal to that which could be actually realized (these improvements may well be optimistic), the issue of steel strain hardening is not considered further.

3.6.5 Proposed modification to employ Modified Compression Field Theory

Figure 33 shows how use of the Modified Compression Field Theory and consideration of two layers of reinforcing steel influence A_{si}, the calculated value of inner steel required at the invert of these pipes.

3.6.6 Relative impact of different potential changes to Direct Design

Figure 34 shows results for pipes of 24 in., 48 in. and 72 in. diameter, considering three different alternatives for Direct Design calculations of A_{si}:

- Calculations based on equation 12.10.4.2.4a-1
- Calculations using equation 12.10.4.2.4a-1 but with required moment capacity reduced to account for thick ring theory
- Calculations based on Modified Compression Field Theory obtained using program RESPONSE, and considering two layers of reinforcing steel

For the smallest diameter pipes, the two changes to the calculation procedure each reduce area of steel required. These could be combined to achieve even greater reductions (i.e. Modified Compression Field Theory could be used to determine area of steel required to achieve moments that were reduced to account for thick ring theory).

The results for pipe of intermediate size (48 in.) are similar, except in the two regions where shear governs. In those regions, the Modified Compression Field Theory yields higher areas of steel.

Results for the largest diameter pipe (72 in.) indicate that correction for thick ring theory consistently reduces the amount of steel required. However, use of Modified Compression Field Theory leads to increases in steel requirements for burial depths between 18 and 21 ft, little change in requirements at burial depths from 23 to 28 ft, and significant increases at greater depths where AASHTO currently requires use of stirrups.

3.6.7 Conclusions

The steel requirements associated with Indirect Design and Direct Design have been compared to three other potential methods of calculating ultimate moment capacity. These comparisons indicate that:

- Indirect design currently leads to more efficient designs compared to Direct Design based on the current procedures, particularly for small diameters
- Reductions in the moment capacity result when the behavior of thick rings is considered instead of the thin ring solutions currently employed in Direct Design; these lead to lower areas of steel required from design; those reductions do not, however, resolve all of the differences between steel outcomes from Indirect and Direct Design in small diameter pipes
- Small reductions might also be possible if the strain-hardening behavior of the reinforcing steel were considered; however, the increased computational effort is not likely warranted given the modest reductions in steel areas that could be achieved
- Use of the Modified Compression Field Theory also results in reductions in the amount of steel required for small diameter pipes, particularly when two layers of steel are considered in the calculation; this resolves almost all of the discrepancies between steel areas resulting from Indirect and Direct Design.

It is recommended, therefore, that moment reductions to account for the behavior of thick rings be included in the AASHTO LRFD Bridge Design Specifications, since the reduction factor is easily calculated. It is also recommended that designers be given the opportunity to employ Modified Compression Field Theory. However, use of this advanced theory should be an option for designers, not a requirement, since it leads to much greater complexity in the calculations.

Table 25. Steel requirements calculated using existing procedures.

Diameter	24in	36in	48in	60in	72in	24in	36in	48in	60in	72in
Thickness	3.75	4.75	5.75	6.75	7.75	3.75	4.75	5.75	6.75	7.75
Cover ft	A_{si} in^2/ft from C76 (for Indirect Design)					A_{si} in^2/ft from PipeCar (Direct Design)				
1	0.12	0.27	0.470	0.700	0.990					
2	0.07	0.08	0.160	0.240	0.360					
3	0.07	0.07	0.140	0.210	0.300					
4	0.07	0.07	0.140	0.210	0.300					
5	0.07	0.07	0.140	0.210	0.300					
6	0.07	0.07	0.140	0.210	0.300					
7	0.07	0.07	0.140	0.210	0.300					
8	0.07	0.07	0.140	0.210	0.300					
9	0.07	0.07	0.140	0.210	0.300	0.070	0.091	0.133	0.181	0.233
10	0.07	0.07	0.140	0.210	0.360	0.070	0.098	0.144	0.194	0.249
11	0.07	0.08	0.160	0.240	0.360	0.070	0.106	0.154	0.207	0.266
12	0.07	0.08	0.160	0.240	0.360	0.070	0.114	0.165	0.221	0.282
13	0.07	0.08	0.160	0.240	0.360	0.070	0.121	0.175	0.235	0.299
14	0.07	0.08	0.160	0.240	0.600	0.078	0.129	0.186	0.248	0.312
15	0.07	0.14	0.260	0.410	0.600	0.082	0.137	0.197	0.262	0.329
16	0.07	0.14	0.260	0.410	0.600	0.087	0.145	0.208	0.276	0.345
17	0.07	0.14	0.260	0.410	0.600	0.092	0.153	0.218	0.290	0.362
18	0.07	0.14	0.260	0.410	0.600	0.097	0.160	0.229	0.334	0.379
19	0.07	0.14	0.260	0.410	0.600	0.102	0.168	0.240	0.396	0.420
20	0.07	0.14	0.260	0.410	0.600	0.107	0.176	0.252	0.459	0.489
21	0.07	0.14	0.260	0.410	0.600	0.112	0.184	0.277	0.521	0.579
22	0.07	0.14	0.260	0.410	0.990	0.117	0.193	0.325	0.584	0.457
23	0.12	0.27	0.470	0.700	0.990	0.120	0.196	0.278	0.365	0.534
24	0.12	0.27	0.470	0.700	0.990	0.125	0.204	0.289	0.379	0.597
25	0.12	0.27	0.470	0.700	0.990	0.130	0.212	0.300	0.412	0.661
26	0.12	0.27	0.470	0.700	0.990	0.135	0.220	0.310	0.462	0.723
27	0.12	0.27	0.470	0.700	0.990	0.140	0.227	0.321	0.512	0.786
28	0.12	0.27	0.470	0.700	0.990	0.145	0.235	0.332	0.562	0.849
29	0.12	0.27	0.470	0.700	0.990	0.150	0.243	0.355	0.612	0.688
30	0.12	0.27	0.470	0.700	0.990	0.155	0.251	0.393	0.662	0.721

Table 26. Inner steel requirements at the invert A_{si} in in^2/ft calculated considering Thick Ring Theory

Diameter	**24**	**36**	**48**	**60**	**72**
Thickness	**3.75**	**4.75**	**5.75**	**6.75**	**7.75**
Cover	**Thickness Correction 1-0.37(t/R)**				
ft	**0.90**	**0.91**	**0.92**	**0.93**	**0.93**
	A_{si} in^2/ft adjusting for thick ring theory				
9	0.063	0.083	0.122	0.167	0.216
10	0.063	0.090	0.133	0.179	0.231
11	0.063	0.097	0.142	0.192	0.247
12	0.063	0.104	0.152	0.204	0.262
13	0.063	0.111	0.161	0.217	0.277
14	0.070	0.118	0.171	0.229	0.290
15	0.074	0.125	0.181	0.242	0.305
16	0.078	0.132	0.192	0.255	0.320
17	0.083	0.140	0.201	0.268	0.336
18	0.087	0.146	0.211	0.309	0.352
19	0.092	0.154	0.221	0.366	0.390
20	0.096	0.161	0.232	0.425	0.454
21	0.101	0.168	0.255	0.482	0.537
22	0.105	0.176	0.299	0.540	0.424
23	0.108	0.179	0.256	0.338	0.496
24	0.113	0.186	0.266	0.351	0.554
25	0.117	0.194	0.276	0.381	0.613
26	0.122	0.201	0.285	0.427	0.671
27	0.126	0.207	0.296	0.474	0.729
28	0.131	0.215	0.306	0.520	0.788
29	0.135	0.222	0.327	0.566	0.639
30	0.140	0.229	0.362	0.612	0.669

Table 27. Inner steel requirements at the invert A_{si} in in^2/ft calculated considering potential benefits of steel strain hardening and thick ring theory

Diameter	**24**	**36**	**48**	**60**	**72**	**24**	**36**	**48**	**60**	**72**
Thickness	**3.75**	**4.75**	**5.75**	**6.75**	**7.75**	**3.75**	**4.75**	**5.75**	**6.75**	**7.75**
Cover ft	**A_{si} in^2/ft (Steel strain hardening)**					**A_{si} in^2/ft thick & steel hardening**				
9	0.07	0.084	0.123	0.166	0.215	0.063	0.077	0.113	0.154	0.200
10	0.07	0.091	0.132	0.179	0.23	0.063	0.083	0.122	0.166	0.213
11	0.07	0.098	0.142	0.191	0.245	0.063	0.090	0.131	0.177	0.227
12	0.07	0.105	0.152	0.204	0.26	0.063	0.096	0.140	0.189	0.241
13	0.07	0.112	0.161	0.216	0.275	0.063	0.102	0.148	0.200	0.255
14	0.071	0.119	0.171	0.229	0.288	0.064	0.109	0.157	0.212	0.267
15	0.076	0.126	0.181	0.241	0.303	0.068	0.115	0.167	0.223	0.281
16	0.081	0.133	0.191	0.254	0.318	0.073	0.122	0.176	0.235	0.295
17	0.085	0.14	0.201	0.267	0.333	0.077	0.128	0.185	0.247	0.309
18	0.09	0.148	0.211	0.334	0.366	0.081	0.135	0.194	0.309	0.340
19	0.094	0.155	0.221	0.396	0.42	0.085	0.142	0.204	0.366	0.390
20	0.099	0.163	0.232	0.459	0.489	0.089	0.149	0.214	0.425	0.454
21	0.103	0.17	0.277	0.521	0.579	0.093	0.155	0.255	0.482	0.537
22	0.108	0.177	0.325	0.584	0.457	0.097	0.162	0.299	0.540	0.424
23	0.111	0.181	0.256	0.347	0.534	0.100	0.165	0.236	0.321	0.496
24	0.115	0.188	0.266	0.374	0.597	0.104	0.172	0.245	0.346	0.554
25	0.12	0.195	0.276	0.412	0.661	0.108	0.178	0.254	0.381	0.613
26	0.124	0.202	0.286	0.462	0.723	0.112	0.185	0.263	0.427	0.671
27	0.129	0.21	0.299	0.512	0.786	0.116	0.192	0.275	0.474	0.729
28	0.133	0.217	0.321	0.562	0.849	0.120	0.198	0.296	0.520	0.788
29	0.138	0.224	0.355	0.612	0.688	0.124	0.205	0.327	0.566	0.639
30	0.142	0.231	0.393	0.662	0.707	0.128	0.211	0.362	0.612	0.656

Table 28. Inner steel requirements at the invert A_{si} in in^2/ft calculated considering potential benefits of both layers of reinforcing steel

Diameter	**24**	**36**	**48**	**60**	**72**
Thickness	**3.75**	**4.75**	**5.75**	**6.75**	**7.75**
Cover ft	**A_{si} in^2/ft**				
9	0.0372	0.0713	0.1116	0.15965	0.2139
10	0.0403	0.0775	0.1209	0.17205	0.2294
11	0.0434	0.0837	0.1302	0.18445	0.2465
12	0.0465	0.0899	0.1426	0.19685	0.2635
13	0.0527	0.093	0.1504	0.20925	0.279
14	0.0589	0.1023	0.1612	0.22475	0.2883
15	0.062	0.1116	0.1705	0.2387	0.3069
16	0.0651	0.1147	0.1798	0.25265	0.3224
17	0.0682	0.1209	0.1922	0.2666	0.3379
18	0.0713	0.1302	0.2015	0.3534	0.355
19	0.0744	0.1364	0.2139	0.372	0.4759
20	0.0775	0.1426	0.2232	0.3937	0.496
21	0.0806	0.1519	0.3131	0.4247	0.5208
22	0.0868	0.1581	0.3379	0.4526	0.4154
23	0.0899	0.155	0.2418	0.33325	0.5549
24	0.093	0.1643	0.2511	0.34565	0.5782
25	0.0961	0.1705	0.262	0.4867	0.6665
26	0.0992	0.1767	0.2728	0.5022	0.7037
27	0.1023	0.186	0.2821	0.5332	0.8122
28	0.1054	0.1922	0.2945	0.5797	0.8556
29	0.1085	0.1984	0.4433	0.6448	0.9889
30	0.1116	0.2077	0.4712	0.6789	1.0385

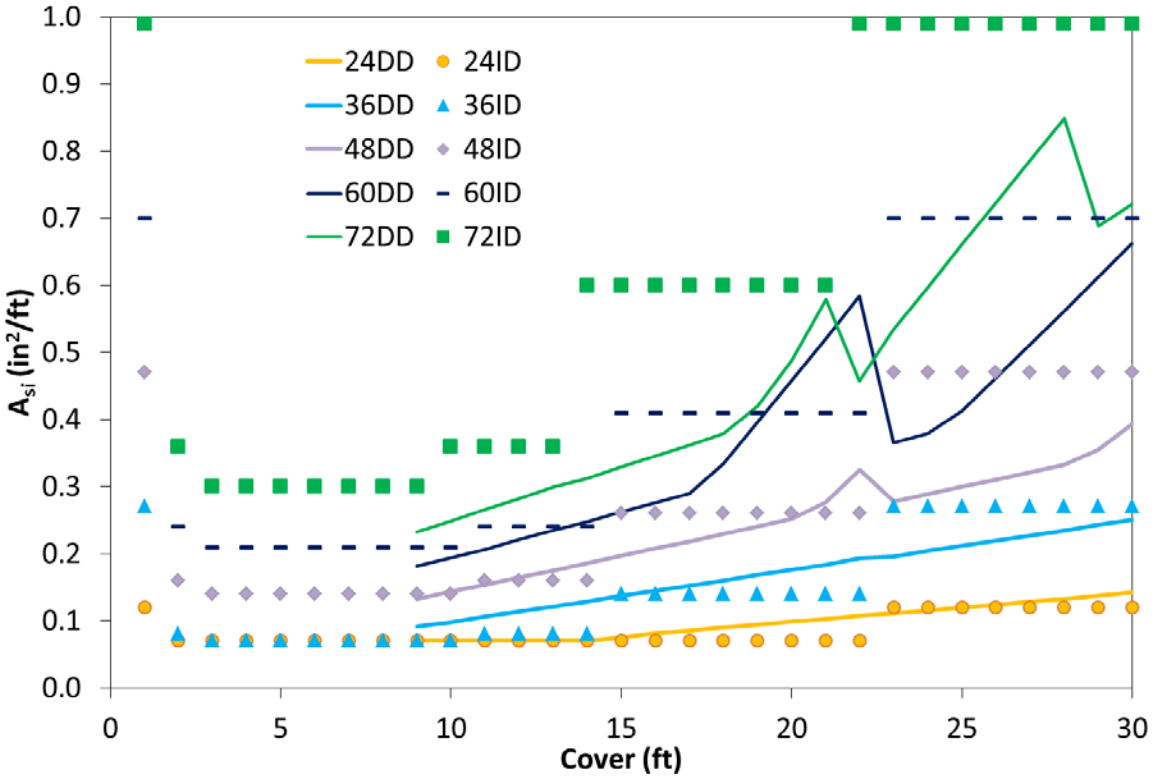

Figure 30. Requirements for inner steel at invert according to ASTM C76 for Indirect Design (Wall C) and current AASHTO requirements for Direct Design (calculated using PipeCar)

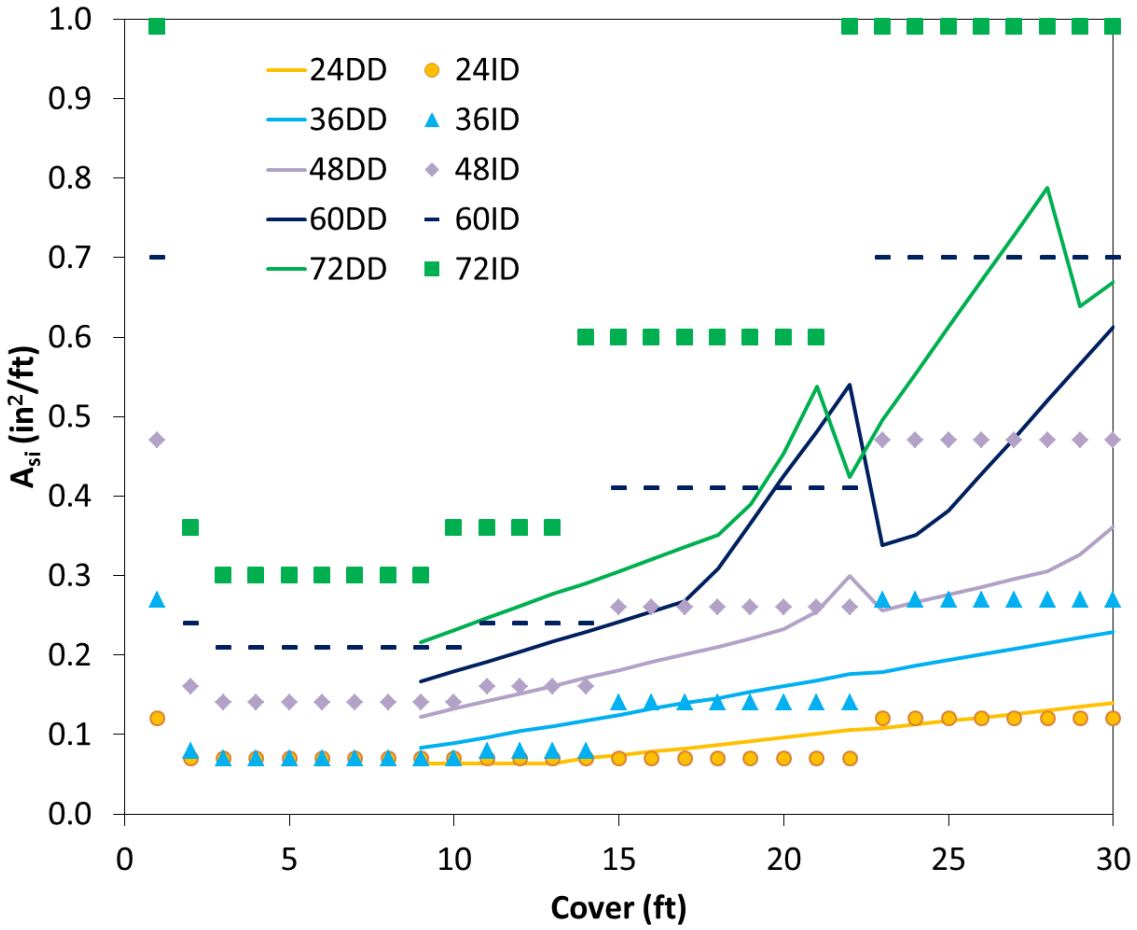

Figure 31. Requirements for inner steel at invert according to ASTM C76 for Indirect Design (Wall C) and current AASHTO requirements for Direct Design modified to account for reductions in moment to account for thick ring behavior.

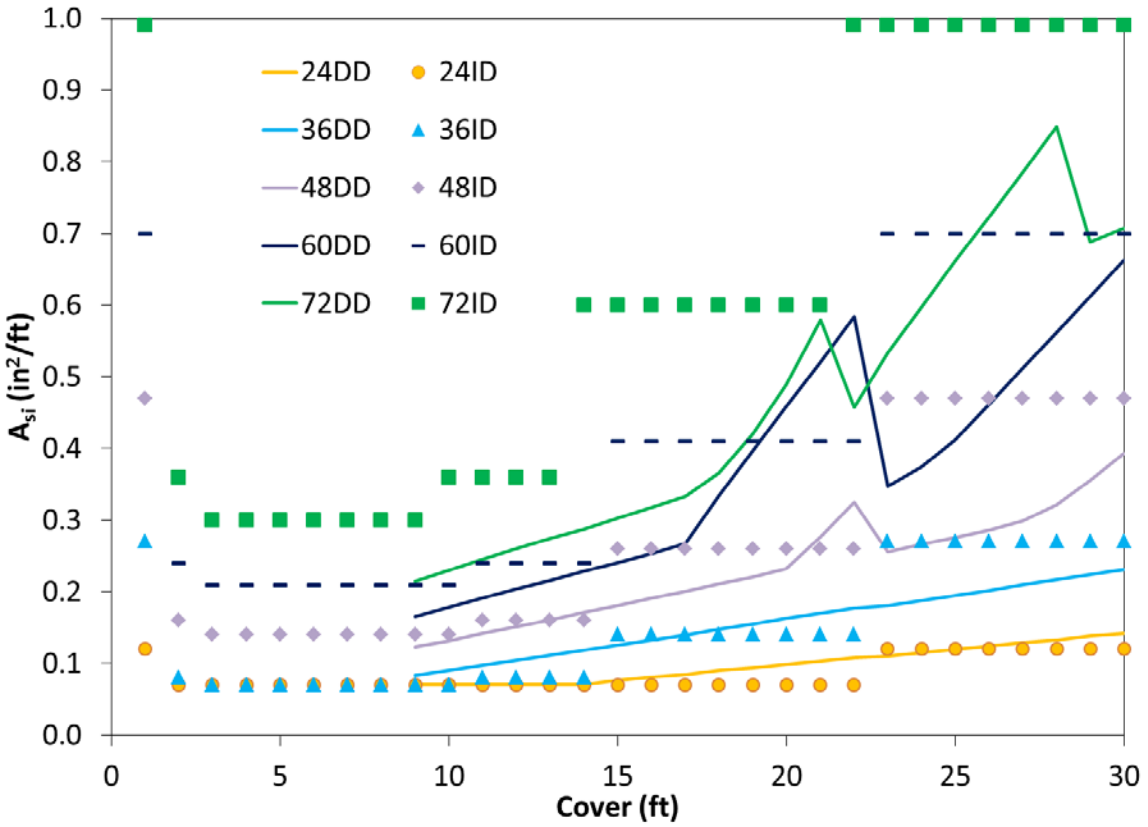

Figure 32. Requirements for inner steel at invert according to ASTM C76 for Indirect Design (Wall C) and current AASHTO requirements for Direct Design modified to account for potential reduction in moment if the steel strain hardens to an ultimate strength of 76 ksi.

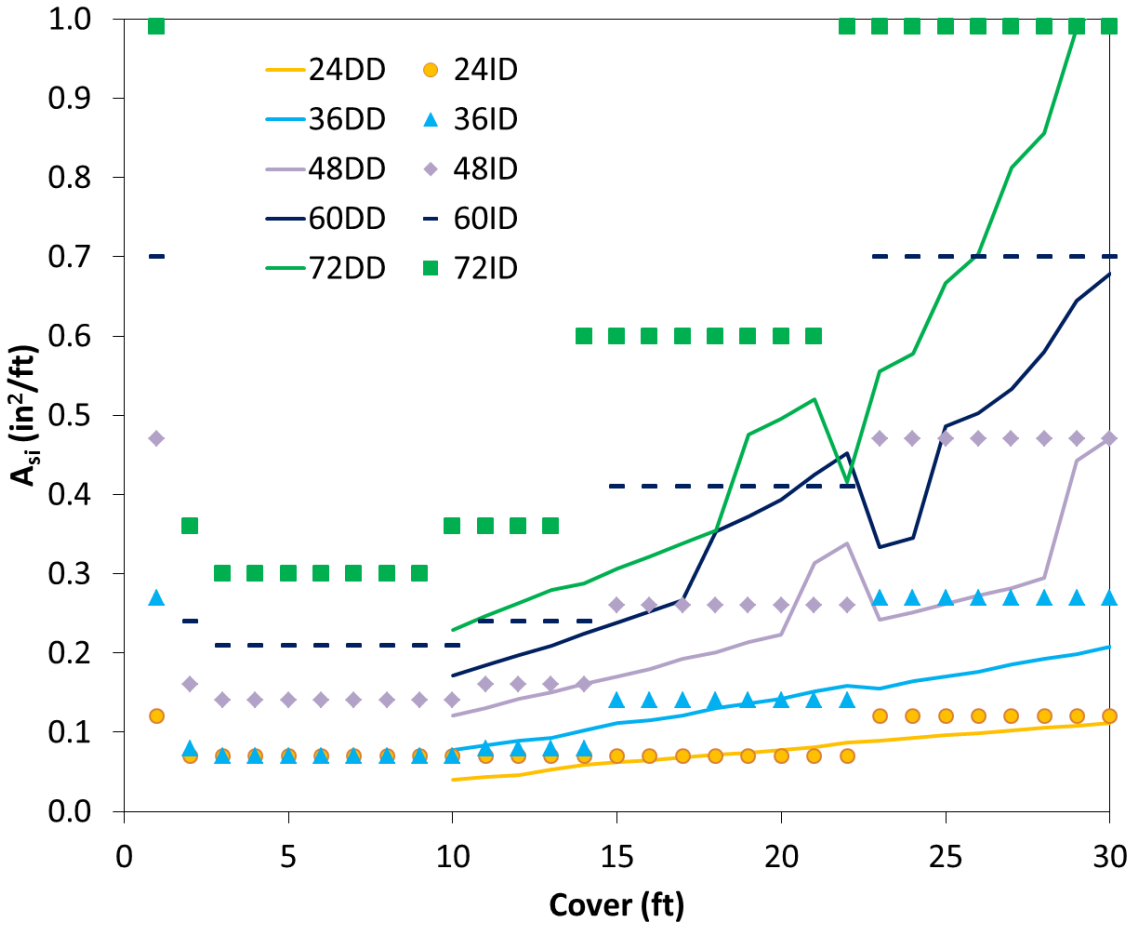

Figure 33. Requirements for inner steel at invert according to ASTM C76 for Indirect Design (Wall C) and current AASHTO requirements for Direct Design modified to employ Modified Compression Field Theory calculations using RESPONSE and two layers of reinforcing steel.

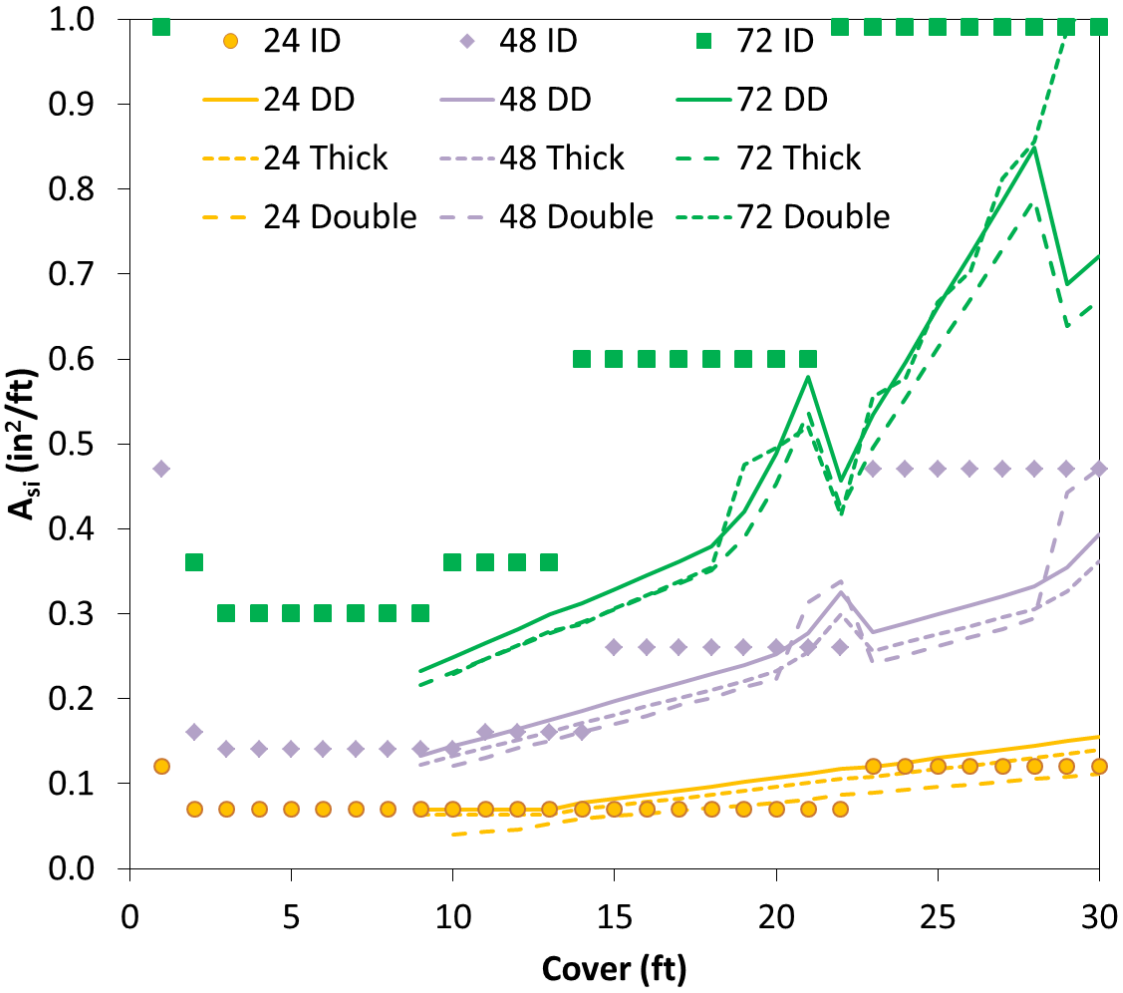

Figure 34. Requirements for inner steel at invert according to ASTM C76 for Indirect Design (Wall C) and current AASHTO requirements for Direct Design and two potential modifications (24 in. and 48 in. and 72in. pipes only).

3.7 Usage guidelines and Design specifications

3.7.1 Overview

Changes to the AASHTO LRFD Bridge Design Specifications are recommended to:

a. Guide usage of the current implementations of Indirect Design and Direct Design
b. Modify calculation of expected live load moments in Direct Design to account for thick ring theory
c. Permit more sophisticated calculations of moment capacity during Direct Design based on the Modified Compression Field Theory
d. Consider load spreading under surface load to the depths of the crown, springline and invert when calculating live load moments at the crown, springline and invert, respectively.

3.7.2 Usage of Indirect Design and Direct Design

The calculations presented in the previous sections show that discrepancies between steel areas associated with Indirect Design and Direct Design pipes under earth loads are resolved if more sophisticated calculations of expected moment and moment capacity are employed. Testing of a 24 in. diameter pipe under simulated deep burial also demonstrated that both Indirect Design and Direct Design produce conservative (safe) estimates of load capacity.

The calculations of the moments expected in shallow buried concrete pipes were compared to moments obtained from measured strains, and these reveal that the Direct Design procedure features conservative estimates of expected moment under vehicle loads at shallow cover. Testing of 24 in. and 48 in. diameter pipes at shallow cover demonstrated that load capacities estimated using Indirect Design and Direct Design are also conservative.

It is recommended therefore that the commentary to the AASHTO LRFD Bridge Design Specifications include reference to these results, supporting the use of whichever design method is most convenient for the user. Therefore, there is no apparent need to prevent use of Indirect Design when it produces more efficient designs relative to Direct Design.

3.7.3 Modification of Expected Moments During Direct Design to Account for Thick Ring Theory

Changes to the AASHTO LRFD Bridge Design Specifications are recommended to incorporate moment correction factors to account for thick ring theory. The recommended changes are given in Appendix D.

3.7.4 Modification of Moment Capacity During Direct Design to Employ Modified Compression Field Theory

Changes to the AASHTO LRFD Bridge Design Specifications are recommended to permit designers to employ more sophisticated estimates of moment capacity during Direct Design. In particular, the use of Modified Compression Field Theory should be mentioned.

3.7.5 Modification of Load Spreading to Consider Depth to Crown, Springline and Invert

Estimates of crown moment resulting from surface loads were reasonable and conservative relative to the moments calculated from measured strains. However, moment estimates at the springline and invert appeared excessively conservative. More consistent estimates of expected invert moment and expected springline result can be obtained considering load spreading down to these specific locations, rather than always calculating load spreading from the surface to the depth of the crown.

CHAPTER 4 CONCLUSIONS AND SUGGESTED RESEARCH

A literature review was undertaken to examine the background of reinforced concrete pipe design and previous comparisons of Indirect Design and Direct Design methods. From that literature review, it was concluded that:

- The degree to which Indirect Design reflects actual buried pipe performance requires assessment, including experimental work for small diameter and large diameter reinforced concrete pipes;
- The performance of Direct Design in estimating the level of moment that develops in buried concrete pipes is unclear, and would benefit from experimental evaluation, both for shallow buried and deeply buried pipes;
- Direct Design examines four different limit states, but would benefit from experimental evaluation to see whether the design method correctly assesses the limit state that controls the performance of shallow buried and deeply buried pipes;
- Modified Compression Field theory might be used to determine the strength limits for reinforced concrete pipe during Direct Design (the moment and shear capacities) instead of the design approximations for flexural and shear strength currently employed; this could include consideration of multiple layers of reinforcing steel and more sophisticated treatment of shear strength;
- Investigation is warranted regarding the level of conservatism that results when the effect of strain hardening in reinforcing steel is neglected during Direct Design.

A program of laboratory testing was undertaken on two 24 in. and two 48 in. diameter pipes in simulations of shallow and deep burial. For those test pipes and the backfill materials and burial conditions examined,

- Indirect Design provided safe estimates of load capacity; the calculated load capacities ranged from 54% to 81% of those observed in the tests;
- Moment estimates during Direct Design based on the ASCE moment factors from two dimensional finite element analysis were conservative; moment estimates at the crown using the LRFD procedures were on average 3 times those observed in the experiments; moment estimates at the springlines were on average 3.6 times those observed in the experiments, and moment estimates at the invert were over 4 times those observed in the experiments;
- Moment estimates at the springline and invert were improved if the load spreading depth was adjusted so that it was the depth of the point in question (i.e. depth to the springline and depth to the invert); this led to a mean ratio of the moment calculation to moment measurement of 2, with a standard deviation of 0.8;

- The capacity limit states predicted using Direct Design were different to the limit states observed during the reinforced concrete pipe tests; in each case, the load capacity was controlled by the service limit (the 0.01 in. crack) instead of flexural failure; the Direct Design estimates of load capacity were between 19% and 77% of the capacities observed during the tests; estimates for 24 in. diameter pipes at shallow cover were 19% and 47% of those observed, whereas estimates for 48 in. diameter pipes were 51% and 71% of the observed strengths; the load capacity calculated for the 24 in. diameter pipe under deep burial was 77% of the design estimate.

Potential changes to the procedures for calculating the ultimate capacity of concrete pipes during Direct Design were examined.

- Expected moments during Direct Design are currently estimated using thin elastic ring theory; since concrete pipes generally have thickness greater than 10% of radius, the use of thin ring theory is conservative; a moment reduction factor that accounts for ring thickness was developed, and its use was examined; the correction is straightforward, and it eliminates some of the discrepancy between required steel areas obtained using Direct Design and Indirect Design;
- Plastic collapse analysis of a buried rigid pipe was examined, where full plastic moment is mobilized at crown, springlines and invert; this calculation procedure would eliminate conservatism associated with Direct Design's matching of maximum elastic moment to moment capacity; however, further work would be required to establish the soil characteristics and earth pressure distributions for each of the standard bedding types (since the pipe would likely respond as a flexible structure once hinges form at the crown, invert and springlines); because the actual load limit seen in the laboratory tests was controlled by the service limit state (the 0.01 in. crack) rather than ultimate strength, the development of the plastic collapse analysis as an alternative to the current approach used during Direct Design is not likely warranted and should not be implemented unless a new procedure that effectively estimates crack widths for specific load levels were implemented;
- Modified Compression Field theory was used to explore how the strength limits for reinforced concrete pipe could be improved during Direct Design, to consider multiple layers of reinforcing steel, strain hardening of the reinforcing steel, and more sophisticated treatment of shear strength; this theory requires iterative calculations that impose compatibility between the layers of steel reinforcing and the concrete;
- Modified Compression Field Theory led to modest reductions in steel requirements when used for a single reinforcing cage in 24 in. and 36 in diameter pipes, with negligible changes for larger structures;

- Modified Compression Field theory for two layers of steel reduced steel requirements for 24 in. diameter pipe by from 24 to 28%, by 18 to 22% for 36 in. diameter pipe, by 11 to 16% for 48 in. diameter pipe, and by less than 12% and 8% for 60 in. and 72 in. diameter pipes.

A comparison of the requirements for area of steel arising from the use of Indirect Design and Direct Design indicated that Direct Design leads to less efficient designs for small diameter structures at shallow cover. Most of that discrepancy is eliminated when thick ring theory is considered (the moment adjustment factor described earlier), and Modified Compression Field Theory is employed, though much of the underlying conservatism of the two procedures would remain. Furthermore, the strength limit tests on shallow buried and deeply buried pipes indicated that both design methods produce conservative estimates of the load capacity of the buried pipe. Therefore, no restrictions are needed on use of Indirect Design and Direct Design. Modifications to the AASHTO LRFD Bridge Design Specifications are proposed, where moment is adjusted to account for thick ring theory, where the commentary specifically mentions the potential for use of Modified Compression Field Theory (at the designer's discretion), and so that the commentary clearly states that both the Indirect Design Method and the Direct Design Method can be employed, at the designer's discretion.

Additional research is recommended to examine the performance of the Indirect Design and Direct Design Methods for large diameter pipes, since testing in the current project was restricted to 24 in. and 48 in. diameter structures. In particular, buried pipe tests in the laboratory for pipes of 60 in. and 72 in. diameter would enable the levels of safety associated with the two design methods to be directly evaluated for these important structures. Other testing that measures the load capacity of buried pipes in other installation conditions would also be of value (the current project examined Type 2 installations only).

It would be valuable to conduct research studies to determine the relationship between crack width and reinforced concrete pipe durability so that the effect of crack width on service life and long term pipe performance can be determined. This research may provide appropriate recommendations for modifications to Direct Design and Indirect Design based on a defined long term performance and limit state condition. Additionally, it could provide guidance for Engineers to evaluate cracks between 0.01" and 0.10" as specified in the AASHTO Bridge Construction Specification Section C27.6.4 or set new width limits based on the defined long term performance condition. However, these studies will likely be complex and time consuming involving work to determine:

- how much deterioration can be tolerated in a reinforced concrete pipe (i.e. answering the question 'how much deterioration is too much deterioration?'), so that the end of service life can

be established (currently there is little information on the effects of deterioration on pipe strength)

- the service life based on relationships between rates of pipe deterioration and crack width, cover depth, total wall thickness, single versus multiple layers of reinforcement, soil conditions (e.g. resistivity), stormwater and groundwater conditions (e.g. salinity), cement and concrete properties and other factors that may influence performance.

ACKNOWLEDGEMENTS

The pipe samples tested in the project were provided by M-CON Products Ltd. of Ottawa, Ontario and Hanson Pipe and Precast of Cambridge, Ontario. We acknowledge the excellent contributions of Graeme Boyd and Brian Westervelt of Queen's University who undertook most of the earthworks and pipe loading, and assisted with the data acquisition, and Trevor Smith who assisted with specimen preparation and who undertook the interpretation of crack widths.

REFERENCES

ACPA (1971). CP Info - Effects of Cracks in Reinforced Concrete Sanitary Sewer Pipes. American Concrete Pipe Association.

ACPA (1976). CP Info - Effects of Cracks in Reinforced Concrete Culvert Pipe. American Concrete Pipe Association.

ACPA (1978) CP Info - Significance of Cracks in Concrete Pipe. American Concrete Pipe Association.

ACPA (1998). Concrete Pipe Design Manual. American Concrete Pipe Association, USA.

ACPA (2007). CP Info – Crack in Installed Reinforced Concrete Pipe. American Concrete Pipe Association.

ACPA (2012). Brief History of ACPA. Retrieved September 26, 2012, from American Concrete Pipe Association: http://www.concrete-pipe.org/pages/history.html

AASHTO (2007) Load and Resistance Factor Design (LRFD) Bridge Design Specifications, 4th Edition, American Association of State Highway and Transportation Officials, Washington, D.C..

AASHTO (2013). AASHTO LRFD Bridge Design Specifications, 6th Edition, 2013 Interim Revisions. AASHTO, Washington, D.C.

ASTM C76-11 (2011) Standard Specification for Reinforced Concrete Culvert, Storm Drain, and Sewer Pipe. ASTM International, 100 Barr Harbor Drive, PO BoxC700, West Conshohocken, PA, 19428-2959 USA

ASTM C497-13 (2013) Standard Test Methods for Concrete Pipe, Manhole Sections or Tile. ASTM International, 100 Barr Harbor Drive, PO BoxC700, West Conshohocken, PA, 19428-2959 USA

ASTM D6938-10 (2010) Standard Test Method for In-Place Density and Water Content of Soil and Soil-Aggregate by Nuclear Methods (Shallow Depth), ASTM International, 100 Barr Harbor Drive, PO BoxC700, West Conshohocken, PA, 19428-2959 USA

Becerril Garcìa, D. (2012) Investigation of Culvert Joints Employing Large Scale Tests and Numerical Simulations, PhD Thesis, Department of Civil Engineering, Queen`s University, Kingston, Ontario.

Bentz, E.C. (2000). Sectional analysis of reinforced concrete members. PhD dissertation, University of Toronto, 2000.

Brachman, R.W.I., Moore, I.D. and Rowe, R.K. (2000). The design of a laboratory facility for evaluating the structural response of small-diameter buried pipes. Canadian Geotechnical Journal, Vol. 37, pp. 281-295.

Brachman, R.W.I., Moore, I.D. and Rowe, R.K. (2001). The performance of a laboratory facility for evaluating the structural response of small diameter buried pipes. Canadian Geotechnical Journal, Vol. 38, pp. 260–275.

Brown, Glenn. (2002). The History of the Darcy-Weisbach Equation for Pipe Flow Resistance. Environmental and Water Resources History 2002. ASCE 2004.

Burns J.Q. and Richard R.M. (1964). Attenuation of stresses for buried cylinders. Arizona University – Symposium of Soil-Structure Interaction – Proceedings (pp. 378-392)

Canadian Standards Association (CSA). 2004. Design of concrete structures, CSA A23. 3–04. CSA, Rexdale, Ontario.

Collins, M. P. (1978). Towards a rational theory for RC members in shear. Journal of the Structural Division, 104(4), 649-666.

Collins, M.P. and Mitchell, D. 1997. Prestressed Concrete Structures, Response Publications, Toronto, 766 pp.

Concrete Pipe Design Manual. (2011). American Concrete Pipe Association.

CSA (2006). Canadian Highway Bridge Design Code, CAN/CSA-S6-06. CSA, Rexdale, Ontario.

CSA (2009). A257 Series-09 Standards for concrete pipe and manhole sections. Canadian Standards Association.

Erdogmus, E. and Tadros, M. (2006).Behavior and Design of Buried Concrete Pipe.Nebraska Department of Roads.

Erdogmus, E. and Tadros, M. (2009).Behavior and Design of Buried Concrete Pipes Phase II - Final Report.Nebraska Department of Roads.

Erdogmus, E., Skourup, B.N., and Tadros, M. (2010) Recommendations for Design of Reinforced Concrete Pipe, Journal of Pipeline Systems Engineering and Practice, ASCE, Vol. 1, No. 1, pp. 25-32.

Heger, F. J. (1982). Structural Design Method for Precast Reinforced-Concrete Pipe.Transportation Research Record, 93-100.

Heger, F. J., & McGrath, T. (1984).Crack Width Control in Design of Reinforced Concrete Pipe and Box Sections. Journal of the American Concrete Institute, 81(2), 149-157.

Heger, F. J., & McGrath, T. J. (1982).Shear Strength of Pipe, Box Sections, and Other One-Way Flexural Members.79, 470-483.

Heger, F. J., & McGrath, T. J. (1983).Radial Tension Strength of Pipe and Other Curved Flexural Members. Journal of the American Concrete Institute, 80(1), 33-39.

Heger, F. J., & Liepins, A. A. (1985).Stiffness of Flexurally Cracked Reinforced Concrete Pipe.Journal of the American Concrete Institute, 82(3), 331-342.

Heger, F.J. (1988). New Installation Design for Buried Concrete Pipe.Pipeline Infrastructure. Proceedings of the Conference Sponsored by the Pipeline Division of the American Society of Civil Engineers.

Heger, F.J., Liepins A.A., Selig, E.T. (1985) SPIDA: An Analysis and Design System for Buried Concrete Pipe. Advances in Underground Pipeline Engineering. Proceedings of the International Conference sponsored by the Pipeline Division of the American Society of Civil Engineers.

Heger, F.J., McGrath T.J. (1980) Design Method for Reinforced Concrete Pipe and Box Sections. Transportation Research Board

Hoeg, K. (1968) Stresses against underground structural cylinders. American Society of Civil Engineers Proceedings, Journal of the Soil Mechanics and Foundations Division July, 1968 (pp.833-858)

Janssen, H.A. (1895). Versuche über Getreidedruck in Silozellen. Zeitschrift des Vereinesdeutscher Ingenieurs.

Lay, G.R. (2012) Response of reinforced concrete and corrugated steel pipes to surface load. Master's Thesis, Department of Civil Engineering, Queen's University, Kingston, Ontario.

Lougheed, A. C. (2008). Limit State Testing of a Buried Deep-Corrugated Large-Span Box Culvert, MASc thesis, Department of Civil Engineering, Queen's University, Kingston On., Canada.

Marston, A., Anderson, A.O. (1913). The theory of loads on pipes in ditches and tests of cement and clay drain tile and sewer pipe. Iowa State College of Agriculture

McGrath, T.J. Tigue, D.B., Heger, F.J. (1988). Pipecar and BOXCAR – Micro Computer Programs for the Design of Reinforced Concrete Pipe and Box Sections. Presented to the January 1988 Annual Meeting of Transportation Research Board (TRB), Washington, D.C.

Moore, I.D. (2012) Large-scale laboratory experiments to advance the design and performance of buried pipe infrastructure, 2nd International Conference on Pipelines and Trenchless Technology, ASCE-China University of Geosciences, Wuhan, China, 11pp, October.

Moore, I.D., Becerril Garcia, D., Sezen, H. and Sheldon, T. (2012) Structural design requirements for culvert joints, NCHRP Web-only document 190, Contractor's Final Report for NCHRP Project 15-38, April 2012 Transportation Research Board, Washington D.C., 387 pp.

Moser, A. (2001). Buried Pipe Design. McGraw-Hill.

OCPA (2010). Concrete Pipe Design Manual, Ontario Concrete Pipe Association, http://www.ocpa.com/_resources/OCPA_DesignManual.pdf

Olander, H.C. (1950). Stress Analysis of Concrete Pipe. United States Department of Interior Bureau of Reclamation.Denver Federal Center. Denver, Colorado

Ontario Concrete Pipe Association. (2011). Ontario Concrete Pipe Association. Retrieved from

Paris, J.M. (1921) Stress Coefficients for large horizontal pipes.Engineering News-Record v87, p768-771.

Petersen, D.,L., Nelson, C.R., Li, G., McGrath, T.J., and Kitane, Y. (2010) Recommended Design Specifications for Live Load Distribution to Buried Structures, 85pp.

Sargand, S.M., Hazen, G.A., Vaithianathan, E, and Hurd, J.O. (1995) Performance verification of a concrete pipe, Concrete International, July, pp. 23-27.

Simpson, Gumpertz & Heger Inc. (2004). PIPECAR. A Computer Program for the Analysis and Design of Circular and Horizontal Elliptical Reinforced Concrete Pipe Culverts.

Spangler, M.G. (1933).The Supporting Strength of Rigid Pipe Culverts, Bulletin 112, Iowa State College.

Standard Practice for Direct Design of Buried and Precast Concrete Pipe Using Standard Installation. (1998). Reston, Virginia: American Society of Civil Engineers.

Tognon, A.R., Rowe, R. K., and Brachman, R.W.I. (2009) Evaluation of side wall friction for a buried pipe testing facility, February 1999. Geotextiles and Geomembranes, 17: 193-212.

Vecchio, F. J., and Collins, M. P. 1986. The modified compression-field theory for reinforced concrete elements subjected to shear. ACI J., 83(2), 219-231.

White D.J. and Take W.A. (2002) GeoPIV: Particle Image Velocimetry (PIV) software for use in geotechnical testing. October 2002. Cambridge University Engineering Department.

Wong, L.S., Allouche, E.N., Dhar, A.S., Baumert, M. and Moore, I.D. (2006). Long term monitoring of SIDD Type IV installations, Canadian Geotechnical Journal Vol. 43, 392–408.

Zhao, J. Q., and Daigle, L. (2001). SIDD pipe bedding and Ontario Provincial Standards. Institute for Research in Construction, National Research Council Canada, Ottawa, Canada.

Appendix A. Thick ring theory

A.1 Introduction

Current design calculations for reinforced concrete pipes employ thin ring theory. However, reinforced concrete pipes often have a wall thickness that is significantly larger than 10% of the pipe radius. As a result, conservative values of bending moment for smaller diameter pipes where this ratio is higher may be the result. Finite element analysis has therefore been used to evaluate how moment values might be adjusted to account for thick ring theory. The following appendix commences with the use of results for thick rings presented in Roark's Formulas for Stress and Strain (Young and Budynas, 2002). It then reports on the results of finite element calculations for pipes under the Paris earth pressure distribution. A simple linear design approximation is provided where moments can be adjusted as a function of the ratio of pipe thickness to radius.

A.2 Moment in thick rings from Roark's Formulas for Stress and Strain

Young and Budynas (2002) provide results for stresses at the inner and outer surface at the crown and springlines of a thick ring under opposing vertical forces. Table A-1 provides details of the calculations. The solutions for circumferential stress σ provided by Young and Budynas (2002) are based on a stress coefficient K where

$$\sigma = K\frac{2p}{\pi b} \qquad \text{A-1}$$

and are given for vertical force *p* and various ratios of inner ring diameter, a, and outer ring diameter, b. Values reported for a/b of 0.6 and 0.7 are provided in Table A-1, and are used to estimate the moment change relative to that of a thin ring.

If stresses are assumed to vary linearly through the ring thickness, then the inner and outer values at the crown and springline can be used to estimate the moment, M normalized by force *p* and average radius *R*, where

$$\frac{M}{pR} = \Delta K \frac{2}{\pi b R} \frac{d^2}{12} = \frac{\Delta K}{3\pi} \frac{(1-\frac{a}{b})^2}{(1+\frac{a}{b})} \qquad \text{A-2}$$

and ring thickness $d = b\text{-}a$. This expression has a value of $\frac{1}{\pi} = 0.31831$ at the crown of a thin ring, and $\frac{1}{\pi} - \frac{1}{2} = -0.18169$ at the springline. Ratios of the thick ring moment divided by the thin ring value can then be determined. The thick ring moment value decreases below the thin ring value at the crown, and increases at the springlines. Linear approximations can then be determined for use in correcting the moments obtained from thin ring theory:

$$\left.\frac{M}{M_{thin}}\right|_{crown} = 1 - 0.373\frac{t}{R} \qquad \text{A-3}$$

$$\left.\frac{M}{M_{thin}}\right|_{springline} = 1 + 0.18\frac{t}{R} \qquad \text{A-4}$$

Those linear estimates of the moment adjustment factor are included in Table A-1. These reveal that the linear moment correction adjustments provide reasonable estimates of moment change (within a few percent of the theoretical value).

Table A-1: Stresses and moments in a thick ring calculated using stress coefficient

	a/b	0.6	0.7	1
Stress coefficient K Young and Budynas (2002)	springline inner	-12.9	-21.4	-
	crown inner	16	31	-
	springline outer	5.8	13.1	-
	crown outer	-8.4	-19	-
t/R= 2(1-a/b)/(1+a/b)		0.5	0.353	0
Crown	Moment	0.2589	0.2808	0.3183
	M/M_{thin}	0.813	0.883	1
	1-0.373 t/R	0.814	0.901	1
Springline	Moment	-0.1984	-0.1938	-0.1817
	M/M_{thin}	1.092	1.067	1
	1+0.18 t/R	1.090	1.064	1

A.3 Moments in thick rings obtained using finite element analysis

Finite element analysis was then used to evaluate how moment estimates are influenced by the thickness of the ring for a buried pipe. Table A-2 summarizes the results of calculations performed for three different pipe thicknesses: t/R=0.04, 0.1 and 0.4. In each case, the pipes featured a unit value of average radius R=1 (e.g. for the thickest pipe, the inner radius was 0.8 and the outer radius was 1.2). The Paris earth pressure distribution has then been employed:

- a uniform vertical stress was applied across the top of the pipe (representing the effect of overburden stress times vertical arching factor)
- a uniform vertical stress three times larger was applied across the middle third of the bottom half of the pipe (to represent the effect of poor haunch soil beside the bedding soil)
- a lateral stress equal to 30% of the vertical stress is applied to both sides of the structure (from the crown to the invert)

The moments have been calculated in two ways. First, stress values near the inner and outer surfaces of the pipe have been used together with a linear approximation through the pipe wall.

Secondly, moment has been calculated considering the nonlinear distribution of stress through the pipe wall (like that shown in Figure A-1 for the thickest pipe, t/R=0.4). The nonlinear calculations produce a reduced value of moment (about 2% less for the thickest pipe). In each case, the moments were then divided by a correction to account for the fact that the external boundary of the pipe is larger for the thicker pipes.

Values of moment were then normalized using the moment for the thinnest pipe examined, t/R=0.04 (denoted $M/M_{0.04}$). This indicates that $M/M_{0.04}$ reduces to 98% when t/R=0.1, and 85% or 87% for t/R=0.4, depending on whether linear or nonlinear moment values are employed.

Table A-2: Moments in a thick ring subjected to the Paris pressure distribution obtained using finite element analysis

t/R	0.04	0.1	0.4
crown stress inner	675	112.0	7.046
crown stress outer	-581	-105.4	-7.274
distance apart	0.0337	0.0901	0.3713
Moment (linear)	0.199	0.201	0.203
Moment/(1+0.5t/R)	0.195	0.191	0.169
$M/M_{0.04}$	1	0.982	0.866
Moment (nonlinear)	0.198	0.201	0.199
Moment/(1+0.5t/R)	0.195	0.191	0.166
$M/M_{0.04}$	1	0.982	0.851
1-0.373 t/R	0.985	0.963	0.851

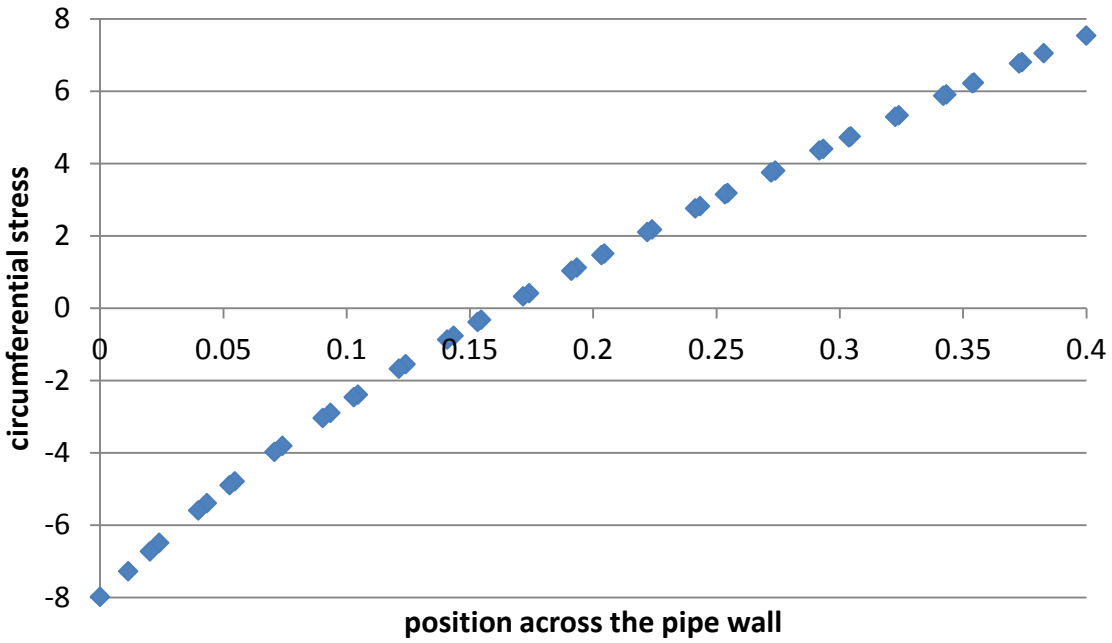

Figure A-1. Nonlinear distribution of circumferential stress across the pipe wall at the crown obtained using finite element analysis (thick pipe, t/R=0.4).

The final row of the table provides values of linear adjustment factor given by equation A-3. This provides corrections that are close to those suggested by the normalized moments $M/M_{0.04}$. Since equation A-3 gives a value of 0.985 when t/R=0.04, the normalized moments $M/M_{0.04}$ are somewhat greater in magnitude than M/M_{thin}, addressing some of the differences seen for t/R=0.1. It indicates that moment reductions for thick rings obtained from equation A-3 are close to those obtained from the finite element calculations, and it appears reasonable to employ the adjustment factors derived from thick rings under opposing vertical forces, rather than developing a slightly different alternative from the finite element calculations.

References

Young, W.C. and Budynas, R.G. 2002. Roark's Formulas for Stress and Strain, McGraw-Hill, New York, NY.

Appendix B. Plastic Collapse Analysis

B.1 Introduction

A potential method for assessing the ultimate capacity of reinforced concrete pipes is to use an upper bound plasticity approach, Heger (1962). To do this, the plastic collapse mechanism for a reinforced concrete pipe must be developed. If the correct mechanism is not selected, an unconservative estimate of the pipe capacity will be calculated. However, due to its geometry, the collapse mechanism for a concrete pipe under standard loading is always the same and involves the development of four plastic hinges (at the crown, invert and springlines) as illustrated in Figure B.1.

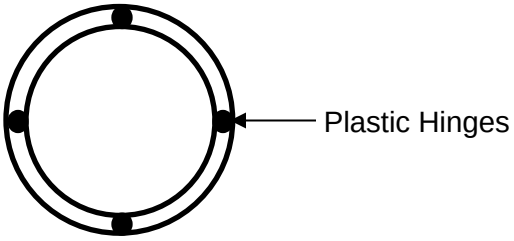

Figure B.1 – Plastic collapse mechanism

B.2 Plastic Collapse Mechanism

In order to develop the work balance for use with this plastic collapse mechanism, both the external work (force acting through a displacement) and internal work (moment acting through a rotation) must be calculated. To do this, tangent lines can be drawn to the pipe at each hinge, which will allow the rotation at each hinge to be determined with respect to the displacement. These lines will also allow the displacement through which the projected vertical and horizontal forces act to be determined. The schematic of the proposed plastic collapse mechanism is shown

in Figure B.2. The tangent lines before rotation are represented by grey dashed lines and the tangent lines after rotation are represented by solid black lines. The outline of the undeformed pipe is also shown for reference.

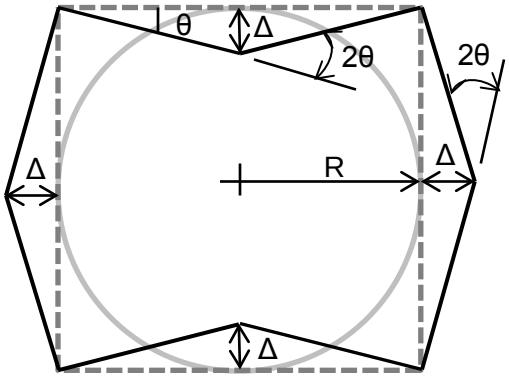

Figure B.2 – Plastic collapse mechanism geometry

Using Figure B.2, the internal work, IW, for the concrete pipe can be expressed in terms of the plastic moment capacity at each hinge, M_p, and the rotation at each, 2θ, as given by equation B-1 (Heger, 1962, considered a similar mechanism, but considered a pair of forces at the invert which lead to a more complex result that is not likely justified by the small error associated with considering a single invert force).

$$IW = M_{pcrown} \times 2\theta + M_{pinvert} \times 2\theta + 2M_{psspringline} \times 2\theta \qquad \text{B-1}$$

By making the assumption that the rotations at each hinge are relatively small compared to the pipe radius, small angle theory can be applied allowing the angle to be related to the displacement as given in equation B-2.

$$\theta = \frac{\Delta}{R} \qquad \text{B-2}$$

In equation B-2, the radius, R, is taken as the distance from the longitudinal axis of the pipe to the centerline of the pipe wall. Finally, by assuming the plastic moment capacities at the crown and the invert are the same, equation B-1 can be rewritten as equation B-3.

$$IW = 4M_{pcrown}\frac{\Delta}{R} + 4M_{psringline}\frac{\Delta}{R} \qquad \text{B-3}$$

The external work varies depending on the loading scenario. For example, for a three edge bearing test, as seen in Figure B.3 (with invert forces represented as a single total force value), the external work, EW, can be approximated using equation B-4.

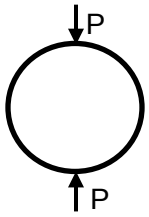

Figure B.3 – Three edge bearing test loading approximation

$$EW = 2P\Delta \qquad \text{B-4}$$

Using conservation of energy (equating internal and external work), the load P required to cause failure of the pipe can be calculated using equation B-5.

$$2P\Delta = 2M_{pcrown}\frac{\Delta}{R} + 2M_{psringline}\frac{\Delta}{R}$$

$$P = \frac{2M_{pcrown}}{R} + \frac{2M_{psringline}}{R} \qquad \text{B-5}$$

The external work mechanism for a pipe under pure soil loading requires an assumption to be made about the soil stress distribution. In the current work the pressure distribution proposed by Paris (1912) is used and given in Figure B.4.

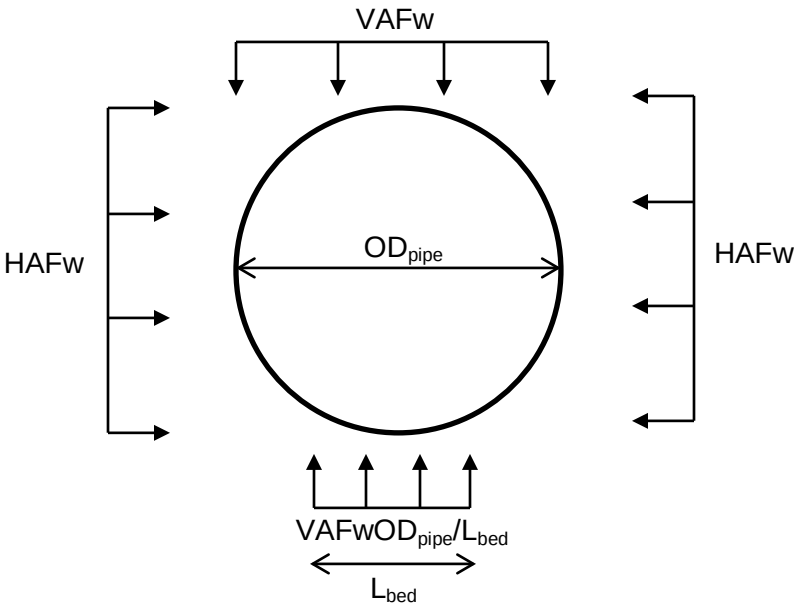

Figure B.4 – Paris pressure distribution

Using the pressure distribution in Figure B.4, the external work, EW, can be calculated using equation B-6.

$$EW = \frac{VAFw \times D_{pipe} \times \Delta}{2} + VAFw \times D_{pipe} \times \Delta\left(\frac{1}{2} + \frac{D_{pipe} - L_{bed}}{2D_{pipe}}\right) - HAFwD_{pipe}\Delta$$

$$EW = VAF \times w \times D_{pipe} \times \Delta\left(1 + \frac{D_{pipe} - L_{bed}}{2D_{pipe}} - \frac{HAF}{VAF}\right) \qquad \text{B-6}$$

The applied load, *w*, can be due to both earth and vehicle loads (depending on the load spreading). The length of bedding, L_{bed}, depends on the assumed bedding conditions and the vertical arching factor, *VAF*, and the horizontal arching factor, *HAF*, are taken as 1.35 and 0.45, respectively. The total applied load, *w*, can be calculated by setting equations B-3 and B-6 equal to each other resulting in equation B-7.

$$VAF \times w \times D_{pipe} \times \Delta\left(1 + \frac{D_{pipe} - L_{bed}}{2D_{pipe}} - \frac{HAF}{VAF}\right) = 4M_{pcrown}\frac{\Delta}{R} + 4M_{psringline}\frac{\Delta}{R}$$

$$w = \frac{4M_{pcrown} + 4M_{psringline}}{VAF \times D_{pipe} \times R\left(1 + \frac{D_{pipe} - L_{bed}}{2D_{pipe}} - \frac{HAF}{VAF}\right)} \qquad \text{B-7}$$

B.3 Evaluation of Three Edge Bearing Test Capacity

As part of the current investigation, three edge bearing tests to failure were performed on two specimens: a 48” class III B-wall (T-48-B) and a 48” class III C-wall (T-48-C). The material properties and geometry are given in Table B-1 for each specimen. The radius for each pipe is calculated as the distance from the longitudinal centreline of the pipe to the centre of the wall. Also included in Table B-1 are three estimates of the plastic moment capacity, which were all determined using a reinforced concrete sectional analysis program called Response-2000 (Bentz, 2000). The first value, M_{py}, is the plastic moment capacity of one pipe length (2440 mm) assuming only the steel yield strength is achieved. The second value, M_{pu}, is the plastic moment capacity of one pipe length assuming the steel reaches its ultimate strength. The third value,

$M_{puaxial}$, is the plastic moment capacity of one pipe length that can be achieved in the presence of a compressive axial force. The axial force was calculated through trial and error as the point where the applied force, P, produced by equation B-5 and the axial compressive force, P/2, required to calculate $M_{puaxial}$ converged to the same value of P.

Table B-1: Material and geometric properties for the three edge bearing test specimens

	T-48-B	T-48-C	D-24-C
f'_c, psi (MPa)	8350 (57.6)	8350 (57.6)	10150 (70)
f_y, ksi (MPa)	70.3 (485)	70.3 (485)	86.3 (595)
f_u, ksi (MPa)	79.8 (550)	79.8 (550)	90.6 (625)
t, in (mm)	5 (127)	5.75 (146)	3.75 (95)
R, in (mm)	26.5 (673)	26.9 (683)	13.9 (352)
A_s, in^2 (mm^2)	0.04 (25.8)	0.04 (25.8)	0.025 (16.1)
s, in (mm)	2 (51)	2.67 (68)	3 (76)
M_{py}, kip.ft (kNm)	51.6 (70)	46.5 (63)	See sec. B.4
M_{pu}, kip.ft (kNm)	53.8 (73)	50.9 (69)	See sec. B.4
$M_{puaxial}$, kip.ft (kNm)	62.7 (85)	60.5 (82)	See sec. B.4

Equation B-5 was then used to determine the load required to fail the pipe in a three edge bearing test using three combinations of the plastic moment capacity: (i) M_{py} at all 4 hinges (P_y), (ii) M_{pu} at all 4 hinges (P_u) and (iii) M_{pu} at the crown / invert and $M_{puaxial}$ at the springlines (P_{uaxial}). The results of each analysis are presented in Table B-2 as well as the actual maximum load applied to the pipes during the three edge bearing test (P_{exp}) and the ratio of the predicted to experimental capacity (Pred / Exp).

Table B-2: Estimated and experimental plastic collapse loads for three edge bearing tests

Pipe	P_{exp} kips (kN)	P_y kips (kN)	P_y / P_{exp}	P_u kips (kN)	P_u / P_{exp}	P_{uaxial} kips (kN)	P_{uaxial} / P_{exp}
48in B wall	119 (530)	93 (416)	0.78	98 (434)	0.82	106 (470)	0.89
48in C wall	110 (489)	83 (368)	0.75	91 (404)	0.83	99 (440)	0.90

From Table B-2 it can be seen that assuming the yield strength of the steel governs the moment capacity leads to a conservative estimate of the failure load. Using a moment based on the ultimate strength of the steel improves the accuracy of the estimate while accounting for the effects of axial load at the springlines leads to an accurate yet conservative estimate of the ultimate limit state capacity.

B.4 Evaluation of Deep Burial Pipe Capacity

A 24" specimen with the properties given in Table B-1 (denoted D-24-C) that was 1.95 m long rather than 2.44 m was tested under simulated deep burial loading. The test was stopped at an applied load of 750kPa, which had caused cracks of the order of 1 mm to develop at the crown and the invert. Although the pipe was not taken to its ultimate limit state, the results of this test will be used to evaluate the plastic collapse model. In order to use equation B-7, values for VAF, HAF and L_{bed} are required. These values were assumed to be VAF = 1.35, HAF = 0.45 and Lbed was taken as taken as half of the pipe diameter (0.4 m). Equation B-7 was then used to determine the applied load required to fail the pipe using three combinations of the plastic moment capacity: (i) M_{py} at all 4 hinges (w_y), (ii) M_{pu} at all 4 hinges (w_u) and (iii) M_{pu} at the crown / invert and $M_{puaxial}$ at the springlines (w_{uaxial}). M_{py} and M_{pu} were taken as 6.1 kNm and 6.4 kNm, respectively, for a unit length of pipe. The value for $M_{puaxial}$ at the springlines and the crown / invert was determined using trial and error, resulted in values of 11.7 and 8.2 kNm, respectively. The results of each analysis are given in Table B-3 along with the ratio of the predicted value to the experimental capacity (assumed to be 750 kPa in this case).

Table B-3: Estimated and experimental plastic collapse loads for deep burial experiment

	VAF = 1.35, HAF = 0.45						VAF=1.13, HAF=0.54	
w_{exp} psi (kPa)	w_y psi (kPa)	w_y / w_{exp}	w_u psi (kPa)	w_u / w_{exp}	w_{uaxial} psi (kPa)	w_{uaxial} / w_{exp}	w_{uaxial} psi (kPa)	w_{uaxial} / w_{exp}
109 (750)	202 (139)	0.19	202 (146)	0.19	326 (225)	0.3	1340 (925)	1.23

Table B-3 indicates that there is not a significant difference between using a plastic moment capacity based on the yield strength or the ultimate strength. Accounting for the axial force acting on the hinge offers considerable benefit in terms of the predicted capacity; however, the results still fall well short of the actual pipe capacity. The three main variables that can affect this estimate are the VAF, HAF and L_{bed}. In terms of VAF, this value is potentially overestimated given the boundary conditions of the pressure cell test. The HAF and L_{bed} are potentially underestimated as the fill material was well compacted and the pipe was installed with a great deal of care. To gain some insights into the sensitivity of the model to these parameters, a second analysis was run with a VAF = 1.13 (a 20% decrease), HAF = 0.54 (a 20% increase) and L_{bed} = OD_{pipe}. The resulting pressure, $w_{uaxial,}$ was 925 kPa, which is greater than the applied pressure reached during the experiment although it is worth noting that the pipe did not fail at that

pressure. The results to this point suggest that the model may have merit although careful thought needs to be given to the correct choice of backfill parameters. This is the subject of ongoing investigation.

References

Bentz, E.C. (2000). Sectional Analysis of Reinforced Concrete Members. Ph.D. Dissertation, University of Toronto, Toronto, Ontario, Canada.

Heger, F. (1962). A theory for the structural behavior of reinforced concrete pipe, DSc thesis, M.I.T., Cambridge, MA, USA.

Paris, J.M. (1912). Stress Coefficients for Large Horizontal Pipes. Engineering News Record, 87(19), 768-771.

Appendix C. Measurement of crack widths using PIV

An analysis was conducted to determine crack widths using particle image velocimetry (PIV). In this technique, digital images are taken of an object as load is applied to it. By comparing images at a given load stage to a reference image of the unloaded object, displacements of regions of interest within the image, known as subsets or patches, can be tracked. In the current research a PIV software package developed in Matlab specifically for geotechnical applications, known as GeoPIV, was used (White et al. 2003) to measure these displacements. The use of this technique has significant advantages over conventional methods:

- use of a crack width gauge requires human access into the pipe during testing, something best avoided given the high surface loads being employed
- use of an extensometer attached to points fixed to the inner surface of the pipe requires advance knowledge of the crack location if the extensometer is to be attached close to either side of the crack or temporary halting of the test to fix the extensometer once the crack has initiated; the accuracy of the measurement could also be influenced by rotations of the pipe segments on either side of the crack, since the length reading is made above (not directly on) the surface

Two cameras were set up, as illustrated in Figure C-1, to capture images of the crown and invert of each reinforced concrete pipe specimen during shallow cover and D-load testing.

Figure C-1: Experimental Set Up of Cameras

Images taken at loading increments of approximately 50kN of applied load were analysed using GEOpiv. To perform the analysis, the locations of the patches need to be selected. Since a PIV analysis can be performed once the test is completed, a priori knowledge of the crack location can be used to determine the required locations for the subsets to measure the crack width. A typical patch arrangement used in this analysis is shown in Figure C-2 using 64 by 64 pixel patches. One can see from the figure that two rows of subsets are used on either side of the crack. This is to overcome two sources of error that can occur when using PIV to measure crack widths: out of plane displacement and inclusion of tensile strains in the measurement. Out of plane displacement errors occur when the distance between the camera and the object being measured varies during the test (as would be the case for the crown of the reinforced concrete pipe that deflects towards the invert of the pipe as it is loaded). Depending on the extent of movement, this effect can lead to significant measurements errors as discussed elsewhere (Hoult et al. 2013). Additionally, when measuring the displacement between two patches, this displacement is due to the combined effects of the crack opening and the tensile strain that is developed between the two patches. By adding an additional two rows of patches the effects of these errors on the crack width measurements can be minimized as will be discussed. The results can then be used to determine the applied load that yielded a 0.25mm crack width in the pipe.

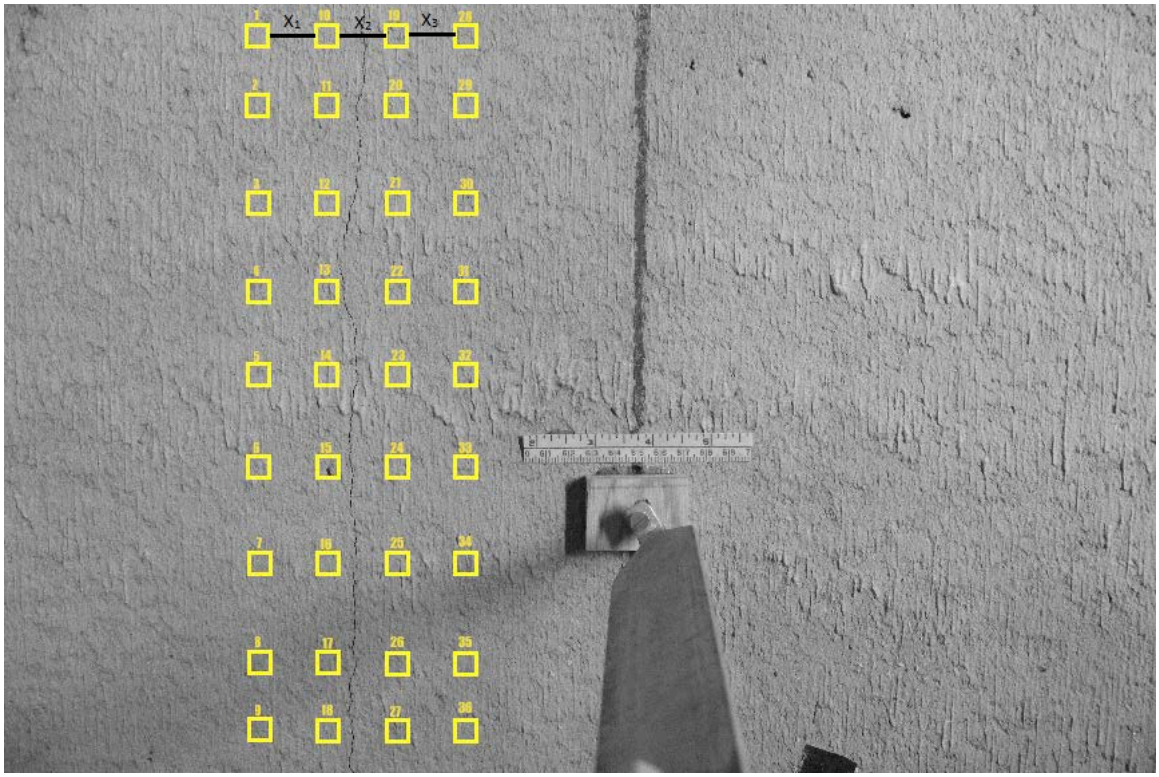

Figure C-2: Crack Width Analysis Patch Arrangement

A total of 36 patches were used to conduct the crack width analysis. Referring to Figure C-2 above, patch numbers 10-27 were created to solely determine uncorrected

crack widths measured as the change in distance x_2 between the central rows of patches. Patches 1-9 and 28-36 were created to adjust the calculated crack widths for any out of plane movement of the pipe and the tensile strains as discussed previously. A correction factor was established using these additional patches. The measured lengths x_1 and x_3 were averaged for each row of patches for each load stage. Since the crack did not form between the two outer rows of patches, any changes in the lengths x_1 and x_3 during the test would be due to effects of out of plane movement and tensile strains. Thus, the x_2 displacement values were adjusted by subtracted the average of x_1 and x_3 from x_2 to determine the total change in length due to crack opening, and accurate crack widths could then be determined. Figure C-3 shows the crack width versus applied load on the pipe relationship. Both uncorrected and corrected values are displayed to indicate the error induced by camera movements and tensile strains.

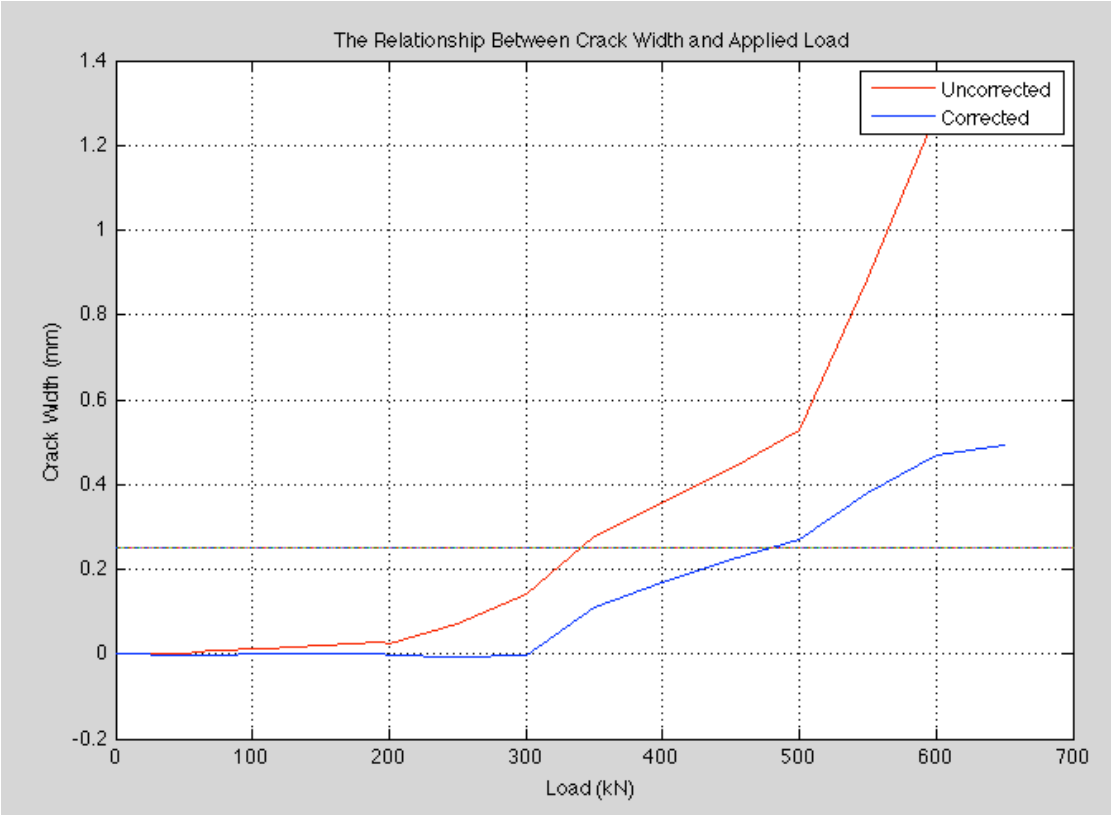

Figure C-3: The Relationship Between Crack Width and Applied Load

Furthermore, the images from the experiment at the critical load as indicated by the PIV analysis were also manually checked. A scale was fixed to the pipe in the field of view of the cameras to determine a pixel to length ratio for the PIV analysis but also so that the 0.25 crack width could be confirmed visually. For the results in Figure C-3, the onset of a crack was not evident until roughly 300kN in the photos; this is also reflected in the figure as the corrected crack width values are also zero up to the 300kN load stage. It was concluded for this test that a 0.25mm crack developed at an applied load of 480kN.

References

Hoult, N.A., Take, W.A., Lee, C., and Dutton, M. (2013). “Experimental Accuracy of Two Dimensional Strain Measurements using Digital Image Correlation.” Eng. Struct., 46, 718-726.

White, D.J., Take, W.A. and Bolton, M.D. (2003). “Soil deformation measurement using particle image velocimetry (PIV) and photogrammetry.” Géotechnique, 50(7), 619-631.

Appendix D: Proposed Usage Guidelines and Other Recommended Changes

D.1 Introduction

Changes are suggested to the AASHTO LFRD Bridge Design Specifications to

- Account for thick ring theory
- Provide guidance on usage of the Indirect Design and Direct Design methods
- Include reference to the use of Modified Compression Field Theory and other more sophisticated approaches for calculation of ultimate strength during Direct Design

D.2 Thick ring theory

The following modifications to the AASHTO LFRD Bridge Design Specifications are recommended. These issues are dealt with in section 3.5.6 of the main report.

12.10.4.2.2 Analysis for Force Effects with the Pipe Ring. Force effects in the pipe shall be determined by an elastic analysis of the pipe ring under the assumed pressure distribution or a soil-structure analysis.	C12.10.4.2.2
If thin ring theory is employed, the expected moments at crown and invert can be adjusted to account for ring thickness by $M_{thick} = M_{thin} (1 - 0.373\ t/R)$ (12.10.4.2.2-1) where: M_{thick} = adjusted moment M_{thin} = moment calculated using thin ring theory t = thickness of the concrete pipe R = average radius of the concrete pipe	NCHRP 20-07 Task 316 established that the discrepancies in areas of flexural steel resulting from Direct and Indirect Design partly result from the use of thin ring theory. Adjustment to account for thick ring theory resolves those discrepancies in part, though much of the conservatism of Direct Design remains (for example, that associated with the estimation of expected moment and consideration of ultimate limit state by considering first plastic moment).

D.3 Usage Guidelines

The following modifications to the AASHTO LFRD Bridge Design Specifications are recommended. The change in text relates to the conclusions drawn about the conservatism of design are in Section 3.7.2 of the main body of the report.

12.10.1 General	C12.10.1
The provisions herein shall apply to the structural	These structures become part of a composite system

design of buried precast reinforced concrete pipes of circular, elliptical, and arch shapes.

The structural design of the types of pipes indicated above may proceed by either of two methods:

- The direct design method at the strength limit state as specified in Article 12.10.4.2, or
  The indirect design method at the service limit state as specified in Article 12.10.4.3.

comprised of the reinforced concrete buried section and the soil envelope.

Standard dimensions for these units are shown in AASHTO M170M, (ASTM C 76M), M 206M (ASTM C 506M), M 207M (AASTM C 507M), and M242M (ASTM C 655M).

NCHRP 20-07 Task 316 established that while Direct Design for small diameter pipes leads to higher steel areas in some cases, these result from simplifying, conservative assumptions during Direct Design, and that either design procedure can be employed.

D.4 Modified Compression Field Theory

The following modifications to the AASHTO LFRD Bridge Design Specifications are recommended, based on the material presented in Sections 3.5.4 and 3.7.4.

12.10.4.2.4 Flexural Resistance at the Strength Limit State

C12.10.4.2.4
NCHRP 20-07 Task 316 established that more sophisticated procedures can be employed for estimating the flexural and shear resistance at the strength limit state, such as Modified Compression Field Theory, to enforce compatibility between and steel and concrete components and account for multiple layers of steel reinforcement and nonlinear concrete and steel behavior.